Université de Montréal

Angiotensin II Type 2 Receptor (AT_2R) in Glomerulogenesis

Par

Min-Chun Liao

Programme de sciences biomédicales

Faculté de médecine

Thèse présentée en vue de l'obtention du grade de docteur en philosophie (Ph.D)

en sciences biomédicales, option générale

Septembre 2019

Université de Montréal

Unité académique : Programme de sciences biomédicales, Faculté de médecine

---

Cette thèse intitulée

Angiotensin II Type 2 Receptor (AT_2R) in Glomerulogenesis

Présenté par

Min-Chun Liao

A été évalué(e) par un jury composé des personnes suivantes

Dre. Jolanta Gutkowska

Président-rapporteur

Dre. Shao-Ling Zhang

Directeur de recherche

Dr. John S.D. Chan

Codirecteur

Dr. Casimiro Gararduzzi

Membre du jury

Dre. Elena Torban

Examinateur externe (pour une thèse)

Dre. Hélène Girouard

Représentante de la doyenne

Résumé

Les données épidémiologiques indiquent que le diabète maternel est associé de manière significative aux anomalies congénitales des reins et des voies urinaires (CAKUT), ce qui implique un risque accru de CAKUT chez la progéniture des mères diabétiques par rapport à la population globale. Les causes de CAKUT sont multifactorielles, impliquant des facteurs génétiques et environnementaux. Le récepteur de l'angiotensine II de type 2 (AT_2R) est l'un des gènes candidats impliqués dans le CAKUT humain et murin. Bien que de nombreuses études soutiennent l'influence des facteurs génétiques et environnementaux sur le développement rénal et la pathogenèse de CAKUT, les effets du gène *AT_2R* et du milieu hyperglycémique *in utero* sur le développement rénal et les effets à long terme chez les enfants de mères diabétiques ne sont pas clairs. Cette thèse a pour objectif d'étudier l'influence de chaque facteur individuellement, ainsi que l'interaction entre ces deux facteurs.

Premièrement, nous avons examiné si le déficit en AT_2R (AT_2RKO) altère la glomérulogenèse via la formation, la maturation et l'intégrité des podocytes. Nous avons observé que la glomérulogenèse était diminuée chez les embryons E15 AT_2RKO, mais le nombre de néphrons ne présentaient aucune différence entre les nouveaux-nés AT_2RKO et les souris de type sauvage. Les souris AT_2RKO présentaient une dysplasie rénale avec un volume de touffes glomérulaires et un nombre de podocytes inférieurs à l'âge de trois semaines. Nos études ont démontré que la perte d'AT_2R via l'augmentation de la génération des dérivés réactifs de l'oxygène (ROS) induite par la NADPH oxydase 4 (Nox4) stimulait l'interaction avec la protéine Hhip ('*Hedgehog interacting protein*'), ce qui déclenchait en outre soit l'apoptose des podocytes par l'activation des voies de la caspase- 3 et de la p53, soit la transition épithéliale-mésenchymateuse des podocytes (EMT) par l'activation de la signalisation TGFβ1–Smad2/3. L'ARNm de Hhip glomérulaire était régulé positivement dans les biopsies rénales chez les patients atteints de glomérulosclérose segmentaire focale (FSGS). Les résultats suggèrent que le déficit en AT_2R est associé à une perte ou un dysfonctionnement des podocytes et est dû, au moins en partie, à une expression accrue de Hhip ectopique dans les podocytes.

Deuxièmement, nous avons cherché à établir les mécanismes sous-jacents par lesquels un milieu hyperglycémique *in utero* et un régime riche en graisses (HFD) après le sevrage accélèrent la programmation périnatale des lésions rénales. Nous avons observé que la progéniture des mères atteintes de diabète sévère avait un phénotype de restriction de croissance intra-utérine (IUGR) et avait développé une hypertension légère et des signes d'atteinte rénale à l'âge adulte. De plus, la progéniture nourrie avec une HFD post-sevrage présentait un rattrapage rapide de la croissance puis des lésions rénales associées à une augmentation de l'expression rénale de TGFβ1 et du collagène de type IV, à la production de ROS et à une accumulation de lipides rénaux, mais sans hypertension systémique. Des études in vitro ont démontré que le HFD ou les acides gras libres accéléraient le processus de programmation périnatale des lésions rénales, via une expression accrue de CD36 et de la protéine de liaison aux acides gras (Fabp4) qui cible les ROS, le facteur nucléaire-kappa B et le TGFβ1. Ces résultats indiquent que l'exposition précoce à l'HFD chez les enfants de mères diabétiques ayant subi une IUGR augmente le risque d'apparition de lésions rénales à l'âge adulte, mais pas d'hypertension.

En résumé, AT_2R joue un rôle essentiel dans la glomérulogenèse et influence l'intégrité et la fonction du podocyte via des altérations de l'expression de Hhip. En outre, les enfants de mères diabétiques ont un risque accru d'hypertension et de lésions rénales; la surnutrition postnatale accélère les lésions rénales chez ces enfants. Bien que le gène *AT_2R* et le milieu hyperglycémique *in utero* aient tous les deux un impact sur le développement du rein et sur les maladies rénales ultérieures, l'interaction entre ces deux facteurs doit encore faire l'objet d'études supplémentaires.

Mots-clés : CAKUT, diabète maternel, déficit en AT_2R, glomérulogenèse, podocytes, Hhip, surnutrition postnatale, programmation périnatale, dérivés réactifs de l'oxygène

Abstract

Epidemiologic data indicate that maternal diabetes significantly associates with congenital anomalies of the kidney and urinary tract (CAKUT), which implies an increased chance of CAKUT in the offspring of mothers with diabetes compared to the general population. The causes of CAKUT are multifactorial, involving genetic and environmental factors. The angiotensin II receptor type 2 (AT_2R) is one of the candidate genes to be implicated in both human and murine CAKUT. Although numerous studies support the influence of genetic and environmental factors on kidney development and the pathogenesis of CAKUT, the impacts of the *AT_2R* gene and hyperglycemic milieu *in utero* on kidney development and long-term outcomes in the offspring of diabetic mothers remain unclear. This thesis aims to investigate the influence of each factor individually, as well as their interaction.

Firstly, we investigated whether AT_2R deficiency (AT_2R knock-out (KO)) impairs glomerulogenesis via podocytes formation, maturation and integrity. We observed that glomerulogenesis is decreased in AT_2RKO embryos at embryonic day 15 (E15), but actual nephron numbers are no different between AT_2RKO and wild-type newborn mice. AT_2RKO mice exhibited renal dysplasia with lower glomerular tuft volume and reduced podocyte numbers at the age of three weeks. Our studies demonstrated that loss of AT_2R via NADPH oxidase 4 (Nox4)-derived reactive oxygen species (ROS) generation stimulates ectopic hedgehog interacting protein (Hhip) expression, which further triggers either podocyte apoptosis by the activation of the caspase-3 and p53 pathways or podocyte epithelial–to–mesenchymal transition (EMT) by the activation of TGFβ1–Smad2/3 signaling. Glomerular *Hhip* mRNA is upregulated in kidney biopsies of patients with focal segmental glomerulosclerosis (FSGS). The results suggest that AT_2R deficiency is associated with podocyte loss/dysfunction and is mediated, at least in part, via increased ectopic Hhip expression in podocytes.

Secondly, we aimed to establish the underlying mechanisms by which a hyperglycemic milieu *in utero* and a post-weaning high-fat diet (HFD) accelerate the perinatal programming of kidney injury. We observed that the offspring of dams with severe maternal diabetes have

an intrauterine growth restriction (IUGR) phenotype and develop mild hypertension and evidence of kidney injury in adulthood. Moreover, those offspring fed with a post-weaning HFD result in rapid catch-up growth and subsequent profound kidney injury associated with the augmentation of renal TGFβ1 and collagen type IV expression, increased production of ROS, and accumulation of renal lipids, but not systemic hypertension. *In vitro* studies demonstrated that HFD or free fatty acids accelerate the process of perinatal programming of kidney injury, via increased CD36 and fatty acid-binding protein 4 (Fabp4) expression, which targets ROS, nuclear factor-kappa B and TGFβ1 signaling. These results indicate that early postnatal exposure to HFD in IUGR offspring of diabetic dams increases the risk of later developing kidney injury, but not hypertension.

In summary, AT_2R plays an essential role in glomerulogenesis and influences the podocyte integrity and function via alterations of Hhip expression. In addition, the offspring of diabetic mothers have an increased risk of hypertension and kidney injury; postnatal overnutrition further accelerates kidney injury in those offspring. Although both AT_2R and hyperglycemic milieu *in utero* have an impact on kidney development and later kidney diseases, the interaction between these two factors still needs further studies.

Keywords: CAKUT, maternal diabetes, AT_2R deficiency, glomerulogenesis, podocytes, Hhip, postnatal overnutrition, perinatal programming, reactive oxygen species

Table of contents

Résumé 3
Abstract 5
Table of contents 7
List of Tables 9
List of Figures 10
List of Abbreviations 13
Acknowledgement 16
Thesis Outlines 17
CHAPTER 1 18
1.1 Introduction 18
1.1.1 Angiotensin II Receptor Type 2 in Glomerulogenesis 18
1.1.1.1 Renin–Angiotensin System (RAS) 18
1.1.1.2 Systemic RAS 18
1.1.1.3 Local RAS 21
1.1.1.4 The Intrarenal RAS 22
1.1.2 AT_2R in the Kidney 23
1.1.2.1 AT_2R Expression in the Developing Kidney 24
1.1.2.2 AT_2R Expression and Functions in the Adult Kidney 25
1.1.2.3 Mouse Models 27
1.1.2.4 Congenital anomalies of the kidney and urinary tract (CAKUT) 27
1.1.2.5. Hypertension and Chronic Kidney Disease 31
1.1.3. Glomerulogenesis and Podocyte 35
1.1.3.1 Kidney and Glomerulus 35
1.1.3.2 Glomerulogenesis 37
1.1.3.3 Podocyte 40
1.1.4 Hedgehog interacting protein (Hhip) 44
1.1.5 Reactive oxygen species (ROS) 47
1.1.6 Objectives 49

1.2 Article 1 52
1.3 Discussion 94
1.4 Summary 98
1.5 Before Chapter 2 99
CHAPTER 2 100
2.1 Introduction 100
2.1.1 Maternal Diabetes-induced Perinatal Programming 100
2.1.2 AT_2R and Perinatal Programming 104
2.1.3 Sex and Gender Effects 105
2.1.4 Research Questions and Hypothesis 109
2.2 Article 2 110
2.3 Discussion 133
2.4 Summary 136
CHAPTER 3 137
3.1 Introduction 137
3.1.1 Interactions of AT_2R with estrogen and its receptors 138
3.1.2 Objectives/ Hypothesis 139
3.2 Materials and Methods 140
3.3 Unpublished Results 144
3.4 Discussions 147
3.5 Future Works 149
CHAPTER 4 – REFERENCES 151

List of Tables

Table 1. Primer sequences 72
Table 2. Nephroseq analysis 73
Table 3. Patient information 74
Table 4. Biological measurements from WT and AT_2RKO mice 74
Table 5. Possible mechanisms for sex differences in CKD progression 108

List of Figures

Figure 1. An enzymatic cascade of angiotensin peptide formation 19
Figure 2. Schematic depiction of the RAS components and selected actions 21
Figure 3. A schematic illustration of the critical signaling pathways of AT_2R 26
Figure 4. Illustrative 3D models of congenital abnormalities of the kidney and urinary tract (CAKUT) 28
Figure 5. A schematic representation of kidney development 30
Figure 6. Pathophysiologic mechanisms of hypertension in chronic kidney disease 32
Figure 7. Schematic depiction of a renal proximal tubule cell showing the principal Na^+ transporters and angiotensin receptors that regulate them 33
Figure 8. Structure of the Bowman's capsule and glomerular capillary tuft 36
Figure 9. Migration of endothelial cells into the developing glomerular tuft 39
Figure 10. Podocyte subcellular compartments showed by conventional SEM and TEM 41
Figure 11. The glomerular filtration barrier and its key molecular components 43
Figure 12. Sources of ROS and the intracellular anti-oxidative defense 48
Figure 13. Physiological measurements of glomerulogenesis and neonatal nephron number. 76
Figure 14. Podocyte marker analysis *in vivo* 78
Figure 15. Hhip expression *in vivo* and *in vitro* 80
Figure 16. Hhip expression and ROS generation 82
Figure 17. Hhip and TGFβ1-induced EMT 84
Figure 18. The interaction of Hhip and TGFβRI 86
Figure 19. Images of freshly isolated neonatal kidneys (whole-mount and frontal versus transverse sections) from Nephrin-CFP-Tg versus Nephrin/AT_2RKO mice. 87
Figure 20. Proliferation study on silencing AT_2R (siRNA) in mPODs under permissive (33°C with 10 U/ml INF-γ) and non-permissive conditions (37°C without INF-γ) 87
Figure 21. Synpo IF staining in mPODs treated with or without PD123319 in a dose-dependent manner. 88
Figure 22. Renal AT_1R protein expression in E18 and neonatal kidneys from wild-type versus AT_2RKO mice analyzed by western blotting. 88

Figure 23. RT-qPCR assessment of *AT_2R* mRNA expression in mPODs treated with AT_2R siRNA (50 nM). 88
Figure 24. RT-qPCR assessment of *Nox1*, *Nox2*, and *Nox4* mRNA expression in mPODs treated with AT_2R siRNA (50 nM). 89
Figure 25. RT-qPCR assessment of *Hhip* and *Nox4* mRNA expression in mPODs treated with GKT (10^{-6} M), PD (10^{-8} M), and PD + GKT. 89
Figure 26. Semi-quantification of Figure 15G *in vitro* 89
Figure 27. Semi-quantification of Figure 15H *in vitro* 90
Figure 28. RT-qPCR assessment of *Nephrin* and *Synpo* mRNA expression in mPODs treated with rHhip in a dose-dependent manner. 90
Figure 29. Synpo IF expression in mPODs treated with rHhip in a dose-dependent manner. . 90
Figure 30. RT-qPCR assessment of *Synpo*, *α-SMA*, and *Fn1* mRNA expression in mPODs treated with rTGFβ1 in a dose-dependent manner. 91
Figure 31. Nephroseq analysis of three publicly available microarray studies performed on human kidney biopsy samples: (1) Nakagawa Chronic Kidney Disease Study; (2) Hodgin Focal Segmental Glomerulosclerosis Glomerular Study; (3) Sampson Nephrotic Syndrome Glomerular Study. 93
Figure 32. A mechanistic proposal on the early developmental origins of 'diabesity' disposition, acquired by pre- and/or neonatal overfeeding, materno-fetal hyperglycemia, and perinatal hyperinsulinism 103
Figure 33. Metabolic parameters in offspring 127
Figure 34. Blood pressure, renal function, and adipocyte morphology 128
Figure 35. Renal morphology 129
Figure 36. Renal CD36 & Fabp 4 gene expression 130
Figure 37. Renal CD36 & Fabp 4 localization 131
Figure 38. BSA-PA effects in IRPTCs 132
Figure 39. Maternal diabetic murine model. 141
Figure 40. Systolic blood pressure in the offspring of non-diabetic (Con) and diabetic (Dia) dams of wild-type (WT) and AT2RKO (KO) mice 144
Figure 41. Renal morphology and function 145
Figure 42. Podocyte number and marker analysis 146

Figure 43. Estrogen receptors expression in isolated glomeruli and effect of estradiol on estrogen receptors and AT_2R expression in cultured podocytes 147
Figure 44. Proposed working model 150

List of Abbreviations

ACE : Angiotensin-converting enzyme

ACE2 : Angiotensin-converting enzyme 2

ACR : Albumin/creatinine ratio

Agt : Angiotensinogen

Ang : Angiotensin

Ang I : Angiotensin I

Ang II : Angiotensin II

Ang III : Angiotensin III

APA : Aminopeptidase A

APN : Aminopeptidase N

ARB : Angiotensin receptor blocker

AT_1R : Angiotensin II receptor type 1

AT_2R : Angiotensin II receptor type 2

AT_2RKO : AT_2R deficiency

ATIP : AT_2R interacting protein

BK : Bradykinin

BP : Blood pressure

BSA : Bovine serum albumin

BSA-PA : BSA-bound sodium palmitate

BW : Body weight

C21 : Compound 21

CAKUT : Congenital anomalies of the kidney and urinary tract

CD2AP : CD2-associated protein

CFP : Cyan fluorescent protein

CKD : Chronic kidney disease

DHE : Dihydroethidium

Dhh : Desert hedgehog

DOHaD : Developmental Origins of Health and Disease

E : Embryonic day

EMT : Epithelial–to–mesenchymal transition

ESRD : End-stage renal disease

Fabp4 : Fatty acid-binding protein 4

FAT1 : Fat cadherin 1

FSGS : Focal segmental glomerulosclerosis

GBM : Glomerular basement membrane

GDM : Gestational diabetes

GFR : Glomerular filtration rate

GPCR : G-protein coupled receptor

GWAS : Genome-wide association study

H&E : Hematoxylin and eosin

H_2O_2 : Hydrogen peroxide

HAPO : Hyperglycemia and adverse pregnancy outcomes

HFD : High-fat diet

Hh : Hedgehog

Hhip : Hedgehog interacting protein

IF : immunofluorescence

IHC : Immunohistochemistry

Ihh : Indian hedgehog

IRAP : Insulin-regulated aminopeptidase

IRPTC : Immortalized rat renal proximal tubular cell line

IUGR : Intrauterine growth restriction

KO : Knockout

KW : Kidney weight

MAPK : Mitogen-activated protein kinase

MCD : Minimal change disease

MM : Metanephric mesenchyme

mPODs : Immortalized mouse podocytes cell line

MrgD : Mas-related G protein-coupled D

ND : Normal diet

NEFA : Non-esterified fatty acids

NEPH1 : Nephrin-like protein 1

NF-κB : Nuclear factor-kappa B

NHE-3 : Sodium-hydrogen exchanger-3

NKA : Sodium-potassium adenosine triphosphatase

NO : Nitric oxide

Nox4 : NADPH oxidase 4

PAS : Periodic acid–Schiff

PGDM : Pre-gestational diabetes

PLZF : Promyelocytic zinc finger protein

RAS : Renin-angiotensin system

rHhip : Recombinant Hhip

ROS : Reactive oxygen species

SBP : systolic blood pressure

Shh : Sonic hedgehog

STZ : Streptozotocin

Synpo : Synaptopodin

Tg : Transgenic

TGFβRI : TGFβ receptor I

TL : Tibia length

TRPC6 : Transient receptor potential channel 6

UB : Ureteric bud

VEGF : Vascular endothelial growth factor

VEGFR2 : Vascular endothelial growth factor receptor 2

WB : Western blotting

ZO-1 : Zonula occludens-1

Acknowledgement

It would not have been possible to complete this dissertation in a period of my study without the great support and help of a number of people whom I would like to acknowledge and thank.

First of all, I would like to express my most profound gratitude to my supervisor Dr. Shao-Ling Zhang, who offered me this opportunity to join her lab and guided me without preconditions throughout my entire journey of pursuing a Ph.D. Without her full support, inspiration and guidance, all the achievements are back to square one. Thank you for your patience, motivation, enthusiasm and perseverance. I am deeply indebted to my co-supervisor Dr. John Chan for his encouragement, helpful comments and academic direction.

I would like to express my deepest appreciation to my dissertation committee: Dr. Jolanta Gutkowska, Dr. Casimiro Gararduzzi, Dr. Elena Torban and Dr. Helene Girouard. I am grateful for their thoughtful insights, expert guidance and enthusiastic commitment.

I also want to offer my sincere thanks to my present colleagues and past lab members: Xing-Ping Zhao, Henry Nchienzia, Chao-Sheng Lo, Shuiling Zhao, Yessoufou Aliou, Shaaban Abdo, Yixuan Shi, Chin Han Wu and Anindya Ghosh for their valuable assistance in collecting data, discussing questions and cooperating experiments at the research site. I would like to extend my special thanks to Mrs. Isabelle Chénier and Dr. Kana Miyata for their insightful comments and suggestions on an earlier version of this dissertation and all the generous help in my studies and life. I owe a debt gratitude to all the people who have helped me throughout the journey of my Ph.D.

Finally, I wish to express my heartfelt gratitude to my parents, sister, brother and in-laws for their constant encouragement and support. The most important is to thank my lovely wife Shiao-Ying Chang for her enduring patience, unconditional support and understanding. Her love is my source of energy to complete this dissertation.

Thesis Outlines

My Ph.D. thesis contains three Chapters bellow:

– Chapter 1: To study the impact of AT_2R deficiency on glomerulogenesis. We aim to investigate whether AT_2R deficiency impairs glomerulogenesis via altered podocytes formation, maturation, and integrity (**Liao MC***, Zhao XP, Chang SY, Lo CS, Chenier I, Takano T, Ingelfinger JR, Zhang SL: AT_2R deficiency mediated podocyte loss via activation of ectopic hedgehog interacting protein (Hhip) gene expression. The Journal of Pathology, 2017; 243 (3): 279-293, Impact Fact (IF): 6.253).

  My paper was chosen as one of 21 original papers highlighted by **The Journal Pathology** as "Recent Advances in Renal Pathology" to celebrate its 125th anniversary (Virtual Issue, September 2018).

– Chapter 2: To study the outcomes of perinatal programming occurring in the offspring of diabetic mothers postnatally fed with a high-fat diet (HFD). We aim to investigate the underlying mechanisms by which a post-weaning HFD accelerates the perinatal programming of kidney injury occurring (Aliou Y*, **Liao MC***, Zhao XP, Chang SY, Chenier I, Ingelfinger JR, Zhang SL: Post-weaning high-fat diet accelerates kidney injury, but not hypertension programmed by maternal diabetes. Pediatric Research, 2016; 79(3): 416-424, Impact Fact (IF): 2.882. *The first two authors contributed equally to this work).

– Chapter 3: To study the impact of AT_2R deficiency on maternal diabetes-induced perinatal programming. We aim to investigate whether AT_2R deficiency accelerates perinatal programming induced by maternal diabetes. (Ongoing studies)

CHAPTER 1

Liao MC*, Zhao XP, Chang SY, Lo CS, Chenier I, Takano T, Ingelfinger JR, Zhang SL: AT_2R deficiency mediated podocyte loss via activation of ectopic hedgehog interacting protein (Hhip) gene expression. The Journal of Pathology, 2017; 243 (3): 279-293

1.1 Introduction

1.1.1 Angiotensin II Receptor Type 2 in Glomerulogenesis

1.1.1.1 Renin–Angiotensin System (RAS)

The renin–angiotensin system plays a pivotal role in controlling renal, vascular and cardiac physiology, and its activation is related to multiple diseases such as chronic kidney disease, hypertension, cardiovascular disease, and diabetes mellitus [1]. Historically, the RAS has been extensively discussed for more than 120 years since the first discovery of the enzyme renin by Tigerstedt and Bergmann in 1898 [2]. The original view of the RAS was thought to be a peptidergic system with endocrine features, which is the systemic RAS or also called the endocrine RAS. However, it is now generally recognized that this original view of the systemic RAS represents an insufficient description of the system. In addition to the systemic RAS, a local RAS exists in different organs and plays a crucial role in physiology and pathophysiology. There are several local RASs that function independently of each other and of the systemic RAS. For instance, angiotensin II (Ang II) generated in the kidney appears to have physiologic effects that are as important as circulating Ang II and, under some circumstances, even more important than circulating Ang II [3]. Thus, the RAS includes both a systemic system with endocrine effects and multiple local systems with autocrine, paracrine, and intracrine effects.

1.1.1.2 Systemic RAS

The systemic RAS begins with renin cleaving its substrate, angiotensinogen (Agt), to form the inactive peptide Angiotensin I (Ang I). Then, Ang I is converted to the biologically active octapeptide Ang II by a dipeptidyl carboxypeptidase named angiotensin-converting

enzyme (ACE), a process that occurs most predominantly on the surface of endothelial cells [1]. Ang II binds to its two receptors, Ang II receptor type 1 (AT_1R) and type 2 (AT_2R), to regulate tissue and cell functions. For example, Ang II acts through AT_1R to initiate and maintain actions that could be harmful to the body, including vasoconstriction, anti-natriuresis, aldosterone secretion, sympathetic nervous system activation, cellular dedifferentiation and growth, inflammation, reactive oxygen species production, and target organ damage [4]. In contrast, Ang II also binds to AT_2R to counterbalance AT_1R-mediated actions, including vasodilation, natriuresis, anti-proliferation, anti-inflammation, anti-oxidative, anti-hypertrophic, and anti-fibrotic actions [5]. Although the expression of this receptor is low in healthy adults, it is activated in certain disease conditions. The RAS also includes several other enzymes, peptides (Ang II metabolites), and receptors, which collectively comprise a "protective arm" to counterbalance the harmful actions of the ACE/Ang II/AT_1R pathway. The components of the protective arm are described below, and Figure 1 provides a schematic illustration of the formation of Ang II and its metabolites.

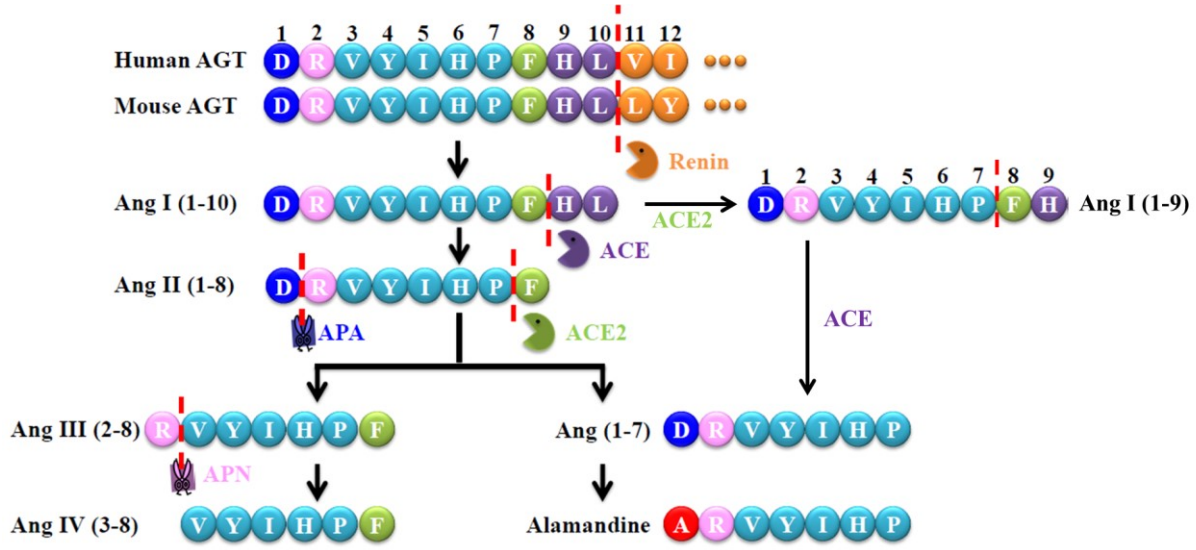

Figure 1. An enzymatic cascade of angiotensin peptide formation. AGT, angiotensinogen; APA, aminopeptidase A; APN, aminopeptidase N.

The RAS plays a critical role in regulating physiological and pathophysiological processes in the cardiovascular system and kidney through autocrine and paracrine as well as endocrine effects [1]. The system is involved in a large range of homeostatic and modulatory

processes that regulate vasoconstriction, salt and water balance, cell growth, tissue remodeling and dysfunction, hormone secretion and sympathetic activity. AT_1R activation is considered to mediate the majority of the biological functions of Ang II [1]. However, the AT_1R is also involved in a variety of pathophysiological conditions in which the RAS is abnormally activated, such as hypertension, cardiac hypertrophy, heart failure, diabetic nephropathy, fibrosis, and inflammation [6]. The AT_1R is widely present in various tissues, including vascular smooth muscle, endothelium, heart, brain, kidney, adrenal gland, and adipose tissue. The classic ACE/Ang II/AT_1R pathway promotes intracellular signaling pathways through the activation of protein kinases, growth factor receptor transactivation, subunits of nicotinamide adenine dinucleotide phosphate (NADPH) oxidase [1]. Those signaling transductions are mostly G-protein-dependent, including $G_{q/11}\alpha$, $G_{12/13}\alpha$, and $G_i\alpha$ [1]. The AT_1R also elicits G-protein-independent signal transduction cascades, forms a heterodimer with other G-protein coupled receptors (GPCRs), and directly interacts with AT_1R interacting proteins [1]. On the contrary, the biological functions of Ang II mediated through AT_2R are considered as regulating vasodilation to counterbalance the vasoconstrictor effects mediated through AT_1R.

A protective arm of the RAS has more recently emerged, which includes the angiotensin-converting enzyme 2 (ACE2) /Ang (1-7)/Mas receptor pathway, the alamandine/Mas-related G protein-coupled D (MrgD) receptor pathway, and the Ang II/Ang III/AT_2R pathway (Figure 2) [7]. In contrast to ACE, a novel mono-carboxypeptidase was identified and called ACE2, which is the pivotal enzyme of the protective arm by converting Ang I and Ang II into Ang (1-9) and Ang (1-7), respectively [1]. Ang (1-9) is then converted to Ang (1-7) by ACE. Ang (1-7) is a ligand of the Mas receptor, which triggers opposite actions to the classic ACE/Ang II/AT_1R pathway, such as vasodilation and anti-fibrosis [1]. Alamandine can be formed from Ang (1-7) in the heart and also has vasodilative and anti-fibrotic effects through binding to MrgD [8]. Ang II is further converted to Ang III and Ang IV by different aminopeptidases (Figure 1). It has been demonstrated that Ang III is a ligand of both AT_1R and AT_2R, as well as the endogenous AT_2R agonist in the kidney [5]. Ang IV binds to its receptor, AT_4R (also known as insulin-regulated aminopeptidase (IRAP)), which causes vasodilation effects by increased endothelial nitric oxide (NO) synthase and also increases renal cortical blood flow and urinary sodium excretion [9]. The updated RAS,

including Ang peptides, their receptors, and actions are summarized in Figure 2. Together, these counter-regulatory pathways work to reduce the harmful impact of the classic ACE/Ang II/AT_1R pathway on blood pressure and kidney function.

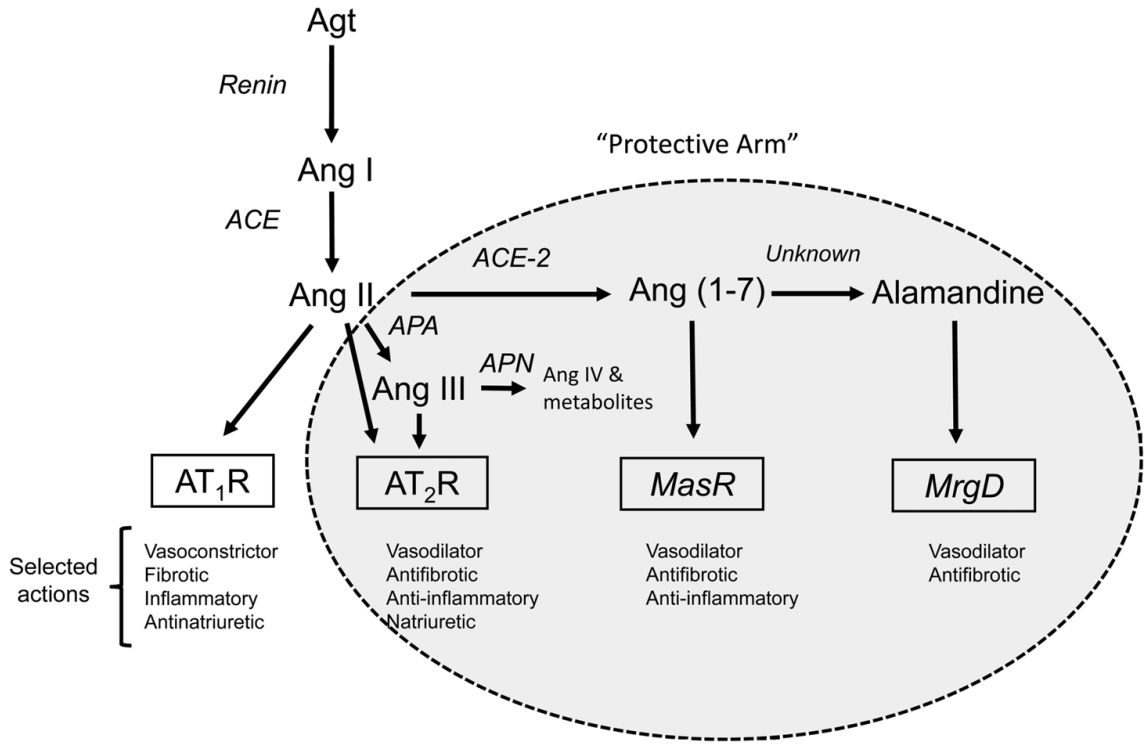

Figure 2. Schematic depiction of the RAS components and selected actions. Receptors are shown in the boxes. Components of the protective arm of the system are shown in the shaded ellipse. AT_2R can be activated by Ang II or the Ang II metabolite, Ang III. Within the kidney, Ang III is thought to be the preferred agonist for AT_2R-induced renal tubular inhibition of Na^+ reabsorption. The "protective arm" of the RAS acts in a counter-regulatory manner to oppose the detrimental actions of Ang II via AT_1R. Adapted from "AT_2 Receptors: Potential Therapeutic Targets for Hypertension," by R.M. Carey, 2017, *American Journal of Hypertension, 30(4)*, p. 340, Copyright 2016, with permission from Oxford University Press. [7]

1.1.1.3 Local RAS

The concept of a local RAS is based on RAS components being expressed in "unlikely" places, and the functions of this system are mostly based on local Ang II synthesis.

Besides, the local RAS exerts diverse physiological and pathophysiological roles, and the RAS components are formed locally by various organs and cells (e.g., kidney, adrenal gland, heart, brain, reproductive tract, skin, digestive organs, white blood cells, and adipocytes) [2]. For example, although renin is secreted from the juxtaglomerular apparatus of the kidney, it is found in the brain after nephrectomy. Circulating renin and its substrate do not pass the blood-cerebrospinal fluid barrier, suggesting that in the brain, the local RAS appears to be regulated independently of the systemic RAS. However, there is the crosstalk between the systemic and local RAS. For instance, heart uptakes renin and Agt from the circulation and stores them locally. Thus, they are used to produce Ang II locally in the heart. Hence, in addition to the systemic RAS, local Ang II synthesis is an essential modulator of tissue function and structure. Also, locally produced Ang II might contribute to the tissue injury via the stimulation of inflammation, proliferation, and apoptosis, the regulation of some gene expressions, and the activation of several intracellular signaling pathways [3].

1.1.1.4 The Intrarenal RAS

Although every organ and tissue in the body has RAS components, the kidney is unique as it has all the RAS components to generate intrarenal Ang II. The level of intrarenal Ang II, expressed as content per mass of tissue, is much higher than the level of that delivered by the circulatory system. In rats, the level of plasma Ang II is in the picomolar range (50-100 pM), whereas the level of luminal Ang II in the renal proximal tubule is in the nanomolar range (30-40 nM) [10, 11]. Intrarenal Ang II plays a pivotal role in regulating renal hemodynamics and functions, which are associated with sodium balance and blood pressure homeostasis [12]. It has further been demonstrated that abnormally increased intrarenal Ang II causes hypertension and renal injury via AT_1R [13].

The main fraction of Ang II in the kidney is produced locally from both plasma Agt and intrarenal Agt generated by the renal proximal tubule [3]. Plasma Ang I in the kidney can also be converted to Ang II by intrarenal ACE, which is expressed in the kidneys predominantly in renal proximal and distal tubules, the collecting ducts, and renal endothelial cells [14]. Renin synthesized by the juxtaglomerular apparatus cells is the primary origin of both plasma and intrarenal renin levels, which also can provide another pathway for the local

Ang I production [15]. Thus, all of the RAS components required to produce intrarenal Ang II are expressed along the nephron, indicating that there is specific compartmentalization of intrarenal RAS with distinct regulatory mechanisms predominating in the separate compartments.

In the view of physiology, the local RAS has abilities to maintain a balance or homeostasis at the tissue level to counterbalance the effects mediated by the systemic RAS [3]. The dual actions of Ang II on its receptors are thought to be the basis of the balance between the systemic and local RAS. Also, the possibility of alternative pathways including different tissue-expressed substrates for ACE, different receptors such as AT_4R, and different Ang II metabolite products such as Ang (1-7) can be responsible for mediating the regulatory and counter-regulatory effects. If this balance is disarranged, the RAS turns into a mediator of the pathophysiological stimulus. Thus, inappropriate activation of the intrarenal RAS leads to alterations in the hemodynamic function that contributes to the development of hypertension. Persistence of this activation results in long-term consequences, including cellular proliferation and renal injury.

1.1.2 AT_2R in the Kidney

AT_2R is generally considered as part of the "protective arm" of the RAS to counterbalance the actions of Ang II via AT_1R [7]. The *AGTR2*, the gene symbol of AT_2R, gene is localized on the X chromosome in human, mouse and rat [5]. The genomic DNA of all three species consists of three exons, two introns, and the whole protein-coding region is contained in the third exon [16]. Because of this uninterrupted protein-coding region, no AT_2R subtypes or splice variants have been identified [17]. The homologous location and structure of the *AGTR2* gene throughout all three species may have important implications in the genetics of the *AGTR2* gene. AT_2R cDNA encodes 363 amino acid residues correlated to a molecular weight of 41 kDa [5]. The AT_2R protein belongs to the family of seven-transmembrane G-protein coupled receptor (GPCR) and functions as a receptor for Ang II [5]. Although AT_1R and AT_2R belong to the same family of GPCRs, both receptors share only approximately 34% amino acid sequence identity [18]. The homologous amino acid sequence of AT_1R and AT_2R is mainly localized in the transmembrane hydrophobic domain, which

forms seven-transmembrane helical columns. Amino acid residues located in these helical domains and considered to be necessary for Ang II binding to AT_1R are also conserved in AT_2R. The divergence regions between AT_1R and AT_2R are in the third intracellular loop and the carboxyl-terminal tail. These structural characteristics of AT_2R establish a potential foundation for its weak coupling to G-proteins and lack of phosphorylation by GPCR kinases, as well as lack of desensitization after Ang II binding [19]. Therefore, due to the differences in amino acid sequence and structural features, it seems that the activation of AT_1R and AT_2R is likely to stimulate distinct signaling mechanisms and induce different biological actions.

1.1.2.1 AT_2R Expression in the Developing Kidney

AT_2R is highly expressed in fetal mesenchymal tissues, suggesting that the actions of Ang II via AT_2R might play a pivotal role in regulating cellular differentiation and organ development [20]. Mouse metanephric development begins on embryonic day (E) 10.5, and kidney development continues until postnatal ten days after birth. In the rodent kidney, AT_2R expression peaks during fetal metanephrogenesis and rapidly declines after birth. Also, AT_2R is expressed earlier than AT_1R. In mice, *AT_2R mRNA* and protein can be detected in the metanephric kidney as early as on E11.5 which is a rapidly developing period of the urogenital system, and its signals are located in the ureteric bud (UB) and the mesenchymal cells adjacent to the UB tip [20]. On E14, AT_2R is expressed in UB branches, nephron progenitors and medullary stroma. AT_2R is detected in inner cortical tubules (i.e., morphologically resembles proximal tubule) on E16 and reaches a maximal level on E19.

On the other hand, AT_1R expression peaks at the end of gestation and subsequently declines gradually. On E12, AT_1R protein is detected at low levels in the UB and the surrounding mesenchyme [20]. On E14, AT_1R immunostaining is highly expressed in both the luminal and basolateral sides of UB branches. On E16, AT_1R is present in proximal tubules and is weakly expressed in the UB branches, stromal mesenchyme and glomeruli.

Nearly simultaneously at E14, both AT_1R and AT_2R are expressed in the metanephros when UB is vigorous branching [21]. However, both receptors show a distinct cellular expression pattern during kidney development. In the fetal kidney, *AT_1R* mRNA is expressed mainly in the glomeruli, S-shaped bodies, and proximal and distal tubules, whereas *AT_2R*

mRNA is expressed primarily in the mesenchymal cells close to the UB tip, and later extended to the nephrogenic area of the superficial cortex and the cells between collecting ducts [21]. Furthermore, it has been demonstrated that in murine, the level of Ang II in the developing fetal kidney is higher than that of adult kidney [20]. In addition to AT_1R and AT_2R, the other RAS components are also expressed in the developing kidney, such as Agt, renin, and ACE, suggesting that the RAS locally plays a role in kidney development.

1.1.2.2 AT_2R Expression and Functions in the Adult Kidney

AT_2R decreases markedly after birth, but it is expressed at low levels in healthy adult tissues including the cardiovascular system, adrenal gland, kidney, brain, reproductive tissues, and skin [5]. In mature kidney, AT_2R protein is expressed predominately in glomeruli and present in small quantities in cortical tubules and interstitial cells. AT_2R is upregulated in adult tissues under certain pathological conditions, including fibrosis, wound healing, tissue remodeling, and inflammation [5]. It has been demonstrated that AT_2R protein is upregulated in adult glomeruli, tubules and interstitium in response to dietary sodium depletion [22].

As mentioned before, the activation of AT_2R is essential to counterbalance the detrimental effects mediated by AT_1R and protect against the progression of organ damage and failure as a result of excessive action of Ang II. The possible signaling pathways involved in AT_2R-mediated biological effects are schematically summarized in Figure 3 [5]. In a sodium-depletion animal model, AT_2R is stimulated to protect the kidney from injury via the bradykinin–nitric oxide (NO)–cGMP pathway. In both vascular smooth muscle cells and cardiomyocytes, AT_2R activation inhibits the phosphorylation of ERK1/2 via stimulation of a variety of phosphatases. It has been reported that inhibition of NADPH oxidase activity stimulates AT_2R-mediated natriuresis [5]. Other potential pathways have been involved in AT_2R-mediated effects, including interaction with AT_2R interacting protein (ATIP) and transcription factor promyelocytic zinc finger protein (PLZF), and activation of several protein phosphatases. Zhang et al. [23] first reported that AT_2R is able to couple the G-proteins $G_{i2}\alpha$ and $G_{i3}\alpha$ in the rat fetus and AT_2R coupling to $G_i\alpha$ is linked with activation of cGMP signaling. Another study has shown that AT_2R-mediated activation of SHP-1 (i.e. phosphatases) is associated with $G_s\alpha$ [24]. Although AT_2R has all of the classic motifs and signature residues of

a GPCR, it lacks the typical mechanisms of rapid desensitization, internalization and degradation. These atypical GPCR features cause a prolonged signaling response. Also, AT_2R may have constitutive activity and exert ligand-independent cellular effects by dimerization with other GPCRs or interaction with different scaffold proteins to mediate its action [5].

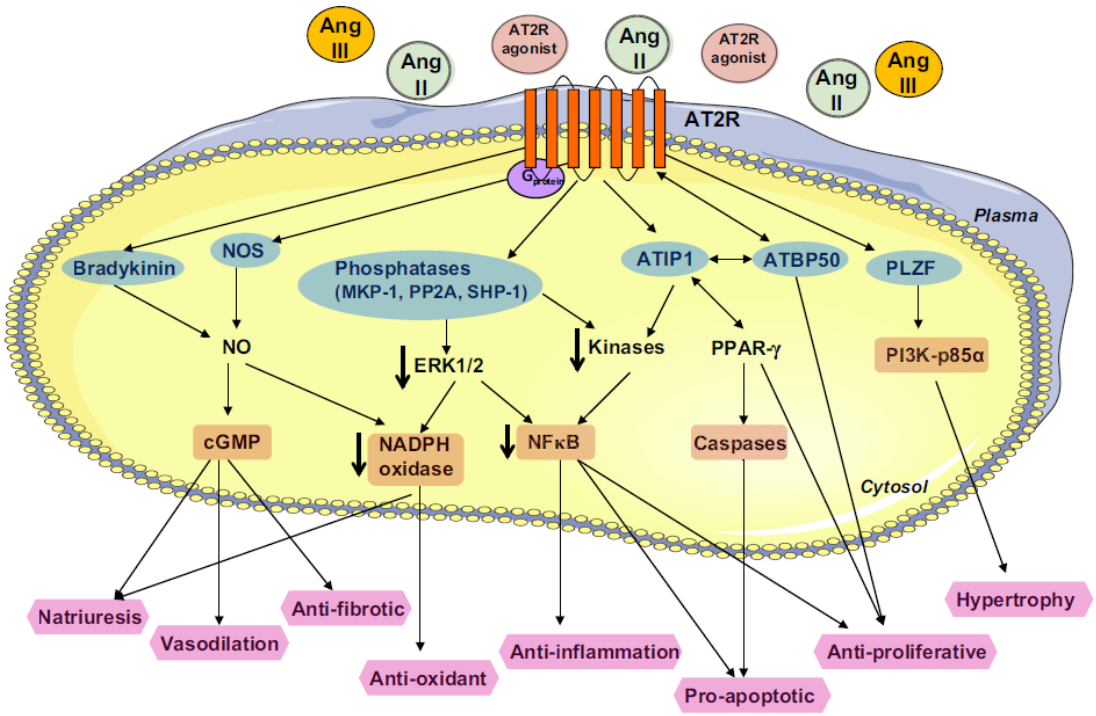

Figure 3. A schematic illustration of the critical signaling pathways of AT_2R. The AT_2R has been shown to activate several pathways which are dependent on its specific action. AT_2R-mediated natriuresis, vasodilation and anti-fibrotic effects involve the activation of a NO–cGMP–dependent pathway, which is likely mediated by the release of bradykinin and an increased NOS activity, whereas its mediated antioxidant, anti-inflammatory and growth inhibition involves the interaction with its interacting protein, ATIP1, and activation of several phosphatases (MKP-1, PP2A, SHP-1) to interfere with ERK1/2 and other kinases' phosphorylation. On the other hand, the interaction with PLZF is involved in its mediated hypertrophic effect, primarily in cardiac tissues. Adapted from "Angiotensin II type 2 receptor (AT_2R) in renal and cardiovascular disease," by B.S. Chow, 2016, *Clinical science (London, England: 1979)*, *130(15)*, p. 1312, Copyright 2016, with permission from Portland Press. [5]

1.1.2.3 Mouse Models

Gene knockout and overexpression mouse models have been useful tools to study the role of AT_2R in cardiovascular and renal diseases. For example, the AT_2R knockout (AT_2RKO) mouse line was reported by two groups in 1995 [25, 26]. There are no dramatically abnormal phenotypes at baseline in AT_2RKO mice, but blood pressure was reported to be either increased [25] or unchanged [26] in these AT_2RKO mice. It has been reported that AT_2RKO mice have increased vascular and anti-natriuretic sensitivity in response to exogenous Ang II, attenuation of exploratory behavior, delay differentiation in the vascular smooth muscle cells, and increased susceptibility to renal-tubular developmental disease [18]. AT_2R deficiency leads to normal or slight blood pressure elevation and augmented vascular sensitivity to exogenous Ang II, suggesting that AT_2R may exert a protective effect in blood pressure regulation by counteracting AT_1R function via downregulation of AT_1R expression [27] and upregulation of bradykinin–NO–cGMP signaling [28]. Although AT_2RKO mice did not produce dramatic morphological abnormalities, those mice display congenital anomalies of the kidneys and urinary tract (CAKUT) with a >23% penetrance [18]. In contrast, transgenic mice that overexpress cardiac-specific AT_2R were found to have no visible morphological or functional changes but a decreased response to AT_1R-mediated vasoconstriction and chronotropic effects [29]. Also, transgenic mice that overexpress AT_2R in vascular smooth muscle cells were found to have activated bradykinin–NO–cGMP pathway and diminished Ang II-induced vascular constriction as well [30].

1.1.2.4 Congenital anomalies of the kidney and urinary tract (CAKUT)

Congenital anomalies of the kidney and urinary tract (CAKUT) are frequent causes of chronic kidney disease (CKD) and end-stage renal disease (ESRD) in children [31]. CAKUT form approximately 20–30% of all congenital malformations, and their frequency has been predicted from three to six per 1,000 births [32, 33]. Because CAKUT play a causative role in 48–59% of cases of CKD and in 34–43% of cases of ESRD in children in developed countries [31, 34], it is imperative to diagnose these anomalies and establish a therapy to preserve renal function and prevent or delay the onset of kidney failure. CAKUT refer to a spectrum of structural malformations that are characterized by defects in morphogenesis of the kidney

and/or urinary tract. The defects of CAKUT involve renal agenesis, renal hypoplasia, renal dysplasia, horseshoe kidney, multicystic dysplastic kidney, ureteropelvic junction obstruction, hydronephrosis, megaureter, duplex collecting system, ectopic ureter, vesicoureteral reflux, and posterior urethral valves (Figure 4) [35]. In Europe, CAKUT account for 41.3% of all children receiving renal replacement therapy [36]. In contrast, CAKUT are a much less frequent cause of ESRD in adult patients who received renal replacement therapy. It has been reported that the estimated median age at the start of renal replacement therapy is 31 and 61 years in patients with and without CAKUT, respectively [37]. However, recent evidence suggests that some patients with asymptomatic or milder forms of CAKUT might develop hypertension, proteinuria, and ESRD in adulthood [37]. Thus, CAKUT progress to ESRD more often at adulthood than in childhood.

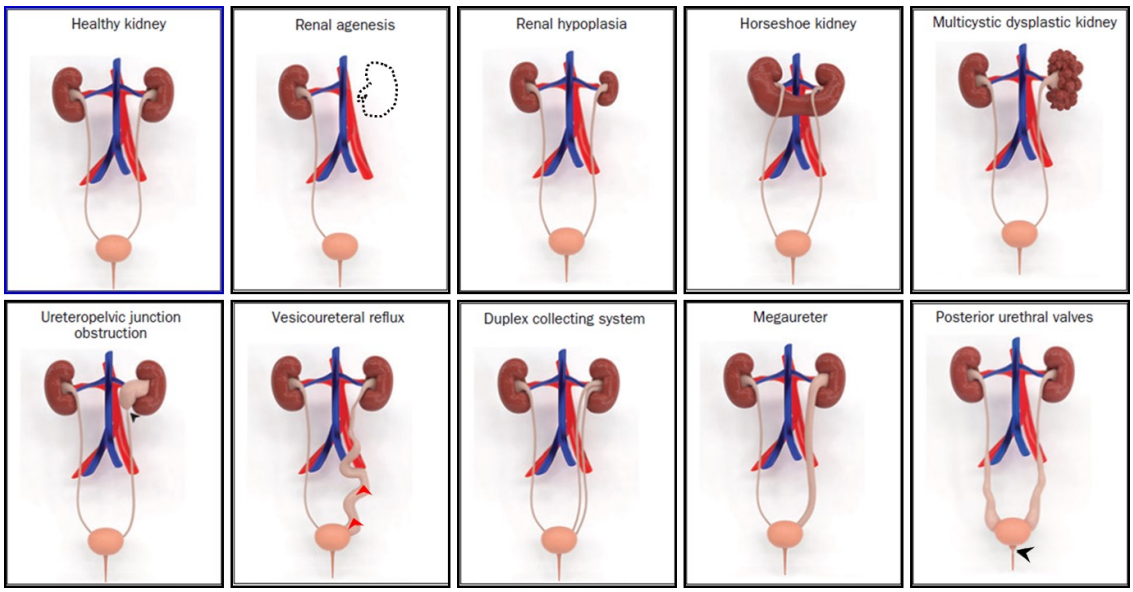

Figure 4. Illustrative 3D models of congenital abnormalities of the kidney and urinary tract (CAKUT) that were created using the modeling tools ZBrush (Pixologic, Inc.) and 3ds Max (Autodesk, Inc.), to illustrate the phenotypic spectrum of CAKUT. The black arrows indicate the site of obstruction in ureteropelvic junction obstruction and posterior urethral valves. The red arrows indicate the abnormal flow of the urine from the bladder to the ureter or kidney occurring in vesicoureteral reflux. Adapted from "Genetic, environmental, and epigenetic factors involved in CAKUT," by N. Nicolaou, 2015,

Nature reviews. Nephrology, *11(12)*, p. 722, Copyright 2015, with permission from Springer Nature. [35]

The etiology of CAKUT is multifactorial, including monogenetic causes, copy number variants, single nucleotide variants, epigenetic influences, and environmental risk factors [35]. Despite the diverse renal structural malformations, all forms of CAKUT stem from defective kidney development. In order to realize the basis of CAKUT, it is indispensable to consider how the kidney develops.

Kidney development (also called nephrogenesis) occurs in three stages, including the pronephros, mesonephros and metanephros, arising sequentially from the intermediate mesoderm [38]. The pronephros is a primitive and transient structure with a non-functional system. Degeneration of the pronephros is required for kidney development. The mesonephros develops caudally to the pronephros and is the first excretory organ, excreting urine via the mesonephric duct (also called Wolffian duct). In mice, the mesonephros becomes inactive and atrophies at E14.5, and, within 24 hours, nearly all of the tubules undergo apoptosis and disappear in a caudal to the cranial direction [39]. At this time point, *AT_2R* mRNA is highly expressed in the mesonephros, suggesting that AT_2R expression might represent a group of specific cells that are programmed to undergo apoptosis [21]. While in the female the mesonephros disappears completely, in the male a part of it develops into the testicular efferent ducts. In contrast to the pronephros and mesonephros, the metanephric kidney persists and is characterized by reciprocal inductive interactions between UB and metanephric mesenchyme. Thus, kidney development occurs with UB outgrowth, followed by UB branching morphogenesis and mesenchyme–to–epithelial transition, and completes with nephron patterning and elongation [39]. The overview of kidney development is schematically summarized in Figure 5.

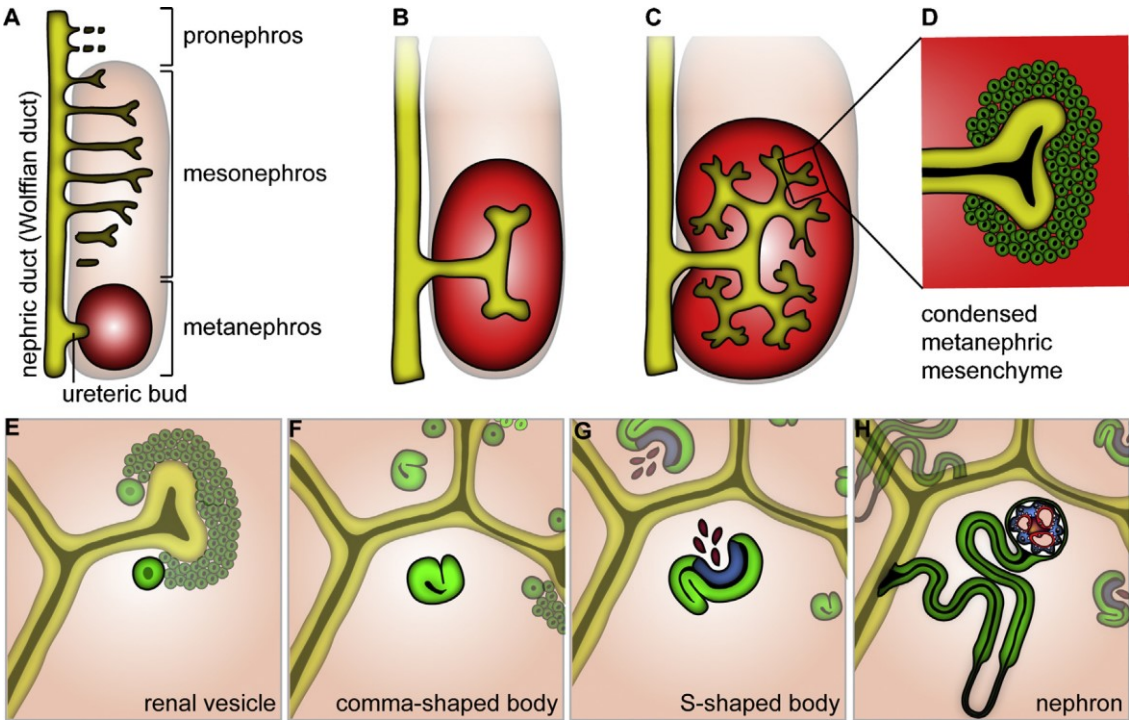

Figure 5. A schematic representation of kidney development. (A) In mammals, the kidney develops from the metanephric mesenchyme upon an invasion of the ureteric bud out of the nephric duct. (B and C) The ureteric bud starts branching within the growing metanephric mesenchyme. (D) The mesenchyme condenses around the ureteric bud tips forming the cap mesenchyme. (E) Renal vesicles form from the condensed cap mesenchyme. (F) A cleft develops in the comma-shaped bodies. (G) Podocyte progenitors start to attract angioblasts in the S-shaped body. (H) The developing nephron connects with the collecting duct. Adapted from "Glomerular development--shaping the multi-cellular filtration unit," by C. Schell, 2014, *Seminars in Cell & Developmental Biology, 36*, p. 41, Copyright 2014, with permission from Elsevier. [40]

The underlying molecular control of nephrogenesis is governed by a large number of genes and signaling pathways. Perturbation in each step of nephrogenesis, due to the dysfunction of genes or exposure to environmental risk factors, can lead to the clinical phenotype of CAKUT. The current understanding of the genes involved in nephrogenesis and the molecular mechanisms involved in the pathogenesis of CAKUT has mainly been obtained from mouse models. As mentioned in the previous section, one of the phenotypes of AT_2RKO

mice is CAKUT, which include a wide range of anatomical anomalies (Figure 4). The observed diversity of anatomical patterns in AT_2RKO mice supports the notion that single-gene mutations might cause CAKUT. These murine and human CAKUT are similar to each other in terms of anatomical anomalies, male preponderance, frequent unilaterality, lack of other structural organ anomalies, and time of onset [41]. However, it has been reported that only 3.1% of AT_2RKO mice have been observed with anatomical defects [41]. Besides, the penetrance of the CAKUT could increase to 23% by interbreeding [41]. Numerous studies demonstrated that epigenetic and gestational environmental risk factors can affect kidney development and might also contribute to the natural history of CAKUT. Thus, it is important to fully understand how disease progression is influenced by genetic and environmental interaction in order to prevent or delay the progression of kidney failure.

1.1.2.5. Hypertension and Chronic Kidney Disease

Hypertension and chronic kidney disease (CKD) are in a closely interlinked cause and effect relationship. Sustained elevations in blood pressure (BP) can lead to worsening kidney function, and the progressive decline in kidney function can conversely lead to worsening BP control. The leading causes of CKD are hypertension and diabetes. CKD affects as many as 10–15% of the adult population worldwide [42]. Patients with CKD are more likely to die from cardiovascular diseases than those without CKD. The prevalence of hypertension ranges from 60% to 90% in CKD patients, depending on the cause of CKD and its stages [43]. Also, it is gaining attention that hypertension and CKD in adulthood have childhood antecedents from as early as *in utero* and the perinatal period [31]. The pathophysiological mechanisms of hypertension in CKD involve multiple factors, including reduced nephron mass, increased sodium retention, activation of the RAS, volume overload, endothelial dysfunction, and sympathetic nervous system overactivity (Figure 6).

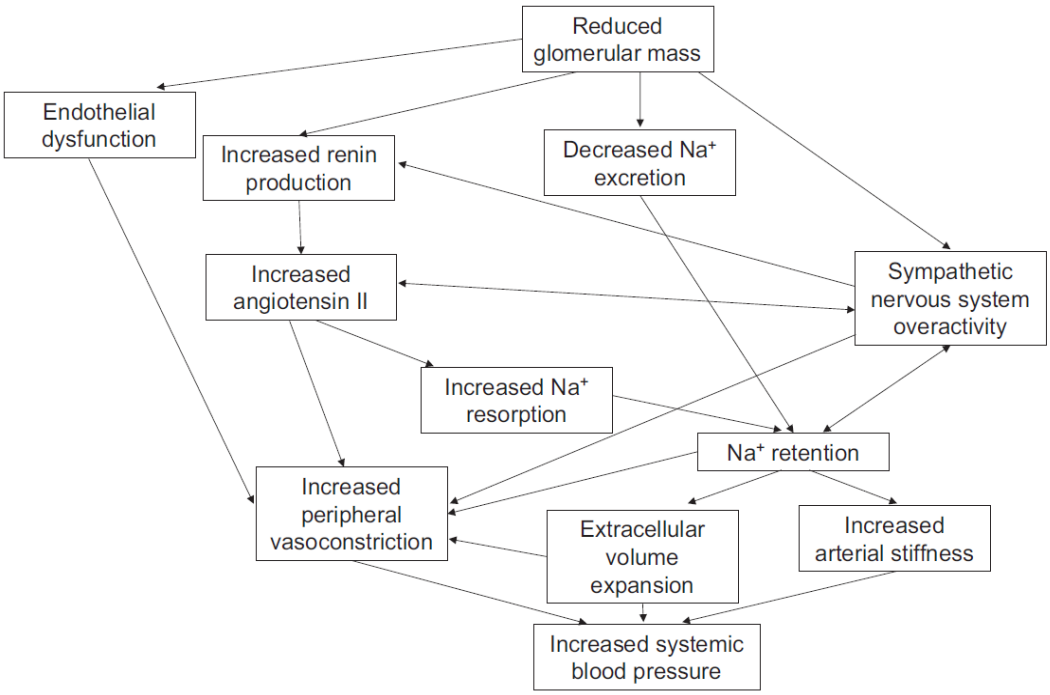

Figure 6. Pathophysiologic mechanisms of hypertension in chronic kidney disease. Adapted from "Hypertension in CKD: Core Curriculum 2019," by E. Ku, 2014, *American Journal of Kidney Diseases, 74(1)*, p. 121, Copyright 2019, with permission from Elsevier. [43]

Sodium homeostasis (i.e., the equivalent of sodium intake by sodium output) plays a pivotal role in extracellular fluid volume homeostasis, which is highly associated with long-term regulation of mean arterial blood pressure. The kidney is a principal organ to excrete sodium from the body, and it plays a central role in maintaining the long-term stability of mean arterial blood pressure. Numerous studies demonstrate that the inability to excrete sodium leads to increased BP in both humans and experimental animals [7]. AT_2R is expressed continuously at a low level in physiological conditions but is upregulated in patients with certain cardiovascular and renal diseases. Accumulating evidences have demonstrated that renal AT_2R plays an essential role in mediating natriuresis. AT_2RKO mice were found to have a hypersensitive anti-natriuretic effect to exogenous Ang II and an abnormal pressure-natriuretic response, suggesting that the natriuretic action of AT_2R is to maintain sodium homeostasis and further to regulate BP. It has been demonstrated that a highly selective

nonpeptide AT_2R agonist, Compound 21 (C21), can markedly promote natriuresis by approximately 10-fold in Sprague-Dawley rats [44]. Besides, renal interstitial infusion of Ang III, an endogenous AT_2R agonist, significantly increases AT_2R-mediated natriuresis, which is abolished in the presence of an AT_2R antagonist, PD123319 [45]. AT_2R-mediated natriuresis is dependent on the bradykinin–NO–cGMP signaling pathway, which can internalize and inactivate major proximal tubule sodium transporters: sodium-hydrogen exchanger-3 (NHE-3) and sodium-potassium adenosine triphosphatase (NKA), therefore decreases sodium reabsorption (Figure 7) [7]. Thus, activation of AT_2R prevents sodium retention and further lowers BP.

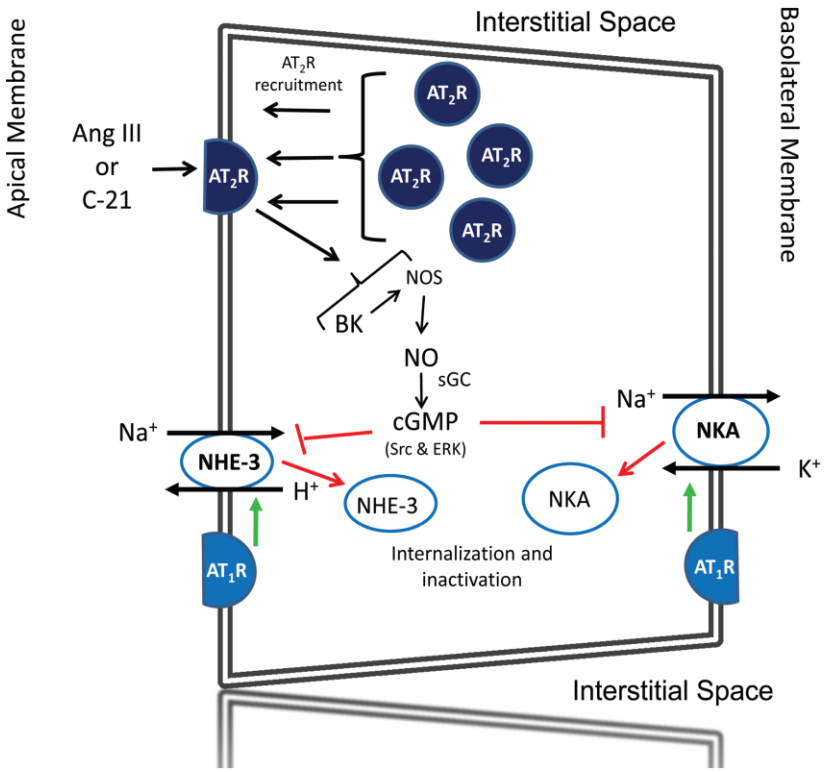

Figure 7. Schematic depiction of a renal proximal tubule cell showing the principal Na^+ transporters and angiotensin receptors that regulate them. AT_1Rs are depicted in light blue and AT_2Rs in dark blue. Green arrows depict stimulation; red arrows depict internalization and inactivation; red lines depict inhibition. AT_2R activation by endogenous agonist Ang III or exogenous nonpeptide agonist C-21 stimulates AT_2R recruitment from intracellular sites to the apical plasma membranes of renal proximal tubule cells, reinforcing, and sustaining the natriuretic response. AT_2R activation via

bradykinin (BK)–NO–cGMP signaling pathway internalizes and inactivates major Na^+ transporter molecules NHE-3 and NKA, counterbalancing AT_1R actions to increase Na^+ reabsorption by stimulating these transporters. Adapted from "AT_2 Receptors: Potential Therapeutic Targets for Hypertension," by R.M. Carey, 2017, *American Journal of Hypertension, 30(4)*, p. 342, Copyright 2016, with permission from Oxford University Press. [7]

AT_2R-mediated vasodilatory responses oppose the vasoconstrictive effects of Ang II via the AT_1R. AT_2RKO mice exhibit higher basal BP than wild-type mice and have increased sensitivity to exogenous Ang II. However, these hemodynamic responses to Ang II are significantly blunted in mice over-expressing AT_2R selectively in vascular smooth muscle cells [30]. Similar to the signaling of the kidney, AT_2R-mediated vasodilation in the vasculature is also dependent on the bradykinin–NO–cGMP signaling pathway. Numerous studies have demonstrated that AT_1R blockade (ARB) is essential to AT_2R-mediated vasodilatory responses in both animal models and human arterioles [5]. For example, Bosnyak et al. [46] reported that a selective AT_2R agonist (C21) alone did not lower BP in conscious experimental animals. However, when given in combination with ARB, C21 lowered BP, and this effect was abolished with the AT_2R antagonist, PD123319. Thus, AT_2R-mediated antihypertensive responses can be revealed by ARB. Nonetheless, the antihypertensive responses mediated by AT_2R appear to be dependent on its expression level in the vasculature, the condition of activation of the RAS, and the presence or absence of ARB.

Fibrosis occurs with all forms of kidney diseases and it accelerates kidney failure. It is a persistent repair response of the normal wound healing process characterized by injury, inflammation, myofibroblast activation, as well as extracellular matrix deposition and remodeling. AT_2R has been shown to have a renal protective ability by preventing fibrosis. It appears that AT_2R deficiency aggravates kidney injury and decreases survival in mice with CKD [47]. Over-expression of the AT_2R in a mouse remnant kidney model ((5/6) nephrectomy) ameliorates glomerular injury via decreased pro-fibrotic cytokines [48]. Thus, AT_2R might be utilized as a therapeutic target to maintain cardiovascular and renal homeostasis in pathological conditions. The potential anti-fibrotic mechanisms of AT_2R are likely to be associated with the reduction of inflammation and pro-fibrotic factors such as

transforming growth factor-β (TGFβ). A selective non-peptide AT_2R agonist, C21, provides the opportunity for the understanding of AT_2R function. It has been shown that C21 could exert an anti-inflammatory effect via inhibited NF-κB activation leading to reduced inflammatory cytokines and chemokines in a variety of animal models [49]. In addition, C21-mediated AT_2R activation has been shown to increase NO and cGMP levels in the kidney and further to inhibit TGFβ signaling which in turn ameliorates TGFβ-mediated myofibroblast activation and extracellular matrix deposition, thereby providing another mechanism to modify fibrosis production [49]. It is reported that the AT_2R may form heterodimers with other GPCR such as relaxin family peptide receptor 1 (RXFP1) to regulate fibrosis progression via the pERK1/2–NOS–NO–cGMP pathway [50].

1.1.3. Glomerulogenesis and Podocyte

1.1.3.1 Kidney and Glomerulus

The kidney is an essential excretory and homeostatic organ. It possesses two primary functions: it excretes various metabolic end products, removing them from the blood and excreting them in urine; and it concentrates certain constituents of the body's fluids to regulate acid-base balance, extracellular fluid volume, and electrolyte concentrations by controlling their excretion and reabsorption. A nephron is the smallest functional unit of the kidney and consists of a renal corpuscle and a tubule unit including proximal tubule, loop of Henle, distal tubule, and collecting duct. The renal capsule, as the beginning of nephron, consists of glomerulus and Bowman's capsule. Each component of the kidney plays distinct and pivotal roles in urine formation as well as in the homeostasis of extracellular fluid.

The glomerulus is an essential functional unit for kidney filtration and a specialized network of capillaries known as a tuft that is practically located between two resistance vessels (i.e., the afferent and efferent arterioles). These capillaries are surrounded by Bowman's capsule and structurally supported by the glomerular mesangial cells. The filter itself has a unique and complex structure and is composed of a multi-layered and multi-cellular barrier, including the fenestrated endothelium of glomerular capillaries, the glomerular basement membrane (GBM), and the filtration slit diaphragm which is connecting adjacent podocyte foot processes (Figure 8). Thus, the primary glomerular filtrate goes through this unique

structure and enters a space defined by the visceral and parietal epithelial cells before flowing into the proximal tubule. Failure in any components of this unique structure causes the loss of size- and charge-selective filtration, clinically characterized by proteinuria [40]. The unique and complex structure of the glomerulus is derived from the metanephric mesenchyme and is based on a tightly regulated developmental program by the processes of glomerulogenesis.

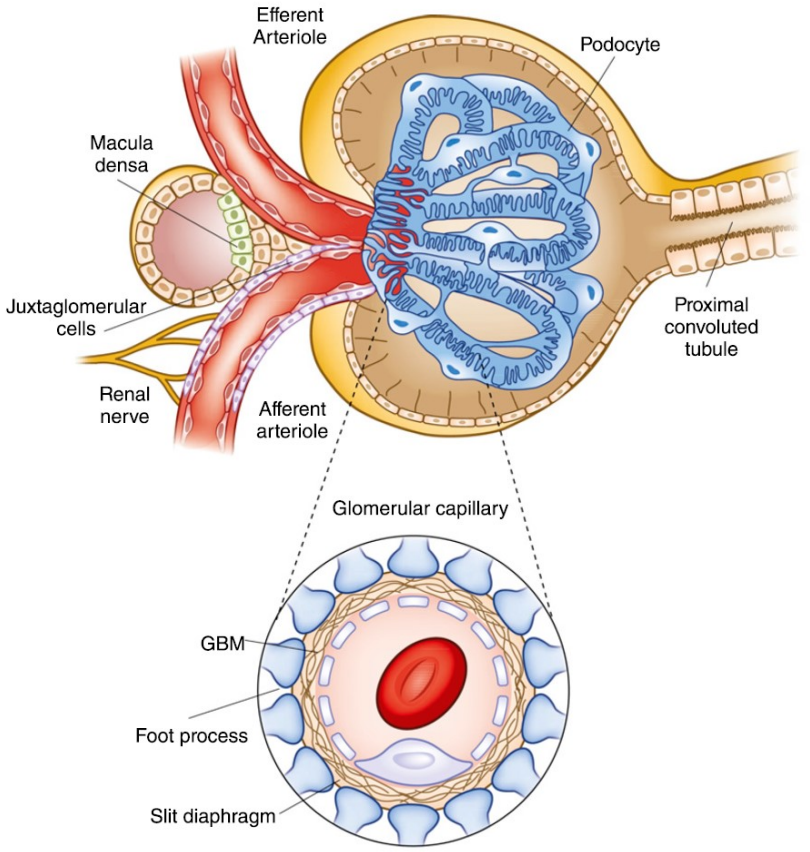

Figure 8. Structure of the Bowman's capsule and glomerular capillary tuft. The capsule is lined with parietal epithelium, which is connected to the cells of the proximal tubule at the urinary pole, which is the right part of the upper picture. Left part of the upper picture is called vascular pole and this includes both the afferent and efferent arterioles. The relationship between these arterioles and the specialized portion of the distal nephron called the macula densa is illustrated. (Inset) The layers that comprise the filtration barrier are displayed below. The outermost layer is composed of the visceral epithelial cells, the podocytes, next to the glomerular basement membrane (GBM) and finally, the fenestrated endothelial cells. Adapted from "The glomerulus: the sphere of influence,"

by M.R. Pollak, 2014, *Clinical journal of the American Society of Nephrology: CJASN, 9(8)*, p. 1462, Copyright 2014, with permission from American Society of Nephrology. [51]

1.1.3.2 Glomerulogenesis

The permanent mammalian kidney (metanephros) stems from metanephric mesenchyme and starts to develop by UB outgrowth (Figure 5) [38, 40]. Kidney development is governed by a cascade of morphogenetic interactions among three cell lineages of different origins: the epithelial cells of the UB, the mesenchymal cells of the metanephric mesenchyme and the endothelial cells of the angioblasts. The development of the embryonic metanephros consists of two different processes: glomerulogenesis and tubulogenesis. Glomerulogenesis proceeds through five morphological stages in embryonic development: renal vesicle, comma-shaped body, S-shaped body, capillary loop, and maturing glomerulus [40]. Glomerulogenesis is divided into two steps, before and after endothelial cell invasion (Figure 9) [52]. In the beginning, mesenchymal cells adjacent and inferior to the tips of UB start to condense, and this group of cells forms a pretubular aggregate. In response to signaling from the UB and surrounding stroma, the pretubular aggregate conducts a mesenchymal–to–epithelial transition forming a polarized renal vesicle [53], which then becomes a comma-shaped body composed of parietal cells and presumptive podocytes. At the same time, the UB continues to branch and induce new aggregates at the bud tips. The polarized renal vesicles remain attached and fuse to the ureteric bud epithelium at their distal part. The renal vesicles elongate along the proximal-distal axis and differentiate into nephron segments in which podocytes are located at the proximal end of the nephron epithelia. This proximal-distal polarity is related to the different gene expression levels [54]. For example, the proximal end of renal vesicle begins to express podocyte-related genes, such as *Wt1*and *MafB*, indicating the possibility that the cells within the proximal part have already been directed toward the podocyte lineage [54].

The functional glomerulus formation initiates at endothelial cells invasion into the vascular cleft observed in the S-shaped body. The S-shaped body is characterized by the presence of a layer of presumptive podocytes and a vascular cleft. At this stage, the S-shaped body is already patterned along the proximal-distal axis [38]. The distal end that had remained

in connect to the ureteric bud epithelium has now fused to form a continuous epithelial tubule. The proximal end assembles the glomerular tuft when endothelial cells migrate to the more proximal cleft. At this stage, the gradient of Wnt/β-catenin activity is generated along the proximal-distal nephron axis, and the proximal end of the S-shaped body, which contains presumptive podocytes, expresses the lowest β-catenin level, suggesting that Wnt signaling might regulate the development of podocytes [55]. The migration of endothelial cells into the vascular cleft depends on the signaling of angiogenic factors such as vascular endothelial growth factor (VEGF), which is produced by presumptive podocytes [52]. Then, endothelial cells proliferate and aggregate to form the first capillary loop without a lumen. It has been demonstrated that TGFβ signaling is associated with the process of lumenation [52]. After the initial migration of endothelial cells, mesangial cells migrate into the glomerulus around the first capillary loop and play a pivotal role in the formation of multiple capillary loops. In the mature glomerulus, the first capillary loop divides into six to eight capillary loops, and endothelial cells acquire a fenestrated morphology. Finally, the fully matured glomerulus includes four highly specified cell populations: the fenestrated endothelial cells, mesangial cells, podocytes, and the parietal epithelial cells of the Bowman's capsule.

In the stages of comma-shaped body and S-shaped body, presumptive podocytes display a layer of columnar-shaped epithelial cells connected by apical junctions, having no foot processes and slit diaphragm, but produce VEGF to attract vascular endothelial growth factor receptor 2 (VEGFR2)-expressing angioblasts [52]. In the subsequent capillary loop stage, podocytes lose their lateral cell attachments to each other, but they remain attached at their basal membrane. At this stage, podocytes begin to form foot processes and slit diaphragm along the basal aspect of the lateral membrane, migrate around the capillary loops, and stop dividing by increasing the cyclin-dependent kinase inhibitors, p27 and p57 [56]. During podocyte development, podocytes gradually increase in size and extend their foot processes to a significant distance from the main cell body as well as exert normal physiological functions.

The mammalian kidney develops by the cells derived from three fundamental lineages: the UB lineage, the nephron lineage, and the stromal lineage. The metanephric mesenchyme consists of nephron progenitor cells (NPCs) and stromal progenitors. NPCs are characterized by expression of *Six2* and differentiate into the entire nephron epithelium, including podocytes,

glomerular parietal epithelial cells, proximal tubule epithelial cells, loop of Henle, and distal tubule epithelial cells [57]. The stromal progenitors express *Foxd1* and differentiate into interstitial fibroblasts, pericytes, mesangial cells and vascular smooth muscle [58]. The kidney vasculature derives from c-kit^{+}/SCL^{+} and CD146^{+} endothelial progenitors [58-60]. The cell-cell interactions among those cells are essential to the growth and continued patterning of the kidney. The Wilms' tumor 1 (WT1) transcription factor is a potent regulator of NPCs in the development of kidney and involved in many genes with essential roles in kidney development [40]. The other transcription factors, including PAX2, SALL1, EYA1, and OSR1also play an important role in kidney development [40, 58].

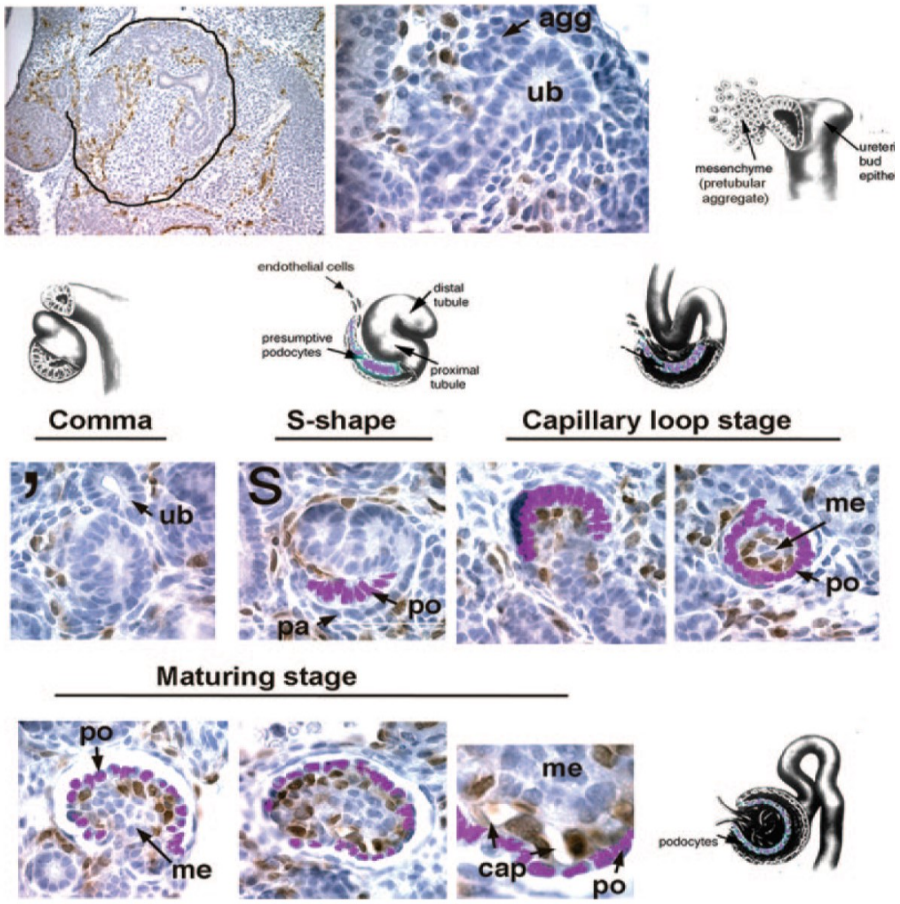

Figure 9. Migration of endothelial cells into the developing glomerular tuft. (Top) An E12.5 mouse metanephros is outlined in black. Endothelial cells express a VEGFR2-GFP transgene and stain brown. The glomerulus develops from a pretubular aggregate (agg) that forms immediately adjacent and below the tips of the ureteric buds (ub). (Middle and

Bottom) VEGFR2-positive cells are seen to "hug" the developing comma-shaped-stage nephron. The S-shaped stage is defined by the presence of a layer of presumptive podocytes (po) and a vascular cleft. Endothelial cells seem to be streaming into this cleft from the metanephric mesenchyme (MM). At the capillary loop stage, pockets of endothelial cells sit right next to the podocytes, and mesangial cells are soon found inside a single capillary loop. By the maturing stage, capillary lumens are beginning to form, and a large population of mesangial cells is present. Schematic diagrams of each developmental stage are shown above the photomicrographs. Podocytes have been digitally colorized for identification (purple). Abbreviation: pa, parietal epithelial cell; po, podocyte; me, mesangial cell; cap, capillary loop. Adapted from "How do mesangial and endothelial cells form the glomerular tuft?" by M.R. Vaughan, 2008, *Journal of the American Society of Nephrology: JASN, 19(1)*, p. 25, Copyright 2008, with permission from American Society of Nephrology. [52]

1.1.3.3 Podocyte

Podocyte is particularly specialized epithelial cell that resides on the visceral side of the Bowman's capsule, wrap around glomerular capillaries, and serves as an essential component of the glomerular filtration barrier. These cells are thought to be the target cell in most forms of inherited and acquired glomerular disease including minimal change disease (MCD), focal segmental glomerulosclerosis (FSGS), and diffuse mesangial sclerosis. Podocytes are structurally divided into three kinds of subcellular compartment: cell body, primary process, and foot process (Figure 10). The cell body of podocyte has several thick primary processes, and many fine foot processes extending from each of the primary processes. The foot processes interdigitate with adjacent foot processes from neighboring podocytes. They are separated from each other by filtration slits and bridged with a specialized intercellular junction known as the slit diaphragm.

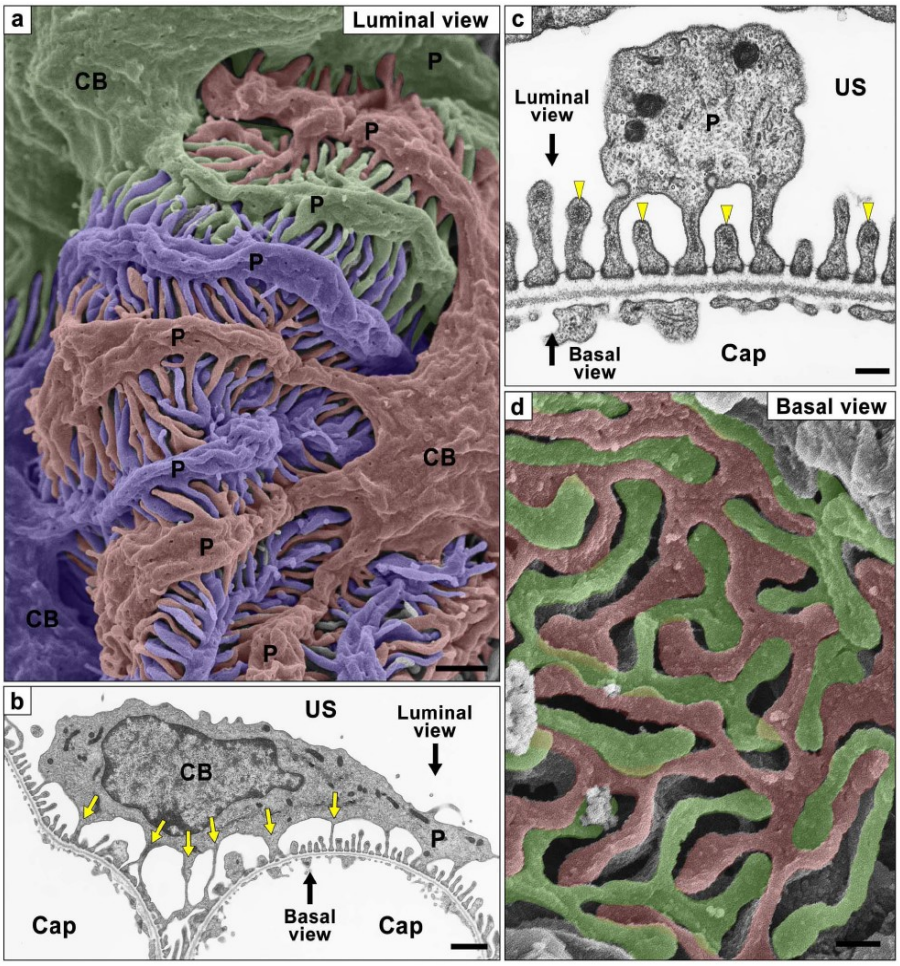

Figure 10. Podocyte subcellular compartments showed by conventional SEM and TEM. (a) Conventional SEM image. Three neighboring podocytes are individually colored with blue, green, and red. (b, c) Conventional TEM images. (d) Alkaline-maceration SEM image. CB, cell body; Cap, capillary lumen; P, primary process; US, urinary space of the Bowman's capsule. Adapted from "Three-dimensional architecture of podocytes revealed by block-face scanning electron microscopy," by K. Ichimura, 2015, *Scientific reports, 5:8993*, p. 2. [61]

The glomerular filtration barrier comprises three layers: glomerular endothelial cell, GBM, and epithelial podocyte. It is widely accepted that damage to any layer might result in leakage of macromolecules passing through the glomerular filtration barrier and ending up in the urine. The slit diaphragm plays a pivotal role as a size barrier for filtration. It is composed of nephrin, podocin, CD2AP (CD2-associated protein), TRPC6 (transient receptor potential

channel 6), ZO-1 (zonula occludens-1), α- and β-catenin, P-cadherin, FAT1 (Fat cadherin 1) and NEPH1 (nephrin-like protein 1) [62]. Podocytes synthesize all of these components and form an extremely specialized adherent junction between adjacent foot processes to establish the molecular sieve known as the slit diaphragm. The podocyte cytoskeleton connects to the extracellular matrix through focal adhesions at the interface with GBM.

The GBM is generated by podocytes and glomerular endothelial cells and composed mainly of laminins and collagen IV [63]. Besides, the GBM is not only a size barrier but also a charge barrier, in cooperation with the glomerular endothelial glycocalyx. The podocyte cytoskeleton not only maintains podocytes physiological functions and morphology but can arrange in response to environmental variations to maintain glomerular filtration barrier integrity. Both the slit diaphragm and podocyte focal adhesions are mainly signaling networks that connect to the podocyte cytoskeleton, maintain a balance between intracellular and extracellular signals, and regulate podocyte function and morphology. The actin cytoskeleton plays an important role in these functions and specialized morphology. Synaptopodin is an actin-associated protein found in renal podocytes and in a restricted population of cells with high synaptic plasticity in the nervous system [64]. This protein plays a role in modulating actin-based shape and motility of renal podocyte foot processes through the regulation of α–actinin–4 activity and the involvement of Rho guanosine triphosphatases (GTPases) [63]. Injury of any filtration components might cause glomerular diseases characterized by glomerular basement abnormalities, podocyte foot process effacement, and proteinuria. The glomerular filtration barrier and its key molecular elements are schematically summarized in Figure 11 [62].

In addition to the podocyte cytoskeleton, the podocyte's cell body contains a nucleus, endoplasmic reticulum, Golgi apparatus, lysosomes, mitochondria, and other organelles. The regulation of podocytes energetics also plays a pivotal role in maintaining podocytes physiological functions and morphology. Numerous studies demonstrated that gene mutation, chemical agents, and environmental changes in podocyte energy metabolism might cause the podocyte injury associated with many glomerular diseases [65]. Therefore, the tight control of podocyte energy metabolism appears to be a new therapeutic strategy for glomerular diseases and recovering podocyte injury.

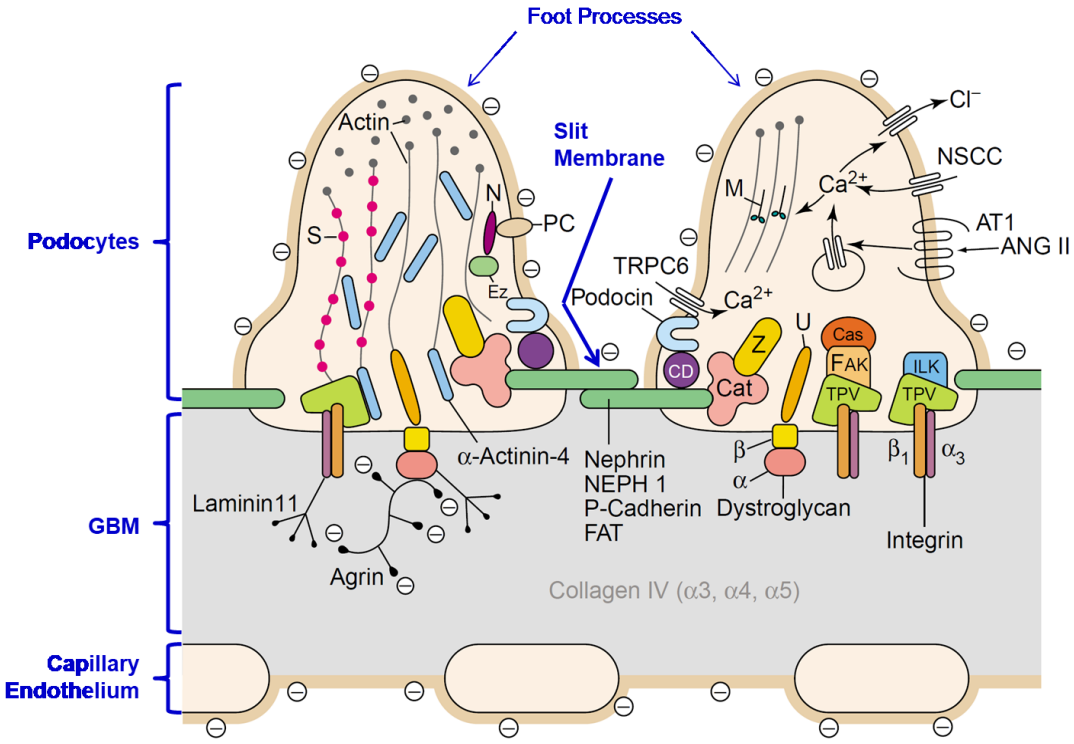

Figure 11. The glomerular filtration barrier and its key molecular components. Two podocyte foot processes bridged by the slit membrane, the glomerular basement membrane (GBM) and the porous capillary endothelium are shown. The surfaces of the podocytes and the endothelium are covered with a negatively charged glycocalyx containing the sialoprotein podocalyxin (PC). The GBM is composed mainly of collagen IV (α3, α4, and α5), laminin 11 (α5, β2, and γ1 chains) and the heparan sulfate proteoglycan agrin. The slit membrane is a porous proteinaceous membrane composed of nephrin, NEPH1, 2 and 3, P-cadherin and FAT1. β1α3 integrin dimers specifically connect the TPV complex (talin, paxillin, and vinculin) to laminin 11; the α and β dystroglycans connect utrophin (U) to agrin. The slit membrane proteins are joined to the cytoskeleton by various adaptor proteins, including podocin, zonula occludens protein 1 (ZO-1; Z), CD2-associated protein (CD) and catenins (Cat). TRPC6 associates with podocin (and nephrin; not shown) at the slit membrane. Among the many surface receptors, only the angiotensin II (ANG II) type 1 receptor (AT_1) is shown. Additional abbreviations: Cas, p130Cas; Ez, ezrin; FAK, focal adhesion kinase; ILK, integrin-linked kinase; M, myosin; N, NHERF2 (Na^+–H^+ exchanger regulatory factor); NSCC, non-

selective cation channel; S, synaptopodin. Modified from "TRPC6 - a new podocyte gene involved in focal segmental glomerulosclerosis," by W. Kriz, 2005, *Trends in Molecular Medicine, 11(12)*, p. 528, Copyright 2005 with permission from Elsevier. [62]

1.1.4 Hedgehog interacting protein (Hhip)

The hedgehog (Hh) proteins are highly conserved proteins, which are critical morphogens for a wide range of developmental processes in embryonic development and that play a pivotal role in tissue homeostasis [66]. Hedgehog-interacting protein (Hhip) is a membrane-bound glycoprotein and an evolutionarily conserved, vertebrate-specific antagonist of Hh signaling [67]. It has high affinity with all three Hh ligands, including Sonic hedgehog (Shh), Indian hedgehog (Ihh), and Desert hedgehog (Dhh) [68]. Hh ligands are lipid-modified proteins that can exert their biological activity via both an autocrine and paracrine manner [69]. In the mammalian developing kidney, only Shh and Ihh expression are detectable [68]. Hh signaling pathway begins with Hh ligands binding to their transmembrane protein receptor Patched1 (Ptch1), which inhibits the repression of Smoothened (Smo) and results in Smo activation to initiate the signal. In the absence of Hh ligands, Ptch1 constitutively represses Hh signaling via the repression of Smo, which is a member of the GPCR superfamily and the switch in this pathway. The derepression of Smo results in the activation of the Glioma-associated oncogenes (Gli) family, leading to the translocation of the Gli transcription factors to the nucleus. The Gli proteins are bi-functional transcription factors that can both activate or inhibit transcription. The balance between the activator and repressor forms of Gli proteins has a key role in the Hh signaling cascade. Gli1 lacks a transcriptional repressor domain and seems to have only a minor role in amplifying the transcriptional response in mammals. Both Gli2 and Gli3 have the transcriptional activation and repressor domains, which are regulated by post-translational proteolytic processing to exert their activator or repressor forms. Mouse mutant studies have reported that Gli2 is mainly in control of the activator function in response to Hh signaling, and Gli3 is in control of the repressor activity [70]. Activated Gli proteins translocate to the nucleus and then control the transcription of target genes. Therefore, the major determining factor of cellular response to Hh ligands is the balance of intracellular Gli activator and repressor.

It has been demonstrated that the Gli proteins control the expression of three classes of genes critical to normal murine renal development, including renal patterning genes (*Pax-2, Sall1*), cell cycle modulators (*Cyclin D1, N-Myc*), as well as Gli family members themselves (*Gli1, Gli2*) [71]. Both paired box 2 *(Pax-2)* and spalt like transcription factor 1(*Sall1*) are transcription factors and play a vital role in murine renal organogenesis. *PAX-2* mutation is associated with renal coloboma syndrome and renal hypoplasia. Mouse mutant studies result in renal aplasia or severe dysgenesis, suggesting that a requirement for Pax-2 for controlling cell proliferation and differentiation and mediating mesenchymal-to-epithelial conversion during outgrowth of the ureteric bud and invasion of the metanephric mesenchyme [72]. Neuroblastoma derived Myc oncogene (*N-Myc*) plays a pivotal role in renal morphogenesis via its effects on cell proliferation and differentiation. In murine, *N-myc* mutation results in fetal death and the hypomorphic *N-myc* mutation studies result in renal hypoplasia with fewer developing glomeruli and collecting ducts, indicating that the renal hypoplasia is due to a decrease in proliferation rather than an increase in apoptosis [73]. Thus, the Gli proteins via the regulation of these genes have a key role in kidney development.

The Hh signaling pathway has a vital role in cell proliferation, differentiation, tissue patterning, and organogenesis during mammalian embryonic development. Aberrant Hh signaling during embryogenesis has been reported in various congenital abnormalities such as renal malformations [68]. For example, in human patients with Pallister-Hall syndrome (PHS), frameshift mutations have been founded in the *GLI3* gene, which express a truncated protein with similarities to the GLI3 repressor [68]. PHS is a rare autosomal dominant disorder characterized by a variable range of anomalies, including hypothalamic hamartoma, pituitary dysfunction, polydactyly and the features of CAKUT (i.e. hydronephrosis, renal hypoplasia, and renal agenesis or dysplasia). The genetic mutation in *SHH* and *GLI2* are also associated with human renal malformations [68, 74]. Dysregulation of Hh signaling may relate to the pathogenesis of ureteropelvic junction obstruction (i.e. a kind of CAKUT) which was demonstrated by the increased expression of Hh-related genes, such as *GLI1* and *HHIP* or the decreased expression of *GLI3* [68]. All these genetic studies indicate that the Hh signaling pathway has an important role in kidney development.

The Hhip is a regulatory component in the vertebrate Hh signaling pathway. It binds all three Hh ligands as a structural decoy receptor with an affinity similar to that of the Ptch1, and its expression is upregulated in response to Hh signaling. Hhip overexpression in murine chondrocytes leads to severe skeletal defects similar to those observed in Ihh mutants, indicating that Hhip is involved in the attenuation of Hh signaling [67]. In murine, Hhip mutation results in both lung and pancreas malformations [75]. Aberrant *HHIP* gene expression is related to several human diseases, such as chronic obstructive pulmonary disease [76], chronic pancreatitis [77], and a variety of tumors [77, 78]. These findings highlight the possibility that aberrant Hhip expression may contribute to the dysregulation of the Hh signaling pathway within embryonic development and the pathogenesis of the different diseases.

Hhip is abundantly expressed in endothelial cells [78], and Hhip-expressing cells are adjacent to the cells that express Shh [67]. Numerous studies demonstrated that Shh is associated with kidney development and tissue repair after various injuries [69]. In the mammalian kidney, Shh, expressed in the distal ureter epithelium and medullary collecting ducts, establishes a gradient of distal high and proximal low levels of Hh signal and controls early morphogenetic events, including ureteric bud growth and metanephric induction. Mutations in the Shh signaling pathway and interruption of the Shh gradient have been linked to renal anomalies such as bilateral renal hypoplasia or a single renal dysplasia [79]. In the embryonic kidney, Hhip is mostly expressed in the differentiated metanephric mesenchyme and UB epithelium, where it might play a role in kidney development via delaying or disorienting the Shh gradient and altering the Shh signaling pathway [80]. In the adult kidney, the interruption of the Shh gradient has been shown to result in fibroblast activation, proliferation and matrix overproduction, ultimately leading to increased kidney fibrosis and aggravated kidney dysfunction [69]. These findings highlight the possibility that Hhip might play a role in the development of renal fibrosis, mostly through the regulation of the Shh gradient. After birth, detection of Hh and its associated genes in healthy human and mouse kidneys is difficult due to their low level of expression. The level of Hhip expression is only a limited amount, and it can be detected at a low level in the mature glomerular endothelial cells, podocytes, and tubulointerstitial cells [80]. Zhao et al. recently reported that Hhip expression

is increased in glomerular endothelial cells in both Type 1 and Type 2 diabetic mice and diabetic heterozygous ($Hhip^{+/-}$) mice showed attenuated features of diabetic glomerular injury [81]. In addition, urinary Hhip is elevated in diabetic kidney disease before the development of microalbuminuria in mice and humans [82]. Thus, abnormal Hhip expression might impact kidney development, the onset of glomerular diseases, and the progress of kidney diseases.

1.1.5 Reactive oxygen species (ROS)

Reactive oxygen species (ROS) have both harmful and beneficial effects according to their concentrations and different environments. ROS were initially known for their detrimental effects on cells and invading microorganisms, whereas they also can serve as specific secondary messengers in various signaling pathways involved in cellular proliferation, differentiation, apoptosis, damage, and inflammation. ROS contain free radicals such as superoxide ($\bullet O_2^-$) and hydroxyl ($\bullet OH$), and non-radical species such as hydrogen peroxide (H_2O_2), singlet oxygen ($^1O_2$), ozone (O_3), hypohalous acids, and organic peroxides. There are numerous intracellular sources of ROS and anti-oxidative defense (Figure 12) [83]. When the production of ROS exceeds the capacity of the intracellular anti-oxidative defense, oxidative stress and oxidant-derived tissue injury occur. As a result, specific macromolecules (proteins, lipids, carbohydrates, and DNA) are oxidized, leading to structural and functional modifications of these macromolecules. Mitochondria are the most significant contributors to intracellular oxidant production. In addition to mitochondria, the primary sources of ROS involved in receptor-mediated signaling pathways are plasma membrane oxidases, especially NADPH oxidases. Numerous studies have indicated that ROS constitute physiologically necessary molecules for organogenesis and pathologically contribute to the progression of various harmful consequences such as inflammation and fibrosis [84].

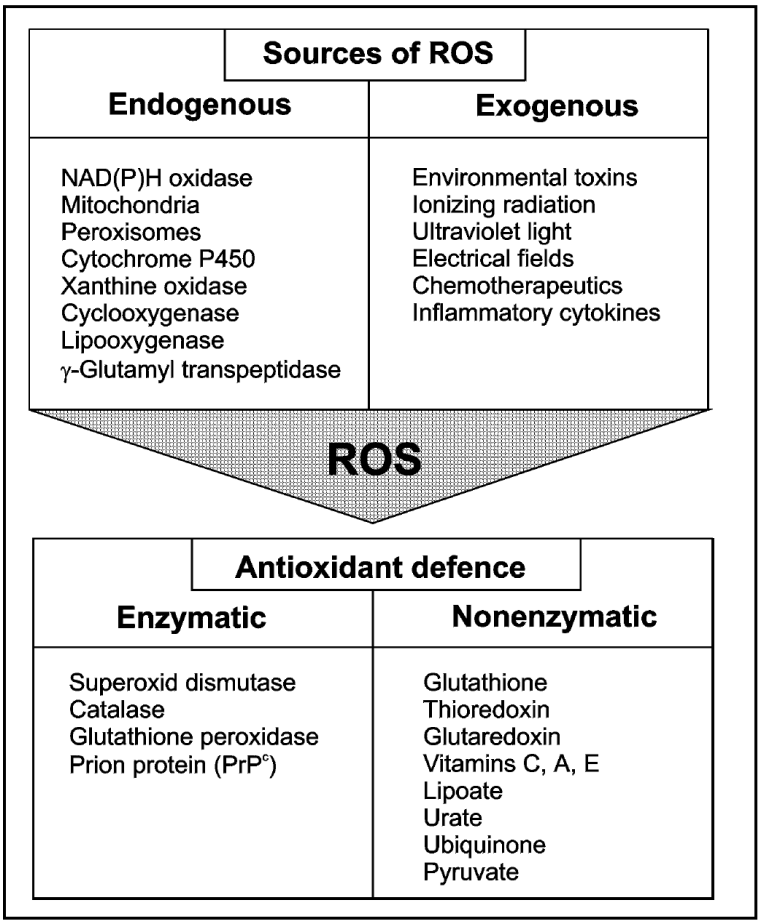

Figure 12. Sources of ROS and the intracellular anti-oxidative defense. ROS are endogenously generated inside cells by a variety of enzymes and through the mitochondrial respiratory chain. Furthermore, intracellular ROS levels can be increased through several exogenous agents. The levels of intracellular ROS are balanced by the intracellular anti-oxidative defense, which consists of enzymatic and non-enzymatic components. Adapted from "Reactive oxygen species as intracellular messengers during cell growth and differentiation," by H. Sauer, 2001, *Cellular Physiology and Biochemistry, 11(4)*, p. 174, Copyright 2001 with permission from Karger Publishers, Basel, Switzerland. [83]

There is a small concentration threshold that governs whether ROS induce the development and progression of kidney diseases or act as second messengers involved in cellular homeostasis and kidney development. Ang II, which produces both $\bullet O_2^-$ and H_2O_2, has been demonstrated to increase ROS generation in vascular smooth muscle cells,

endothelial cells, renal proximal tubule cells, and glomerular mesangial cells via active NADPH oxidase [85]. NADPH oxidase, which is a cytosolic enzyme complex, consists of a membrane-associated $p22^{phox}$ and $gp91^{phox}$ subunit and four cytosolic subunits: $p47^{phox}$, $p67^{phox}$, $p40^{phox}$, and GTPase rac1 or rac2. In humans, there are seven NADPH oxidase isoforms: Nox1, Nox2 ($gp91^{phox}$), Nox3, Nox4, Nox5, and dual oxidases (Duox1, Duox2). Among them, Nox1, Nox2 and Nox4 are expressed in the kidney and have been identified as primary sources of ROS in renal cells, such as epithelial cells, podocytes, mesangial cells, endothelial cells, and fibroblasts [86].

Nox4 is abundantly expressed in the kidney and is the leading source of renal ROS. It has been characterized in the renal pathophysiology of diabetic nephropathy, hypertensive nephropathy, acute kidney injury, and other kidney diseases. In mouse models of Type 1 and Type 2 diabetes, Nox4 expression is significantly increased in the kidney. Also, high glucose increases Nox4 expression in tubular epithelial cells, mesangial cells, and podocytes via activation of several signaling pathways such as TGFβ1/Smad2/3 in podocytes, and PI3 kinase/Akt/PKC in mesangial cells [86]. Thus, NADPH oxidase plays a role as a potential pathogenic mediator of ROS generation. Previous studies conducted by Kondo et al. [87] have demonstrated that ROS produced by NADPH oxidase play a pivotal role in UB branching and kidney development by regulating proliferation and apoptosis. In general, these studies suggest that NADPH oxidase-dependent ROS might not only play roles in kidney damage at the cellular and tissue level but also contribute to physiological processes of kidney development in a precisely controlled manner.

1.1.6 Objectives

CAKUT account for the largest classification of CKD and ESRD in children and include renal hypoplasia/dysplasia and renal pelvis/ureteral abnormalities [31]. Although monogenic causes of CAKUT have been demonstrated, the identified mutations lack substantial evidence to support a pathogenic role in CAKUT. AT_2RKO mice have been found to have anatomical abnormalities, which are similar to human CAKUT. Additionally, both Pax-2 and N-myc play essential roles in renal morphogenesis via their effects on cell proliferation and differentiation [72, 73]. Previously, our lab has reported that AT_2R

deficiency impairs kidney development, leading to renal hypoplasia (reduced kidney and glomerular size with lower glomerular tuft volume) by down-regulation of Pax-2 and N-myc which are essential to UB branching and mesenchymal–to–epithelial transition in kidney development [88]. However, the association between glomerular size and numbers/sizes of glomerular resident cells in AT_2RKO mice is incompletely delineated.

CKD affects 10–15% of the adult population worldwide [42]. Glomerular diseases account for 90% of CKD. The most significant feature of glomerular diseases is podocyte injury, dysfunction and loss. Furthermore, podocytes play an essential role to attract endothelial cells migration in glomerulogenesis. Although AT_2RKO mice exhibit a spectrum of CAKUT with a >23% penetrance by interbreeding alone, lack of AT_2R might influence on podocytes maturation, integrity and function without apparent renal abnormalities in childhood and have higher possibilities to develop kidney diseases such as glomerular diseases and CKD in adulthood. Hence, our overall goal in the present study was to further delineate the regulation and function of AT_2R in both kidney development and later, with the onset of kidney injury in adulthood, with a particular focus on podocytes. The first aim was to investigate whether AT_2R deficiency impairs glomerulogenesis via mediated podocytes formation, maturation and integrity.

It has been reported that infants exposed early to diabetes mellitus had increased risks of CAKUT, suggesting that a hyperglycemic intrauterine environment might impair human fetal kidney development [35]. Rodents maternal diabetes induced by streptozotocin (STZ) also supports the effect of gestational diabetes on CAKUT risk, as exposure to hyperglycemia *in utero* might result in reduced nephron endowment, such as renal dysplasia (a small kidney with abnormal internal structures) and renal hypoplasia (a kidney with abnormal structures and the different degree of reduction in the number of nephrons) [35]. Previous studies demonstrated that high glucose specifically stimulates Pax-2 expression in mouse embryonic metanephric mesenchymal cells (MK4 cells) and embryonic kidney explants via ROS generation and activation of the NF-κB signaling pathway [89]. Also, high glucose alters UB branching in kidney development via increased ROS generation derived from the activation of NADPH oxidases and upregulation of Pax-2 expression [90]. Thereafter, we found that neonatal offspring from maternal diabetic mice had smaller kidneys with smaller glomeruli

size as compared with the kidneys of control offspring and this phenotype was due to inducing nascent nephron cell apoptosis via enhanced intrarenal RAS activation and NF-κB signaling [91]. Furthermore, the upregulation of Hhip is associated with maternal diabetes and further impairs kidney development [80]. Overall, these findings indicate that the hyperglycemic milieu *in utero* impairs kidney development with renal hypoplasia features in the offspring. This renal hypoplasia phenotype (i.e. small kidney and small glomeruli with lower glomerular tuft volume) accompanied by augmented Hhip expression also displays in AT_2RKO mice, suggesting that AT_2R may directly or indirectly be associated with Hhip expression. Taken together, we hypothesized that lack of AT_2R alters podocyte biology via the upregulation of Hhip expression.

1.2 Article 1

- **AT_2R deficiency mediated podocyte loss via activation of ectopic hedgehog interacting protein (Hhip) gene expression**
- **The Journal of Pathology, 2017; 243 (3): 279-293**
- **Min-Chun Liao[1]**, Xin-Ping Zhao[1], Shiao-Ying Chang[1], Chao-Sheng Lo[1], Isabelle Chenier[1], Tomoko Takano[2], Julie R. Ingelfinger[3] and Shao-Ling Zhang[1]*

  [1]Université de Montréal, Centre de Recherche du Centre Hospitalier de l'Université de Montréal (CRCHUM), Tour Viger, Montréal, Québec, Canada

  [2]McGill University Health Centre, Montréal, Québec, Canada

  [3]Pediatric Nephrology Unit, Massachusetts General Hospital and Harvard Medical School, Boston, Massachusetts, USA

  *Correspondence to: S-L Zhang, Université de Montréal, Centre de Recherche du Centre Hospitalier de l'Université de Montréal (CRCHUM), Tour Viger, 900 Rue Saint-Denis, Montréal, Québec, H2X 0A9, Canada. E-mail: shao.ling.zhang@umontreal.ca
- **Author Contribution**

SLZ is the guarantor of this work, had full access to all study data, and takes responsibility for data integrity and the accuracy of data analysis. SLZ was principal investigators and was responsible for the study conception and design. SLZ also wrote, reviewed, and edited the manuscript. TT and JRI contributed to discussion and reviewed/edited the manuscript. MCL (Table 4 and Figures 13A~B, 14~30), XPZ (Figures 13D~F, 17C), SYC (Figures 13C~E), CSL (Figure 31), IC (animal management and discussion) and SLZ contributed to the experiments and collection of data. All authors were involved in the analysis and interpretation of data and contributed to the critical revision of the manuscript. MCL contributed to 72.5% of work.

Abstract

Angiotensin II Type 2 receptor (AT_2R) deficiency in AT_2R knockout (KO) mice has been linked to congenital abnormalities of the kidney and urinary tract; however, the mechanisms by which this occurs are poorly understood. In this study, we examined whether AT_2R deficiency impaired glomerulogenesis and mediated podocyte loss/dysfunction *in vivo* and *in vitro*. Nephrin-cyan fluorescent protein (CFP)-transgenic (Tg) and Nephrin/AT_2RKO mice were used to assess glomerulogenesis, while wild-type and AT_2RKO mice were used to evaluate maturation of podocyte morphology/function. Immortalized mouse podocytes (mPODs) were employed for *in vitro* studies. AT_2R deficiency resulted in diminished glomerulogenesis in E15 embryos, but had no impact on actual nephron number in neonates. Pups lacking AT_2R displayed features of renal dysplasia with lower glomerular tuft volume and podocyte numbers. *In vivo* and *in vitro* studies demonstrated that loss of AT_2R was associated with elevated NADPH oxidase 4 levels, which in turn stimulated ectopic hedgehog interacting protein (Hhip) gene expression in podocytes. Consequently, ectopic Hhip expression activation either triggers caspase-3 and p53-related apoptotic processes resulting in podocyte loss, or activates TGFβ1–Smad2/3 cascades and α-SMA expression to transform differentiated podocytes to undifferentiated podocyte-derived fibrotic cells. We analyzed HHIP expression in the kidney disease database (Nephroseq) and then validated this using HHIP immunohistochemistry staining of human kidney biopsies (controls versus focal segmental glomerulosclerosis). In conclusion, loss of AT_2R is associated with podocyte loss/dysfunction and is mediated, at least in part, via augmented ectopic Hhip expression in podocytes.

Keywords: Hhip expression; podocytes and AT_2R deficiency

Introduction

Congenital abnormalities of the kidney and urinary tract (CAKUT) occur in 3–6 per 1000 live births in humans, and are responsible for 34–59% of childhood cases of chronic kidney disease (CKD) and 31% of cases of pediatric end-stage renal disease in the United States (1,2). The term CAKUT covers all nephrogenic defects, ranging from abnormalities in the developmental sequence to gene regulation profiles. The wide range of abnormalities, which include renal parenchymal anomalies (from renal agenesis to renal hypoplasia/dysplasia), collecting system abnormalities (hydronephrosis and megaureter), bladder abnormalities (ureterocele and vesicoureteral reflux), and/or urethral (posterior urethral valves) abnormalities, corresponds to aberrant events at specific stages of development (2,3). Although genetic studies over the last decade have increased our understanding of the genes involved in CAKUT [e.g. angiotensin II (Ang II) type 2 receptor (AT_2R) – AT_2R knockout mice (AT_2RKO) exhibit a spectrum of CAKUT (i.e. renal hypoplasia/dysplasia and renal pelvis/ureteral abnormalities) (2–5)], the underlying mechanisms causing the renal malformations require further elucidation, particularly with respect to the possible molecular and developmental interactions that lead to the abnormalities in a renal cell-specific manner, for example, in the podocyte.

The hedgehog (Hh) pathway is a key signaling pathway for proper vertebrate embryonic development (6-8), as well as for the maintenance and regeneration of various adult tissues (9-11). Hedgehog interacting protein (Hhip) was discovered as a putative antagonist of three Hh ligands, including Sonic hedgehog (Shh), Indian hedgehog (Ihh), and Desert hedgehog (Dhh) (6,12). Acting as a structural decoy receptor, Hhip regulates cell function via either canonical or non-canonical Hh pathways (6,12-18). The importance of Hhip is highlighted by the findings that (i) Hhip overexpression in chondrocytes leads to severe skeletal defects (6,14); (ii) deficient Hhip expression results in lung and pancreas malformations (6,14); and (iii) altered *Hhip* gene expression is linked to several human diseases, such as pancreatitis (19), chronic obstructive pulmonary disease (18,20), and various tumors (21,22).

We recently established the expression pattern of Hhip in both embryonic and mature mouse kidney (23). During kidney development, Hhip is activated and is largely expressed in

differentiated ureteric bud (UB) and metanephric mesenchyme (MM) lineages, where it may participate in nephrogenesis (23). A counterbalance between Hhip and Shh signaling (the most studied Hh ligand in the kidney (7,24)) appears to be important for maintaining a normal Shh gradient [distal (high) to proximal (low)], and interruption of this gradient has been shown to result in renal anomalies such as renal dysplasia/hypoplasia (24) and fibrosis (25,26). After birth, Hhip expression is quiescent; only a limited amount of Hhip expression is detectable in mature glomerular endothelial cells, podocytes and glomerular/tubular epithelial cells, and tubulointerstitial cells (23).

We (27) and others (28,29) have documented that AT_2R deficiency impairs UB branching nephrogenesis during embryogenesis; AT_2R deficiency results in newborn kidneys that display some hypoplastic features (e.g. small glomeruli with lower glomerular tuft volume). However, it is unclear whether such renal anomalies are associated with podocyte malformation and/or malfunction. In the present study, we tested whether loss of AT_2R impacts on glomerulogenesis and podocyte formation, maturation, and integrity. We hypothesized that loss of AT_2R would be associated with ectopic activation of Hhip expression in podocytes. We aimed to investigate NADPH oxidase 4 (Nox4), oxidative stress (reactive oxygen species, ROS), and TGFβ as intracellular pathways involved in Hhip activation mediating podocyte loss.

Materials and Methods

Animal Models

AT_2RKO mice (C57BL/6) (4,5) were obtained from Dr. Tadashi Inagami (Vanderbilt University School of Medicine, Nashville, TN, USA). Nephrin-cyan fluorescent protein (CFP)-transgenic (Tg) mice 30, which are fertile, with a normal phenotype at birth and during adult life, were obtained from Dr. Susan Quaggin (Northwestern University Feinberg School of Medicine, Chicago, IL, USA). For embryonic studies, we chose to work with Nephrin-CFP-Tg mice because they carry the fluorescent marker CFP driven by the podocyte-specific nephrin promoter, permitting us to monitor glomerulogenesis in real time with the use of fluorescence microscopy. In the current project, we changed the genetic background of Nephrin-CFP-Tg from the original CD1 (30,31) to C57BL/6 (≥ 10 generations) and then created hybrid mice (Nephrin/AT_2RKO in C57BL/6) by cross-breeding AT_2RKO mice with

Nephrin-CFP-Tg mice, which permits the direct visualization of glomerulogenesis under a fluorescent microscope so that we might study the impact of AT_2R deficiency on podocyte formation. Also, since rodent nephrogenesis continues until postnatal day 10, we followed suckling pups from birth to 3 weeks of age and studied mature podocytes at 3 weeks of age in both wild-type (WT, C57BL/6) and AT_2RKO mice.

Animal care in these experiments met the standards set forth by the Canadian Council on Animal Care, and the procedures utilized were approved by the Institutional Animal Care Committee of the Centre de Recherche du Centre Hospitalier de l'Université de Montréal (CRCHUM). All mouse lines were housed under standard humidity and lighting conditions (12 h light–dark cycles). Animals were allowed free access to standard mouse chow and water *ad libitum*.

Isolation and Analysis of Metanephroi and Glomeruli

Mouse embryos were dissected aseptically from timed-pregnant Nephrin-CFP-Tg and Nephrin/AT_2RKO mice from embryonic day 14 (E14) to neonate. Since CFP-positive glomeruli are convincingly seen in E14 kidneys isolated from Nephrin-CFP-Tg, we followed the nephron formation starting from day E14 to neonate in both Nephrin-CFP-Tg and Nephrin/AT_2RKO mice. The isolation of metanephroi was performed under sterile conditions, and quantitative assessment of the number of CFP-positive glomeruli was analyzed by using 2D images taken by an Eclipse TE 2000-S Microscope (Nikon, Melville, NY, USA) (31). Mature glomerular isolation from both WT and AT_2RKO mice was performed by using the iron-magnet method (32).

Renal Morphology, Mean Glomerular Volume, and Nephron and Podocyte Number

Renal morphology was assessed with hematoxylin and eosin (H&E) staining. Mean glomerular volume (V_G) was determined by the method of Weibel and Gomez with the aid of an image analysis software system (Motics Images Plus 2.0; Motic, Richmond, BC, Canada) (27); stereological quantification of neonatal nephron number was carried out using serial sections with 2D H&E images as previously reported (33).

Podocytes were identified by immunofluorescence (IF) staining of podocyte markers including anti-Wilms tumor-1 (WT-1) (C-19) and p57 (H-91) antibodies (1:100, both from

Santa Cruz Biotechnology, Santa Cruz, CA, USA) in paraffin-embedded mouse kidney sections (23,27,33). Podocyte density per glomerular area (number per μm^2) was performed in a blind fashion by counting both WT-1 and p57 positively stained cells in glomerular cross-sections (30–35 glomeruli per mouse, N = 6) (34).

Real-Time Quantitative Polymerase Chain Reaction (RT-qPCR)

RT-qPCR [The Fast SYBR® green master mix kit and the 7500 Fast Real-Time PCR system (Applied Biosystems, Life Technologies, Foster City, CA, USA)] was performed as reported previously (23,27,33). The change in mRNA for each gene was determined and normalized to its own *β-actin* (*Actb*) mRNA, and the percentage change was compared with the expression of the corresponding gene in WT (100%) by using the $2^{(-\Delta\Delta CT)}$ method. The primers used are listed in Table 1.

Immunohistochemical Studies and Reagents

Western blotting (WB), immunohistochemistry (IHC), immunofluorescence (IF), and dihydroethidium (DHE) staining were each performed based on the standard protocols, as described elsewhere (23, 27, 35). The antibodies used included anti-Hhip (5D11) (WB, 1:2000; IHC/IF, 1:100), α-SMA (1A4) (WB, 1:10000; IHC/IF, 1:500), and β-actin antibodies (WB, 1:10000) from Sigma-Aldrich, Canada (Oakville, ON, Canada); anti-WT-1 (C-19) (IF, 1:100), AT_1R (WB, 1:1000), nephrin (N-20) (WB, 1:1000; IF, 1:100), synaptopodin (Synpo) (P-19) (WB, 1:1000; IF, 1:100), cyclin-dependent kinase inhibitor p57 (H-91) (IF, 1:100), and p53 (Pab240) (WB, 1:1000) antibodies from Santa Cruz Biotechnology (Santa Cruz, CA, USA); acetyl-p53 (Lys379) (AC-p53) (WB, 1:2000; IHC, 1:100), cleaved caspase-3 (Asp175) (WB, 1:2000), and caspase-3 antibodies (WB, 1:2000) from Cell Signaling (Danvers, MA, USA); anti-TGFβ1 antibody (WB, 1:500; IHC, 1:100) from R&D Systems, Inc (Burlington, ON, Canada); phospho-Smad2 (Ser465/467)/Smad3 (Ser423/425) antibody (WB, 1:2000) (New England Biolabs, Whitby, ON, Canada); Smad2/3 antibody (WB, 1:2000) (Cedarlane-Millipore, Burlington, ON, Canada); and anti-NADPH oxidase 4 (Nox4) (WB, 1:2000; IHC, 1:500), phospho-p53 (S15) antibodies (WB, 1:2000; IHC, 1:100) (Abcam, Cambridge, MA, USA).

Chemical reagents included small interfering RNA (siRNA) of AT_2R from Life Technology Inc (Mississauga, ON, Canada); recombinant Hhip (rHhip) and TGFβ1 (rTGFβ1) from R&D Systems, Inc; PD123319 from Santa Cruz Biotechnology; and GKT137831 (dual inhibitor of both Nox1 and Nox4) from Cayman Chemical (Ann Arbor, MI, USA).

Podocyte Cell Line

We obtained an immortalized mouse podocyte cell line (mPODs) from Dr. Stuart J Shankland (University of Washington, WA, USA) (36). In brief, mPODs were grown on a collagen I-coated plate in DMEM medium supplemented with 10% FBS (Invitrogen, Burlington, ON, Canada), 100 U/ml penicillin–streptomycin (Invitrogen), and 10 U/ml recombinant mouse interferon-γ (Sigma) at 33°C (defined as a permissive condition). Then the differentiated mPODs were cultured under non-permissive conditions, i.e. without interferon-γ at 37°C, for 10 days before the desired experiments. The treatment periods of rHhip, rTGFβ1, and PD123319 were for 24 h. We cloned the rat TGFβ1 promoter (pGL4.20/rTGFβ1, N-1016/+143, NM_021578.2) by PCR. pGL4.20/rTGFβ1 promoter activity under rHhip was analyzed by luciferase assay in mPODs.

Nephroseq Analysis

Nephroseq analysis (https://www.nephroseq.org/resource/login.html) was performed on three publicly available microarray studies performed on human kidney biopsy samples – the Nakagawa Chronic Kidney Disease (CKD) Study, the Sampson Nephrotic Syndrome Glomerular (Glom) Study, and the Hodgin Focal Segmental Glomerulosclerosis (FSGS) Glomerular (Glom) Study (Table 2). We compared the original microarray mRNA value (presented with log2 median-centered intensity) of each individual subject on several relevant genes [*HHIP*, *AGTR2*, *TP53* (tumor protein p53), *FN1*, *WT-1*, *NPHS1*, and *NPSH2*].

HHIP Expression in Kidney Biopsy Samples by Immunohistochemistry

Kidney biopsy samples were obtained from the McGill University Health Centre Kidney Disease Biorepository (REB #14-466). All participants provided written consent and the study was approved by the institutional review board. Patient characteristics are summarized in Table 3.

Statistical Analysis

For animal studies, groups of 6–12 mice were studied. *In vitro*, three to four separate experiments were performed for each protocol. All values represent mean ± SEM. Statistical significance between the experimental groups was analyzed by Student's *t*-test or one-way ANOVA, followed by the Bonferroni test using Prism 5.0 software (GraphPad, San Diego, CA, USA). A probability level of $p \leq 0.05$ was considered to be statistically significant (23, 27, 35).

Results

Physiological measurements of glomerulogenesis, nephron number, and glomerular tuft volume (VG)

Since CFP-positive glomeruli are convincingly seen in E14 kidneys isolated from Nephrin-CFP-Tg mice, we followed the time course of glomerulogenesis from E14 to neonate in both Nephrin-CFP-Tg mice and Nephrin/AT_2RKO mice (Figure 13A). Compared with Nephrin-CFP-Tg mice, E14–E15 metanephroi isolated from Nephrin/AT_2RKO mice displayed fewer CFP-positive glomeruli (i.e. on E15, Nephrin-CFP-Tg, 27.25 ± 3.155, N = 8 litters versus Nephrin/AT_2RKO, 20.11 ± 2.239, N = 9 litters, Figure 13B) with grossly smaller kidney size. However, those gross differences were less apparent after E17 (Figure 13A). We then examined kidneys from live newborns to determine renal morphology (Figure 13C; supplementary material, Figure 19) and nephron number (Figure 13D). The kidneys of AT_2RKO neonates had smaller glomeruli, typical of delayed maturation (Figure 13C); the actual nascent nephron numbers in AT_2RKO as analyzed by serial 2D sections, however, did not differ from those of WT control mice (Figure 13D) (WT, 3038.4 ± 175.52, N = 6 versus AT_2RKO, 2963.25 ± 178.47, N = 5). We did not observe significant differences in other biological measurements including body weight (BW, g), kidney weight (KW, mg), and KW/BW ratio between WT and AT_2RKO pups from neonate until 3 weeks of age (Table 4). Compared with WT, AT_2RKO mice exhibited a significantly lower mean glomerular tuft volume (V_G, μm^3) throughout the entire suckling period (Figure 13E). Nephrin protein (Figure 13F) expression was significantly decreased in isolated glomeruli from 3-week-old AT_2RKO mice, compared with WT mice. Since AT_2R siRNA significantly decreases mPOD proliferation under a non-permissive condition, and there was no impact under a permissive condition (supplementary material, Figure 20), *in vitro* studies with mPODs were performed

under non-permissive conditions. Our data indicated that the AT_2R antagonist (PD123319) appeared to interrupt the integrity of the actin cytoskeleton, resulting in decreased Synpo expression in a dose-dependent manner (supplementary material, Figure 21).

Podocyte morphology/numbers

Next, we examined several podocyte markers and their gene and protein expression in both WT and AT_2RKO mice at 3 weeks of age (Figure 14). RT-qPCR data (Figure 14A) revealed that mRNA expression of *Wt1*, *Nphs1* (nephrin), *Synpo* (synaptopodin), and *Nphs2* (podocin) was significantly decreased in isolated glomeruli of AT_2RKO mice compared with WT animals. These observations were further confirmed by IF staining, i.e. WT-1 (Figure 14B), p57 (Figure 14C), nephrin (Figure 14D), and Synpo (Figure 14E). We analyzed both WT-1 and p57-IF positive podocytes (number per μm^2) and observed that AT_2RKO mice had fewer podocytes (average 30% reduction) compared with the WT control, and these results were indeed in line with nephrin and synaptopodin expression levels as observed by IF.

Hhip expression impact on podocyte morphology

AT_2R mRNA (Figure 15A) expression was confirmed by RT-qPCR in AT_2RKO mice. (It should be noted that we could not perform WB to quantify AT_2R protein expression, mainly due to the non-specificity of all commercial AT_2R antibodies (37).) Compared with WT animals, Hhip expression (mRNA and protein) was significantly increased, while AT_1R remained unchanged in isolated glomeruli of AT_2RKO mice at 3 weeks of age (Figure 15A, B). Additionally, no difference in renal AT_1R protein expression between AT_2RKO mice and WT mice was observed in E18 and neonatal kidneys (supplementary material, Figure 22). Enhanced Hhip-IHC expression (localized to glomerular, tubular, and adjacent tubulointerstitial cells) was observed in the kidneys of AT_2RKO mice (Figure 15C). Co-localization experiments revealed that the podocytes of AT_2RKO mice expressed less Synpo and p57, but more Hhip (Figure 15D).

To establish the further link among AT_2R, Synpo, and Hhip expression, we performed knockdown of AT_2R signaling either by AT_2R siRNA [N.B. *AT_2R* mRNA expression (approximately 50%) was knocked down by using AT_2R siRNA (50 nM) in mPODs (supplementary material, Figure 23)] or by using the AT_2R antagonist PD123319 (10^{-8} M). IF

staining (Figure 15E, F) revealed that loss of AT_2R results in decreasing Synpo but increasing Hhip expression in the cytosolic compartments in mPODs, respectively. Both AT_2R siRNA and PD123319 significantly stimulated Hhip and Nox4 expression (at both mRNA and protein levels), and increased cleaved caspase-3, α-SMA, and TGFβ1 levels and the phosphorylation of Smad2/3 protein, but attenuated Synpo protein expression and had no impact on AT_1R protein expression in mPODs (Figure 15G, H; supplementary material, Figures 24–27). Moreover, recombinant Hhip (rHhip) dose dependently decreased *Synpo/nephrin* mRNA (supplementary material, Figure 28) and inhibited Synpo protein expression, which was associated with interruption of cytoskeletal integrity in mPODs (supplementary material, Figure 29).

Hhip expression on ROS generation

Compared with WT animals, enhanced Hhip, Nox4, AC-p53, and phosphorylated p53 expression, as well as elevated ROS generation reviewed by dihydroethidium (DHE) staining, was observed in the glomeruli of AT_2RKO mice (Figure 16A). *Bax* and *Nox4* mRNA expression was significantly elevated in isolated glomeruli of AT_2RKO mice, whereas *Bcl-2*, *Nox1*, and *Nox2* (*Cybb*) mRNA expression remained unchanged (Figure 16B). The enhanced Nox4 protein expression was further confirmed in isolated glomeruli of AT_2RKO mice (Figure 16C). *In vitro*, *Nox4* mRNA was selectively increased, while *Nox1* and *Nox2* mRNA remained unchanged in AT_2R siRNA-treated mPODs (supplementary material, Figure 24). PD123319 (10^{-8} M) significantly enhanced DHE staining (Figure 16D) and elevated *Hhip* and *Nox4* mRNA expression (supplementary material, Figure 25), which was attenuated by GKT137831 (a dual inhibitor of both NOX1 and NOX4) in mPODs. Together, these data underscore the importance of AT_2R in ROS generation.

To further confirm the functional impact of ROS on Hhip expression, we applied hydrogen peroxide (H_2O_2), which dose dependently stimulated Hhip and α-SMA protein expression (Figure 16E). In addition to the stimulatory effect of PD123319 (10^{-8} M) on cleaved caspase-3 expression (Figure 15H), rHhip stimulated ROS generation and this stimulatory effect could be completely abolished by GKT137831 (Figure 16F). Meanwhile, rHhip also increased the expression of cleaved caspase-3, acetyl-p53 (Lys379) (AC-p53), and phospho-p53 protein in mPODs in a dose-dependent manner (Figure 16G).

Hhip expression impact on podocyte transition

Our RT-qPCR data indicated that *TGFβ1* and *α-SMA* (*Acta2*) mRNA expression was significantly elevated in isolated glomeruli of AT_2RKO mice at 3 weeks of age (Figure 17A) – which we further confirmed by IHC/IF staining (Figure 17B). *In vitro*, under the stimulatory effects of PD123319 (Figure 15H), rHhip also dose dependently stimulated TGFβ1 (*Tgfb1*) promoter activity (Figure 17C) and enhanced TGFβ1 expression and the phosphorylation of Smad2/3 (Figure 17D), as well as upregulating *α-SMA* mRNA (Figure 17E) and protein expression (Figure 17F).

When we blocked TGFβ receptor I (TGFβRI) with SB431532 (an inhibitor of TGFβRI), the rHhip effect on Synpo, Nox4, and the phosphorylation of Smad2/3 protein expression was prevented (Figure 18A), as was ROS generation (Figure 18B). Also, recombinant TGFβ1 (rTGFβ1) stimulated *α-SMA* and *fibronectin* (*Fn1*) mRNA expression, while it inhibited *Synpo* mRNA expression in a dose-dependent manner (supplementary material, Figure 30). Coomassie Blue gel staining showed that AT_2RKO mice at the age of 3 weeks had detectable albumin leakage in their urine compared with WT animals (Figure 18C).

Nephroseq analysis and HHIP-IHC expression in kidney biopsy samples

In the Nakagawa CKD Kidney study, compared with normal kidney (NK, $N = 9$), significantly decreased mRNA values of *NPHS1*, *NPHS2*, and *WT1* were seen, while increased mRNA levels of *HHIP*, *TP53*, and *FN1* were observed in CKD kidneys ($N = 53$). *ATGR2* mRNA levels were not different between the two groups (supplementary material, Figure 31). Although glomerular HHIP levels were higher in FSGS patients ($N = 8$), compared with NK ($N = 9$) and minimal change disease (MCD, $N = 7$) in the Hodgin FSGS dataset ($N = 30$), the difference did not reach statistical significance (supplementary material, Figure 31).

Finally, we validated HHIP-IHC expression in human kidney biopsies (controls, $N = 2$ versus FSGS, $N = 4$). Compared with the controls with minimal HHIP staining in the glomerulus, glomerular HHIP staining in four patients with FSGS was increased in variable degrees (Figure 18D).

Discussion

In the present study, we demonstrated that AT_2R deficiency is associated with podocyte transition from normal morphology to an apoptotic and/or a fibrotic-like phenotype. The underlying mechanism appears to be mediated, at least in part, via augmented ectopic Hhip expression in podocytes.

While the expression pattern of AT_2R in both embryonic (in both UB and MM lineage derivatives) and mature stages (glomerular endothelial cells, podocytes, tubular epithelial cells, and inner medullary collecting duct) is well defined (4,38-40), AT_2R regulation and function with respect to expression during development in a renal cell-specific manner have not been fully delineated. For instance, aberrant UB budding is seen in 60% of E11 AT_2RKO embryos (4,5), and decreased UB branching nephrogenesis around E14 AT_2RKO embryos has been documented by us (27) and others (28,29). However, it is unclear whether those anomalies would occur throughout the entire nephrogenic process and subsequently affect the final nephron number. Taking advantage of Nephrin/AT_2RKO mice carrying the fluorescent marker CFP, we confirmed that E14–E15 embryonic kidneys isolated from Nephrin/AT_2RKO mice had fewer CFP-positive glomeruli with a grossly smaller kidney size. However, those differences disappeared after E17.

Although neonatal kidneys of AT_2RKO mice display some renal hypoplastic features (small glomeruli with less nephron maturation) as reported previously (27), the actual nascent nephron formation (nephron number) and several biological measurements including BW, KW, and the KW/BW ratio in AT_2RKO mice did not differ from those of WT animals. AT_2RKO mice displayed a significantly lower mean glomerular tuft volume during the entire suckling period. Together, these data suggested that the lack of AT_2R might not interrupt the sequence of the final nephron formation, but instead modify the maturation, integrity, and function of specialized renal cells, such as podocytes. In line with the observations that AT_2R enhanced the expression of slit diaphragm molecules (40) and AT_2R had a renoprotective effect to prevent diabetic nephropathy occurring in Zucker rats (41), we found that several podocyte markers, such as p57, WT-1, nephrin, and Synpo expression, were significantly decreased in the glomeruli of AT_2RKO mice at 3 weeks of age that had a detectable amount of albumin leakage in their urine. Together, these data underscore the functional role of AT_2R in

podocyte formation and integrity. Further, we found no evidence that AT_2R deficiency results in a compensatory change in AT_1R expression, since AT_1R expression (mRNA and protein) remains unchanged both *in vivo* and *in vitro*.

Evidence of both increased oxidative stress (as 'read' by DHE staining and Nox4 expression) and activation of TGFβ1 signaling was present in the kidneys of AT_2RKO mice, as reported elsewhere (35). Although the mechanisms of ROS-induced apoptosis and/or TGFβ1-related epithelial–mesenchymal transition (EMT) have been well recognized in the pathogenesis of podocyte loss/dysfunction (42-45), and TGFβ1 can upregulate mitochondrial Nox4 in cultured podocytes, promoting apoptosis (43,46), it is unclear whether AT_2R deficiency directly or indirectly mediates increased ROS and TGFβ1 activation, resulting in the podocyte phenotypes seen in AT_2RKO mice. Previously, we established that the ROS, Hhip, and TGFβ1 signaling cross-talk mediates impaired renal development in the progeny of diabetic dams (23,33). The neonatal kidneys of such offspring display similar renal hypoplastic features (small glomeruli with immature nephrons) to those seen in AT_2RKO mice. Thus, we hypothesize that AT_2R deficiency might promote Hhip ectopic expression in podocytes, leading to podocyte loss/dysfunction, given the fact that Hhip plays a critical role in cell apoptosis, angiogenesis, and tumorigenesis (21,22).

To test our hypothesis, we conducted the molecular and immunohistochemical experiments both *in vivo* and *in vitro*. Indeed, we observed that Hhip expression was significantly augmented in the podocytes of AT_2RKO mice. The loss of AT_2R in mPODs upregulated Hhip and Nox4 expression (mRNA/protein), leading to the collapse of cytoskeleton actin integrity, likely due to the activation of cleaved caspase-3 and the EMT-related TGFβ1–Smad2/3 pathway in podocytes. Next, we explored whether ROS/TGFβ1 and Hhip act separately or in concert to contribute to podocyte dysfunction. *In vitro*, H_2O_2 stimulated Hhip protein expression and rHhip elevated ROS generation, both in a dose-dependent manner, underscoring the presence of a positive autocrine feedback loop of ROS–Hhip. Similar to PD123319, rHhip was associated with an increase in cleaved caspase-3 and acetylated p53 protein expression in podocytes. Together, these results indicate that loss of AT_2R results in Hhip stimulation, which then may trigger podocyte apoptosis; this process may be mediated, at least in part, via ROS generation.

We noted that AT_2R deficiency increased the expression of EMT-related genes, as shown by activation of TGFβ1–Smad2/3 signaling and enhanced α-SMA expression (mRNA/protein) in podocytes both *in vivo* and *in vitro*. When TGFβRI was blocked with SB431532, the action of rHhip on Synpo and Nox4 protein expression, as well as TGFβ1–Smad2/3 signaling in podocytes, was completely inhibited, suggesting that activated Hhip targeting podocytes occurs through a TGFβRI-dependent manner. Currently, we do not know how Hhip functionally interacts with TGFβRI. At least our data suggested that Hhip could directly stimulate TGFβ1 expression transcriptionally (mRNA) and translationally (protein). On the other hand, it has been reported that the TGFβ1/PKA/SMAD/Gli signaling axis promotes cancer progression, EMT, and metastasis (47). Whether or not this oncogenic axis applies to our model merits further investigation.

Finally, we extended our findings by applying them to the data obtained from human subjects with kidney diseases that may involve regulation of *HHIP* and *AGTR2*. First, we queried the publicly available gene expression database in kidney diseases (Nephroseq) to analyze the expression of *HHIP* and associated genes. The Nakagawa CKD Kidney dataset reflects gene expression in both the glomerulus and the tubulointerstitial compartment, and the results indicate that *HHIP*, *TP53*, and *FN1* mRNAs are upregulated, while *NPHS1*, *NPHS2*, and *WT1* mRNAs are downregulated in CKD, a condition of progressive loss of kidney function. *AGTR2* mRNA was unchanged in CKD kidneys.

FSGS is a pathological change in the glomerulus following podocyte loss both in experimental models and in humans (48, 49). Of interest, glomerular *HHIP* mRNA tended to be upregulated in patients with FSGS (Nephroseq, Hodgin FSGS dataset), and HHIP-IHC expression was increased in the glomeruli of FSGS patients; some staining was clearly outside of the capillary lumen, consistent with the staining of podocytes. The results support the notion that HHIP is upregulated in glomerular cells, including podocytes, in patients with FSGS. Upregulation of HHIP in podocytes may contribute to podocyte loss in humans, consistent with our findings in mice.

In summary, the present results lead us to propose a working model (Figure 18E) of AT_2R deficiency and its association with podocyte loss/dysfunction. In brief, loss of AT_2R via ROS generation (probably mediated by Nox4) stimulates ectopic Hhip expression, which in

turn triggers podocyte apoptosis by activation of the caspase-3 and p53 pathways. Concomitantly, the augmented Hhip interacts with TGFβRI to trigger TGFβ1/Smad2/3 signaling and then transform differentiated podocytes into undifferentiated podocyte-derived fibrotic cells. In conclusion, our data suggest that loss of AT_2R is associated with podocyte loss/dysfunction, likely via augmented ectopic Hhip expression in podocytes.

Acknowledgements

We owe special thanks to Dr. John SD Chan (CRCHUM, Montreal, QC, Canada) for his unconditional support and valuable comments on this manuscript. This project was supported by grants to SLZ from the Canadian Diabetes Association (OG-3-13-4073-SZ). SYC is a Canadian Diabetes Association Doctoral Student. Editorial assistance was provided by the CRCHUM's Research Support Office.

Author Contributions Statement

MCL, XPZ, SYC, CSL, IC, and TT contributed to researched data. TT and JRI contributed to discussion and reviewed/edited the manuscript. SLZ contributed to researched data and discussion and also wrote, reviewed, and edited the manuscript.

Abbreviations

AC-p53, acetyl-p53 (Lys379); AT_1R, angiotensin II type 1 receptor; AT_2R, angiotensin II type 2 receptor; CAKUT, congenital abnormalities of the kidney and urinary tract

References of Article 1

1. Yosypiv, I.V., Renin-angiotensin system in ureteric bud branching morphogenesis: insights into the mechanisms. Pediatr Nephrol, 2011. 26(9): p. 1499-512.
2. Yosypiv, I.V., Congenital anomalies of the kidney and urinary tract: a genetic disorder? Int J Nephrol, 2012. 2012: p. 909083.
3. Schedl A. Renal abnormalities and their developmental origin. Nat Rev Genet 2007; 8: 791– 802.
4. Ichiki T, Labosky PA, Shiota C, et al. Effects on blood pressure and exploratory behaviour of mice lacking angiotensin II type-2 receptor. Nature 1995; 377: 748– 750.
5. Nishimura H, Yerkes E, Hohenfellner K, et al. Role of the angiotensin type 2 receptor gene in congenital anomalies of the kidney and urinary tract, CAKUT, of mice and men. Mol Cell 1999; 3: 1– 10.
6. Chuang PT, McMahon AP. Vertebrate Hedgehog signalling modulated by induction of a Hedgehog-binding protein. Nature 1999; 397: 617– 621.
7. Ingham PW, McMahon AP. Hedgehog signaling in animal development: paradigms and principles. Genes Dev 2001; 15: 3059– 3087.
8. McMahon AP, Ingham PW, Tabin CJ. Developmental roles and clinical significance of hedgehog signaling. Curr Top Dev Biol 2003; 53: 1– 114.
9. Onishi H, Katano M. Hedgehog signaling pathway as a therapeutic target in various types of cancer. Cancer Sci 2011; 102: 1756– 1760.
10. Thayer SP, di Magliano MP, Heiser PW, et al. Hedgehog is an early and late mediator of pancreatic cancer tumorigenesis. Nature 2003; 425: 851– 856.
11. Zhou D, Li Y, Zhou L, et al. Sonic hedgehog is a novel tubule-derived growth factor for interstitial fibroblasts after kidney injury. J Am Soc Nephrol 2014; 25: 2187– 2200.
12. Bosanac I, Maun HR, Scales SJ, et al. The structure of SHH in complex with HHIP reveals a recognition role for the Shh pseudo active site in signaling. Nat Struct Mol Biol 2009; 16: 691– 697.

13. Bishop B, Aricescu AR, Harlos K, et al. Structural insights into hedgehog ligand sequestration by the human hedgehog-interacting protein HHIP. Nat Struct Mol Biol 2009; 16: 698– 703.

14. Chuang PT, Kawcak T, McMahon AP. Feedback control of mammalian Hedgehog signaling by the Hedgehog-binding protein, Hip1, modulates Fgf signaling during branching morphogenesis of the lung. Genes Dev 2003; 17: 342– 347.

15. Coulombe J, Traiffort E, Loulier K, et al. Hedgehog interacting protein in the mature brain: membrane-associated and soluble forms. Mol Cell Neurosci 2004; 25: 323– 333.

16. Holtz AM, Griffiths SC, Davis SJ, et al. Secreted HHIP1 interacts with heparan sulfate and regulates Hedgehog ligand localization and function. J Cell Biol 2015; 209: 739– 757.

17. Kwong L, Bijlsma MF, Roelink H. Shh-mediated degradation of Hhip allows cell autonomous and non-cell autonomous Shh signalling. Nat Commun 2014; 5: 4849.

18. Lao T, Jiang Z, Yun J, et al. Hhip haploinsufficiency sensitizes mice to age-related emphysema. Proc Natl Acad Sci U S A 2016; 113: E4681– E4687.

19. Kayed H, Kleeff J, Esposito I, et al. Localization of the human hedgehog-interacting protein (Hip) in the normal and diseased pancreas. Mol Carcinog 2005; 42: 183– 192.

20. Zhou X, Baron RM, Hardin M, et al. Identification of a chronic obstructive pulmonary disease genetic determinant that regulates HHIP. Hum Mol Genet 2012; 21: 1325– 1335.

21. Nie DM, Wu QL, Zheng P, et al. Endothelial microparticles carrying hedgehog-interacting protein induce continuous endothelial damage in the pathogenesis of acute graft-versus-host disease. Am J Physiol Cell Physiol 2016; 310: C821– C835.

22. Olsen CL, Hsu PP, Glienke J, et al. Hedgehog-interacting protein is highly expressed in endothelial cells but down-regulated during angiogenesis and in several human tumors. BMC Cancer 2004; 4: 43.

23. Zhao XP, Liao MC, Chang SY, et al. Maternal diabetes modulates kidney formation in murine progeny: the role of hedgehog interacting protein (HHIP). Diabetologia 2014; 57: 1986– 1996.

24. Cain JE, Rosenblum ND. Control of mammalian kidney development by the Hedgehog signaling pathway. Pediatr Nephrol 2011; 26: 1365– 1371.

25. Ding H, Zhou D, Hao S, et al. Sonic hedgehog signaling mediates epithelial–mesenchymal communication and promotes renal fibrosis. J Am Soc Nephrol 2012; 23: 801– 813.

26. Fabian SL, Penchev RR, St-Jacques B, et al. Hedgehog–Gli pathway activation during kidney fibrosis. Am J Pathol 2012; 180: 1441– 1453.

27. Chen YW, Tran S, Chenier I, et al. Deficiency of intrarenal angiotensin II type 2 receptor impairs paired homeo box-2 and N-myc expression during nephrogenesis. Pediatr Nephrol 2008; 23: 1769– 1777.

28. Oshima K, Miyazaki Y, Brock JW III, et al. Angiotensin type II receptor expression and ureteral budding. J Urol 2001; 166: 1848– 1852.

29. Song R, Spera M, Garrett C, et al. Angiotensin II AT2 receptor regulates ureteric bud morphogenesis. Am J Physiol Renal Physiol 2010; 298: F807– F817.

30. Cui S, Li C, Ema M, et al. Rapid isolation of glomeruli coupled with gene expression profiling identifies downstream targets in Pod1 knockout mice. J Am Soc Nephrol 2005; 16: 3247– 3255.

31. Tran S, Chen YW, Chenier I, et al. Maternal diabetes modulates renal morphogenesis in offspring. J Am Soc Nephrol 2008; 19: 943– 952.

32. Zhong F, Wang W, Lee K, et al. Role of C/EBP-alpha in adriamycin-induced podocyte injury. Sci Rep 2016; 6: 33520.

33. Chang SY, Chen YW, Zhao XP, et al. Catalase prevents maternal diabetes-induced perinatal programming via the Nrf2–HO-1 defense system. Diabetes 2012; 61: 2565–2574.

34. Zhang J, Pippin JW, Vaughan MR, et al. Retinoids augment the expression of podocyte proteins by glomerular parietal epithelial cells in experimental glomerular disease. Nephron Exp Nephrol 2012; 121: e23– e37.

35. Chang SY, Chen YW, Chenier I, et al. Angiotensin II type II receptor deficiency accelerates the development of nephropathy in type I diabetes via oxidative stress and ACE2. Exp Diabetes Res 2011; 2011: 521076.

36. Mundel P, Reiser J, Zuniga Mejia BA, et al. Rearrangements of the cytoskeleton and cell contacts induce process formation during differentiation of conditionally immortalized mouse podocyte cell lines. Exp Cell Res 1997; 236: 248– 258.

37. Hafko R, Villapol S, Nostramo R, et al. Commercially available angiotensin II At(2) receptor antibodies are nonspecific. PloS One 2013; 8: e69234.

38. Norwood VF, Craig MR, Harris JM, et al. Differential expression of angiotensin II receptors during early renal morphogenesis. Am J Physiol 1997; 272: R662– R668.

39. Ozono R, Wang ZQ, Moore AF, et al. Expression of the subtype 2 angiotensin (AT2) receptor protein in rat kidney. Hypertension 1997; 30: 1238– 1246.

40. Suzuki K, Han GD, Miyauchi N, et al. Angiotensin II type 1 and type 2 receptors play opposite roles in regulating the barrier function of kidney glomerular capillary wall. Am J Pathol 2007; 170: 1841– 1853.

41. Castoldi G, di Gioia CR, Bombardi C, et al. Prevention of diabetic nephropathy by compound 21, selective agonist of angiotensin type 2 receptors, in Zucker diabetic fatty rats. Am J Physiol Renal Physiol 2014; 307: F1123– F1131.

42. Daehn I, Casalena G, Zhang T, et al. Endothelial mitochondrial oxidative stress determines podocyte depletion in segmental glomerulosclerosis. J Clin Invest 2014; 124: 1608– 1621.

43. Das R, Xu S, Nguyen TT, et al. Transforming growth factor β1-induced apoptosis in podocytes via the extracellular signal-regulated kinase-mammalian target of rapamycin complex 1–NADPH oxidase 4 axis. J Biol Chem 2015; 290: 30830– 30842.

44. Lee HS. Mechanisms and consequences of TGF-β overexpression by podocytes in progressive podocyte disease. Cell Tissue Res 2012; 347: 129– 140.

45. Loeffler I, Wolf G. Epithelial-to-mesenchymal transition in diabetic nephropathy: fact or fiction? Cells 2015; 4: 631– 652.

46. Das R, Xu S, Quan X, et al. Upregulation of mitochondrial Nox4 mediates TGF-beta-induced apoptosis in cultured mouse podocytes. Am J Physiol Renal Physiol 2014; 306: F155– F167.

47. Javelaud D, Pierrat MJ, Mauviel A. Crosstalk between TGF-beta and hedgehog signaling in cancer. FEBS Lett 2012; 586: 2016– 2025.

48. Wharram BL, Goyal M, Wiggins JE, et al. Podocyte depletion causes glomerulosclerosis: diphtheria toxin-induced podocyte depletion in rats expressing human diphtheria toxin receptor transgene. J Am Soc Nephrol 2005; 16: 2941– 2952.

49. Wiggins RC. The spectrum of podocytopathies: a unifying view of glomerular diseases. Kidney Int 2007; 71: 1205– 1214.

50. Nakagawa S, Nishihara K, Miyata H, et al. Molecular markers of tubulointerstitial fibrosis and tubular cell damage in patients with chronic kidney disease. PloS One 2015; 10: e0136994.

51. Sampson MG, Robertson CC, Martini S, et al. Integrative genomics identifies novel associations with APOL1 risk genotypes in black NEPTUNE subjects. J Am Soc Nephrol 2016; 27: 814– 823.

52. Hodgin JB, Borczuk AC, Nasr SH, et al. A molecular profile of focal segmental glomerulosclerosis from formalin-fixed, paraffin-embedded tissue. Am J Pathol 2010; 177: 1674– 1686.

Tables and Figures

Table 1. Primer sequences

Gene name (HUGO symbol)	**Primer sequences (S = sense; AS = antisense)**	**Reference Sequence**
Angiotensin II receptor type 1/ AT_1R (*Agtr1a*)	S: CTGGCAGGCACAGTTACATAT AS: TCAGCAAAAAGCATAAGTCAG	NM_177322.3
Angiotensin II receptor type 2/ AT_2R (*Agtr2*)	S: CAGCAGAAACATTACCAGCAG AS: GAGTAATAGGTTGCCCAGAG	NM_007429.5
α-Smooth muscle actin/ α-SMA (*Acta2*)	S: GACGCTGAAGTATCCGATAGAACA AS: CACACGAAGCTCGTTATAGAAA	NM_007392.3
BCL2 associated X, apoptosis regulator (*Bax*)	S: TAGCAAACTGGTGCTCAAGG AS: TCTTGGATCCAGACAAGCAG	NM_007527.3
BCL2, apoptosis regulator (*Bcl2*)	S: AGAGACAGCCAGGAGAAATCAAAC AS: CTGTGGATGACTGAGTACCTGAAC	NM_009741.5
Fibronectin (*Fn1*)	S: TAGCAGGCTACCGACTGACCG AS: CACCCAGCTTGAAGCCAATCC	NM_010233.2
Hedgehog interacting protein (*Hhip*)	S: CCCATCGGCTCTTCATTCTA AS: CCTTTCGTCTCCTCCCTTTA	NM_020259.4
Nephrin (*Nphs1*)	S: GTGCCCTGAAGGACCCTACT AS: CCTGTGGATCCCTTTGACAT	NM_019459.2
NADPH oxidase 1 (*Nox1*)	S: GGTCACTCCCTTTGCTTCCA AS: GGCAAAGGCACCTGTCTCTCT	NM_172203.2
NADPH oxidase 2/ cytochrome b-245 beta chain (*Cybb*)	S: CCCTTTGGTACAGCCAGTGAAGAT AS: CAATCCCGGCTCCCACTAACATCA	NM_007807.5
NADPH oxidase 4 (*Nox4*)	S: TGGCCAACGAAGGGGTTAAA AS: GATGAGGCTGCAGTTGAGGT	NM_001285835.1
Podocin (*Nphs2*)	S: CTTGGCACATCGATCCCTCA AS: CGCACTTTGGCCTGTCTTTG	NM_130456.4
Synaptopodin/ Synpo (*Synpo*)	S: CTTTGGGGAAGAGGCCGATTG AS: GTTTTCGGTGAAGCTTGTGC	NM_001109975.1
Transforming growth factor beta 1/ TGFβ1 (*Tgfb1*)	S: CTTCAGCTCCACAGAGAAGAACTG AS: TCAGCTGCACTTGCAGGAGCG	NM_011577.2
Wilms tumor 1/ WT-1 (*Wt1*)	S: GAGAGCCAGCCTACCATCC AS: GGGTCCTCGTGTTTGAAGGAA	NM_144783.2

Table 2. Nephroseq analysis

Study	Sample size	Subgroups (sample number)	Tissue type	Microarray	Measured gene number	Reference
Nakagawa CKD Kidney	61	1. Normal kidney (NK, 8) 2. Chronic kidney disease (CKD, 53)	Kidney	Agilent Whole Human Genome Microarray 4x44K (Probe Name Version)	19 063	[50]
Sampson Nephrotic Syndrome Glom	38	1. Focal segmental glomerulosclerosis (FSGS, 15) 2. Membranous glomerulonephropathy (MG, 9) 3. Minimal change disease (MCD, 7) 4. Other nephrotic syndrome (ONS, 7)	Glomeruli	Affymetrix Human Gene 2.1 ST Array (altCDF v19)	22 150	[51]
Hodgin FSGS Glom	30	1. Normal kidney (NK, 9) 2. Collapsing focal segmental glomerulosclerosis (CFSG, 6) 3. Focal segmental glomerulosclerosis (FSGS, 8) 4. Minimal change disease (MCD, 7)	Glomeruli	Affymetrix Human X3P Array	19 139	[52]

Nephroseq website (https://nephroseq.org/resource/main.html).

Table 3. Patient information

Patient ID	**Age (years); sex (M/F)**	**Diagnosis**
Control #1	62; M	–
Control #2	Not known; transplantation donor	–
FSGS #1	31; F	FSGS
FSGS #2	30; F	FSGS
FSGS #3	19; M	FSGS
FSGS #4	42; M	FSGS

Table 4. Biological measurements from WT and AT_2RKO mice

	Body Weight (BW, g)		**Kidney Weight (KW, mg)**		**Ratio KW/BW (mg/g)**	
Age	**WT**	**AT_2RKO**	**WT**	**AT_2RKO**	**WT**	**AT_2RKO**
Neonate	1,38±0,02	1,46±0,04	15,60±0,26	15,52±0,64	11,35±0,11	10,59±0,23
1 week	3,82±0,07	4,02±0,07	42,67±0,91	44,84±0,85	11,18±0,12	11,15±0,09
2 weeks	7,44±0,27	7,72±0,22	101,2±3,80	99,28±3,50	13,63±0,17	12,79±0,15
3 weeks	10,55±0,23	10,96±0,27	146,30±2,94	149,70±4,00	13,92±0,13	13,69±0,15

Figure 13

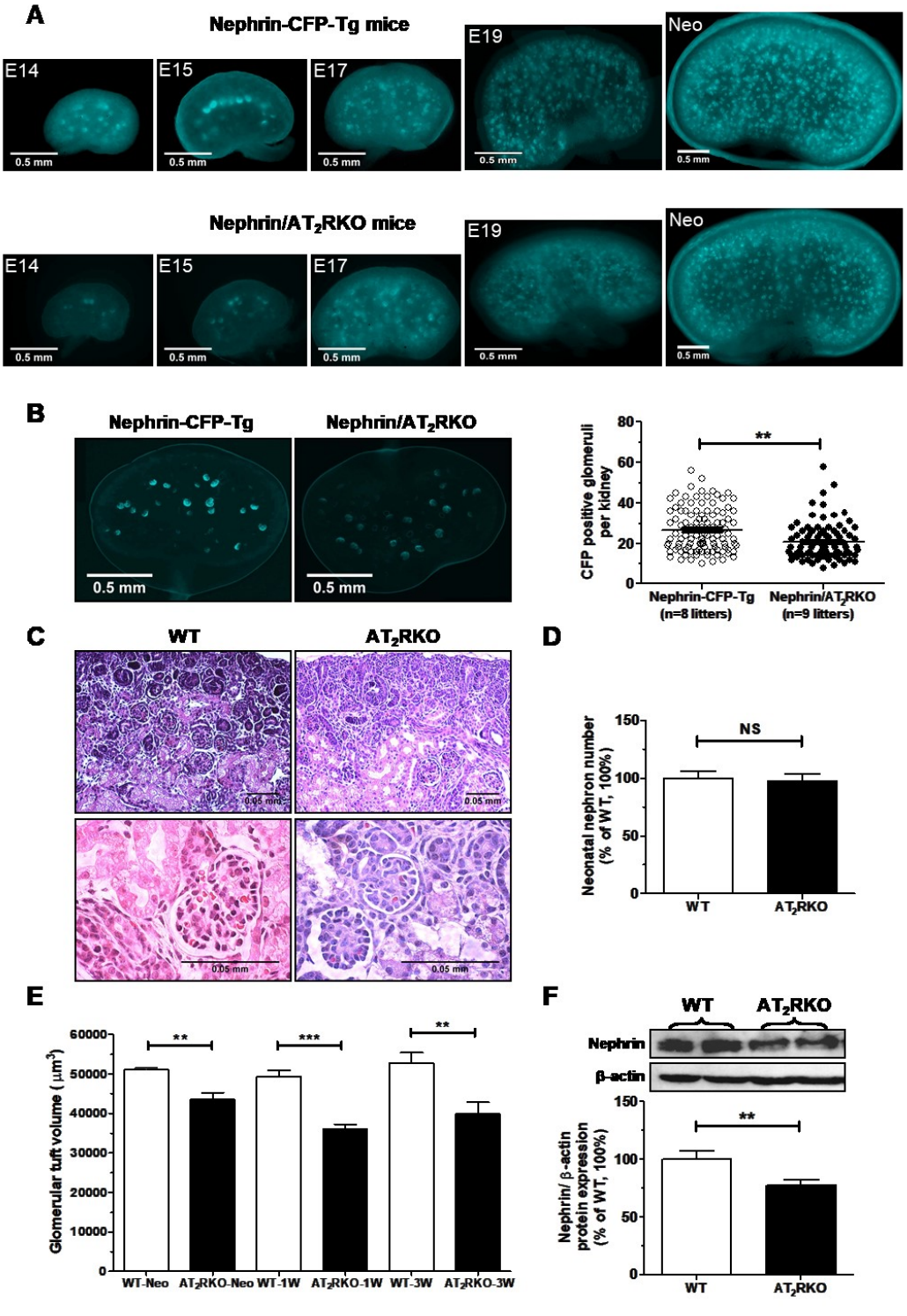
A
Nephrin-CFP-Tg mice
E14
E15
E17
E19
Neo
0.5 mm
Nephrin/AT2RKO mice
B
Nephrin-CFP-Tg
Nephrin/AT2RKO
CFP positive glomeruli per kidney
**
Nephrin-CFP-Tg (n=8 litters)
Nephrin/AT2RKO (n=9 litters)
C
WT
AT2RKO
D
Neonatal nephron number (% of WT, 100%)
NS
E
Glomerular tuft volume (μm3)
WT-Neo
AT2RKO-Neo
WT-1W
AT2RKO-1W
WT-3W
AT2RKO-3W
F
Nephrin
β-actin
Nephrin/ β-actin protein expression (% of WT, 100%)

Figure 13. Physiological measurements of glomerulogenesis and neonatal nephron number. (A) Metanephroi isolated from timed-pregnant Nephrin-CFP-Tg and Nephrin/AT_2RKO mice from E14 to neonate. (B) Quantification of E15 CFP-positive glomeruli of Nephrin-CFP-Tg (n = 8 litters) and Nephrin/AT_2RKO (n = 9 litters) mice. (C) Neonatal kidney morphology by H&E staining. (D) Quantification of neonatal nephron number of WT (n =6, white bar) and AT_2RKO (n =5, black bar) mice. The y-axis shows the percentage of nephron number compared with WT mice (100%). (E) Quantification of glomerular tuft volume (VG) measurement in WT (white bar, neonate: n = 6; 1 week old: n = 8; 3 weeks old: n = 9) and AT_2RKO mice (black bar, neonate: n = 15; 1 week old: n = 9; 3 weeks old: n = 6). (F) Nephrin protein expression analyzed by WB in isolated glomeruli from 3-week-old WT (white bar, n = 6) and AT_2RKO (black bar, n = 6) mice. Nephrin levels were normalized by their corresponding β-actin levels. **$p \leq 0.01$; ***$p \leq 0.001$. NS = non-significant.

Figure 14

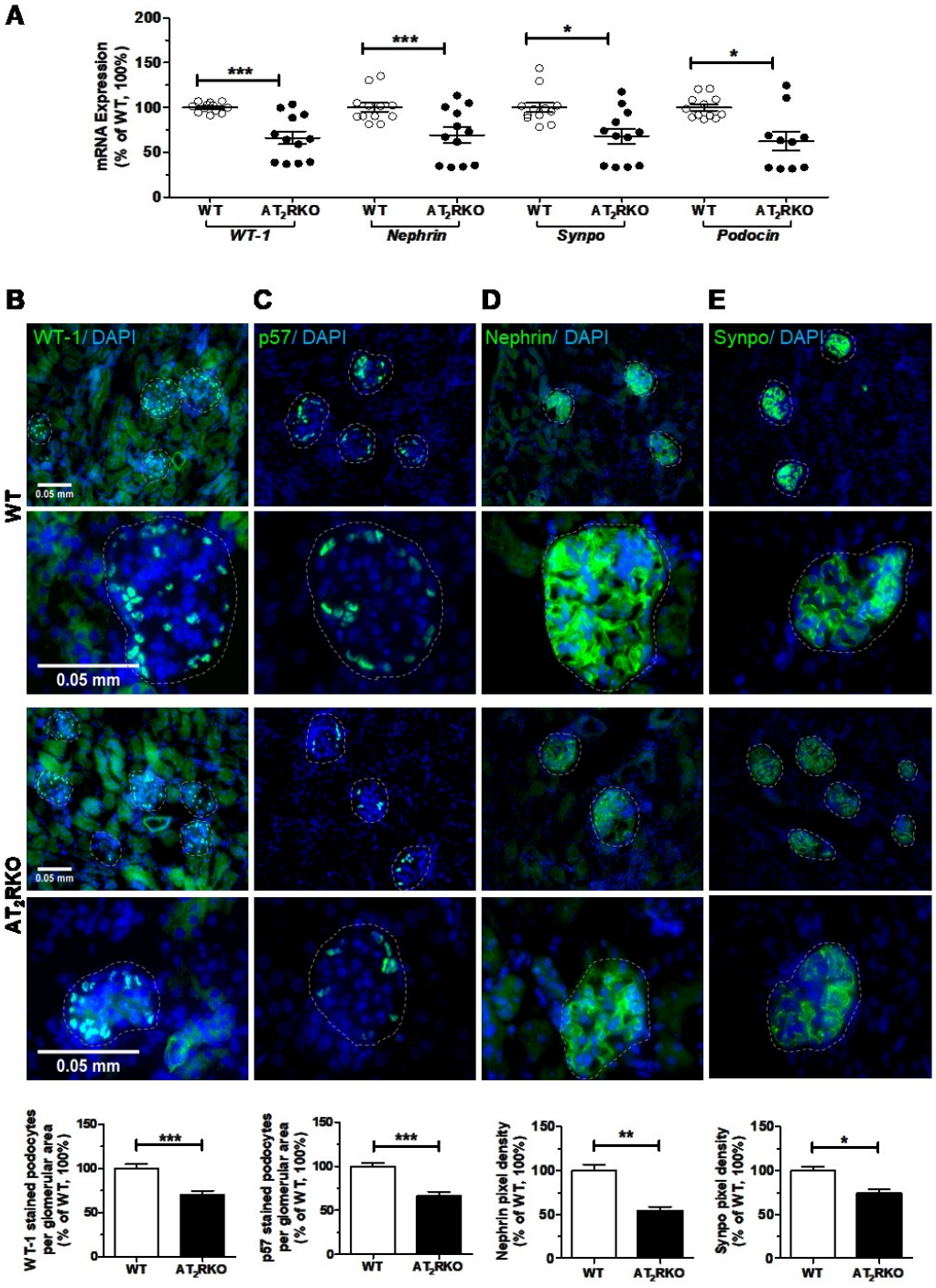
A
mRNA Expression (% of WT, 100%)
200
150
100
50
0
***
***
*
*
WT
AT2RKO
WT-1
Nephrin
Synpo
Podocin
B
C
D
E
WT-1/ DAPI
p57/ DAPI
Nephrin/ DAPI
Synpo/ DAPI
WT
AT2RKO
0.05 mm
WT-1 stained podocytes per glomerular area (% of WT, 100%)
p57 stained podocytes per glomerular area (% of WT, 100%)
Nephrin pixel density (% of WT, 100%)
Synpo pixel density (% of WT, 100%)
***
***
**
*

Figure 14. Podocyte marker analysis *in vivo*. (A) RT-qPCR analysis in isolated glomeruli from WT and AT_2RKO mice at the age of 3 weeks. (B–E) Podocyte markers' IF staining in glomeruli of kidneys from WT and AT_2RKO mice at the age of 3 weeks; % of podocyte numbers per glomerular cross-section in analysis of podocyte density per glomerular area (number per μm^2) based on WT-1 (B) and p57 (C) IF staining. Semi-quantification of fluorescent nephrin (D) and Synpo (E) staining. *$p \leq 0.05$; **$p \leq 0.01$; ***$p \leq 0.001$.

Figure 15

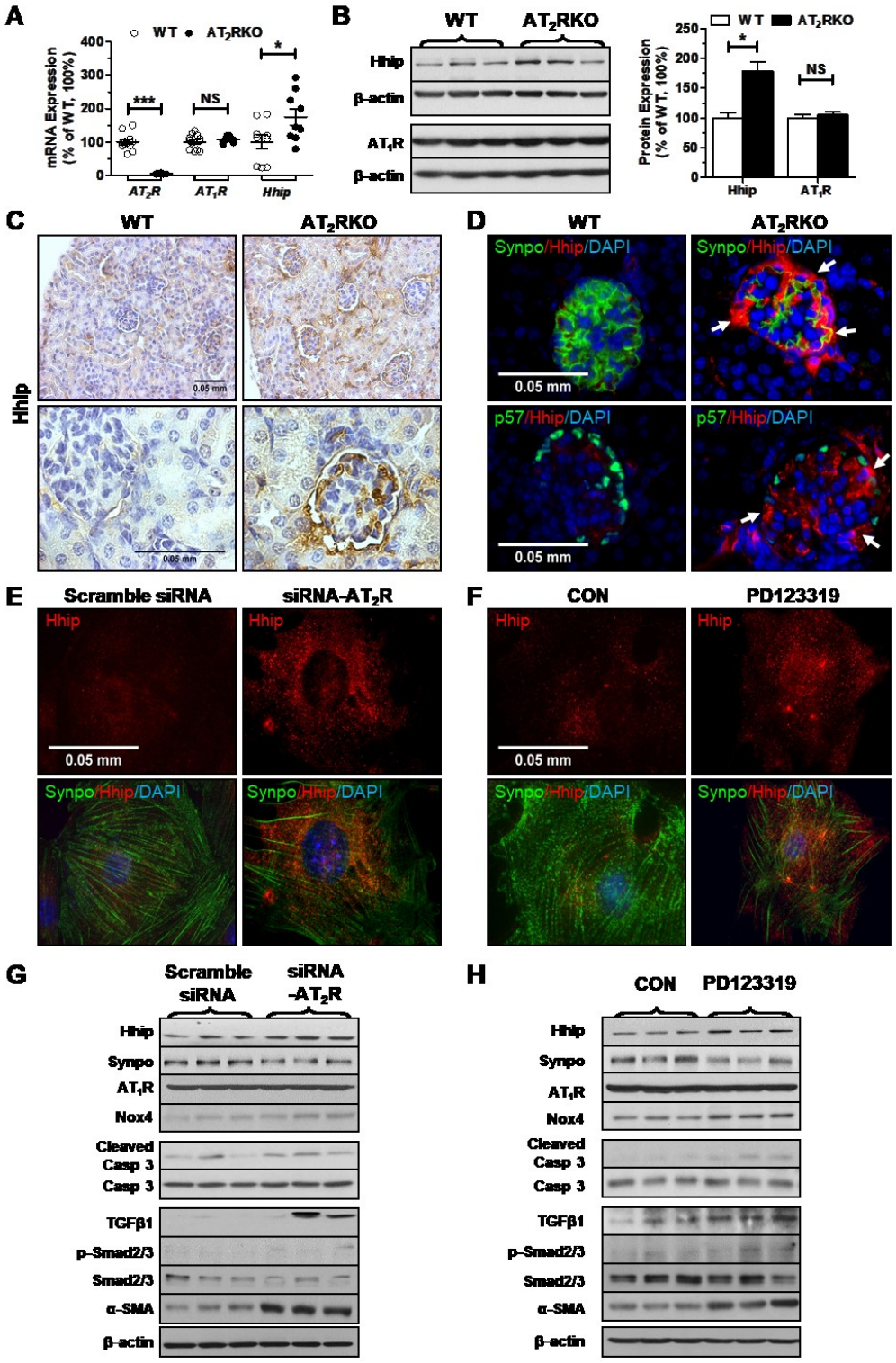
A
WT
AT2RKO
mRNA Expression (% of WT, 100%)
400
300
200
100
0
***
NS
*
AT2R
AT1R
Hhip
B
WT
AT2RKO
Hhip
β-actin
AT1R
β-actin
WT
AT2RKO
Protein Expression (% of WT, 100%)
250
200
150
100
50
0
*
NS
Hhip
AT1R
C
WT
AT2RKO
Hhip
0.05 mm
0.05 mm
D
WT
AT2RKO
Synpo/Hhip/DAPI
Synpo/Hhip/DAPI
0.05 mm
p57/Hhip/DAPI
p57/Hhip/DAPI
0.05 mm
E
Scramble siRNA
siRNA-AT2R
Hhip
Hhip
0.05 mm
Synpo/Hhip/DAPI
Synpo/Hhip/DAPI
F
CON
PD123319
Hhip
Hhip
0.05 mm
Synpo/Hhip/DAPI
Synpo/Hhip/DAPI
G
Scramble siRNA
siRNA -AT2R
Hhip
Synpo
AT1R
Nox4
Cleaved Casp 3
Casp 3
TGFβ1
p-Smad2/3
Smad2/3
α-SMA
β-actin
H
CON
PD123319
Hhip
Synpo
AT1R
Nox4
Cleaved Casp 3
Casp 3
TGFβ1
p-Smad2/3
Smad2/3
α-SMA
β-actin

Figure 15. Hhip expression *in vivo* and *in vitro*. (A–D) *In vivo*. (A, B) AT_1R, AT_2R, and Hhip expression (A, RT-qPCR; B, WB) in isolated glomeruli from 3-week-old WT and AT_2RKO mice. mRNA and protein levels were normalized by their corresponding β-actin levels. *$p \leq 0.05$; ***$p \leq 0.001$. NS = non-significant. (C, D) Hhip-IHC staining (C) or IF co-staining (Synpo and Hhip; p57 and Hhip) in kidneys of WT and AT_2RKO mice at the age of 3 weeks (D). (E–H) *In vitro*. (E, F) Synpo and Hhip IF co-staining in mPODs treated with 50 nM AT_2R siRNA (E) or PD123319 (10^{-8} M) (F). (G, H) WB analysis in mPODs treated with 50 nM AT_2R siRNA (G) or PD123319 (10^{-8} M) (H).

Figure 16

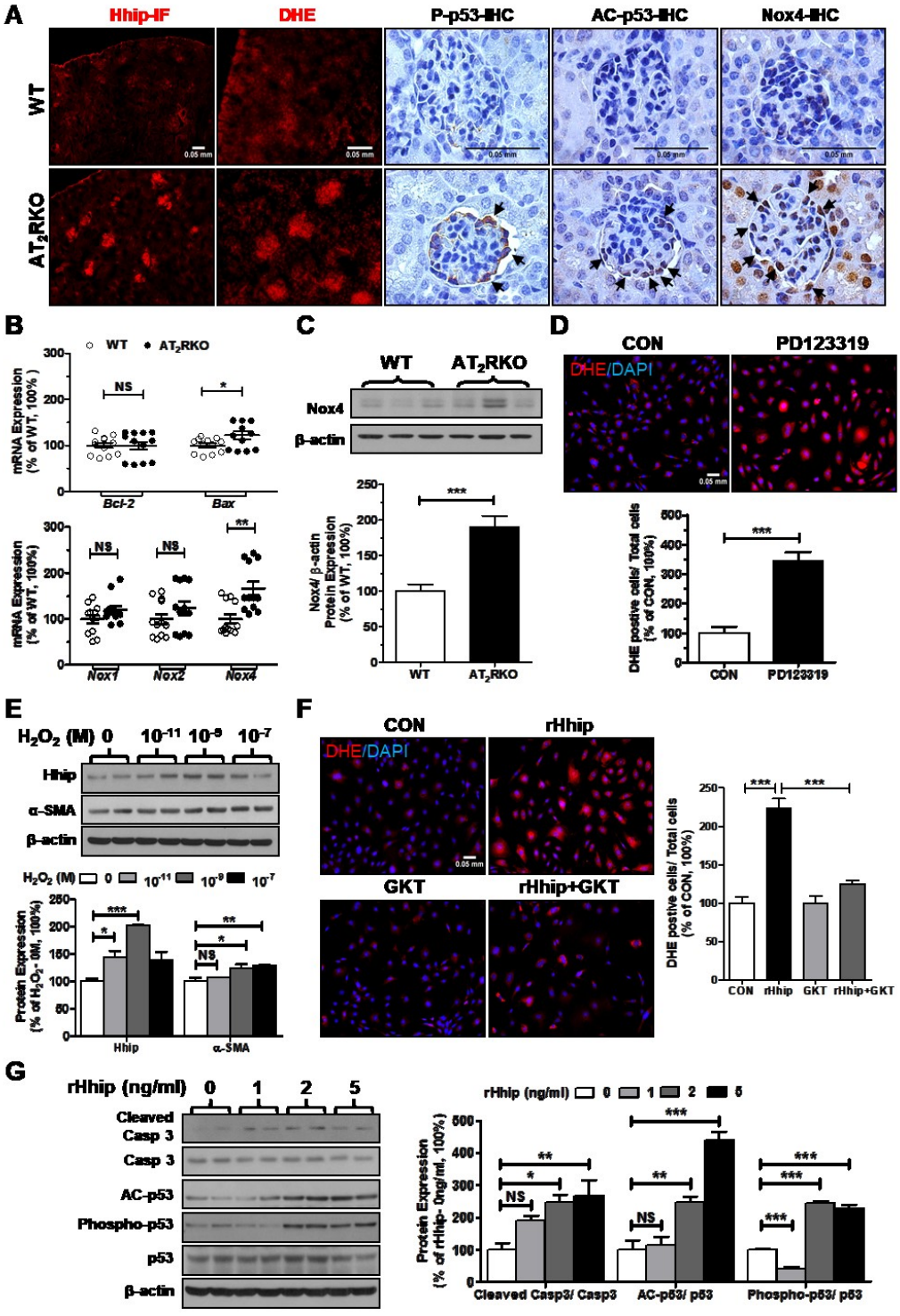
A
Hhip-IF
DHE
P-p53-IHC
AC-p53-IHC
Nox4-IHC
WT
AT2RKO
B
WT
AT2RKO
mRNA Expression (% of WT, 100%)
NS
*
Bcl-2
Bax
mRNA Expression (% of WT, 100%)
NS
NS
**
Nox1
Nox2
Nox4
C
WT
AT2RKO
Nox4
β-actin
Nox4/ β-actin Protein Expression (% of WT, 100%)
***
WT
AT2RKO
D
CON
PD123319
DHE/DAPI
DHE postive cells/ Total cells (% of CON, 100%)
***
CON
PD123319
E
H2O2 (M) 0
10-11
10-9
10-7
Hhip
α-SMA
β-actin
H2O2 (M) 0 10-11 10-9 10-7
Protein Expression (% of H2O2- 0M, 100%)
Hhip
α-SMA
F
CON
rHhip
DHE/DAPI
GKT
rHhip+GKT
DHE postive cells/ Total cells (% of CON, 100%)
CON
rHhip
GKT
rHhip+GKT
G
rHhip (ng/ml) 0 1 2 5
Cleaved Casp 3
Casp 3
AC-p53
Phospho-p53
p53
β-actin
rHhip (ng/ml) 0 1 2 5
Protein Expression (% of rHhip- 0ng/ml, 100%)
Cleaved Casp3/ Casp3
AC-p53/ p53
Phospho-p53/ p53

Figure 16. Hhip expression and ROS generation. (A–C) *In vivo*. (A) IF (Hhip), DHE, and IHC staining (phospho-p53, AC-p53, and Nox4) in kidneys of WT and AT_2RKO mice at the age of 3 weeks. (B) RT-qPCR of *Bcl-2*, *Bax*, *Nox1*, *Nox2*, and *Nox4* mRNA in isolated glomeruli of WT and AT_2RKO mice at the age of 3 weeks. (C) Nox4 protein expression analyzed by WB in isolated glomeruli from 3-week-old WT (white bar, n = 6) and AT_2RKO (black bar, n = 6) mice. Nox4 levels were normalized by their corresponding β-actin levels. (D–G) *In vitro*. (D) DHE staining in mPODs treated with or without PD123319 (10^{-8} M). (E) WB analysis in mPODs treated with or without H_2O_2. Hhip and α-SMA levels were normalized by their corresponding β-actin levels. (F) DHE staining in mPODs treated with or without rHhip. (G) WB analysis in mPODs treated with or without rHhip. *$p \leq 0.05$; **$p \leq 0.01$; ***$p \leq 0.001$. NS = non-significant.

Figure 17

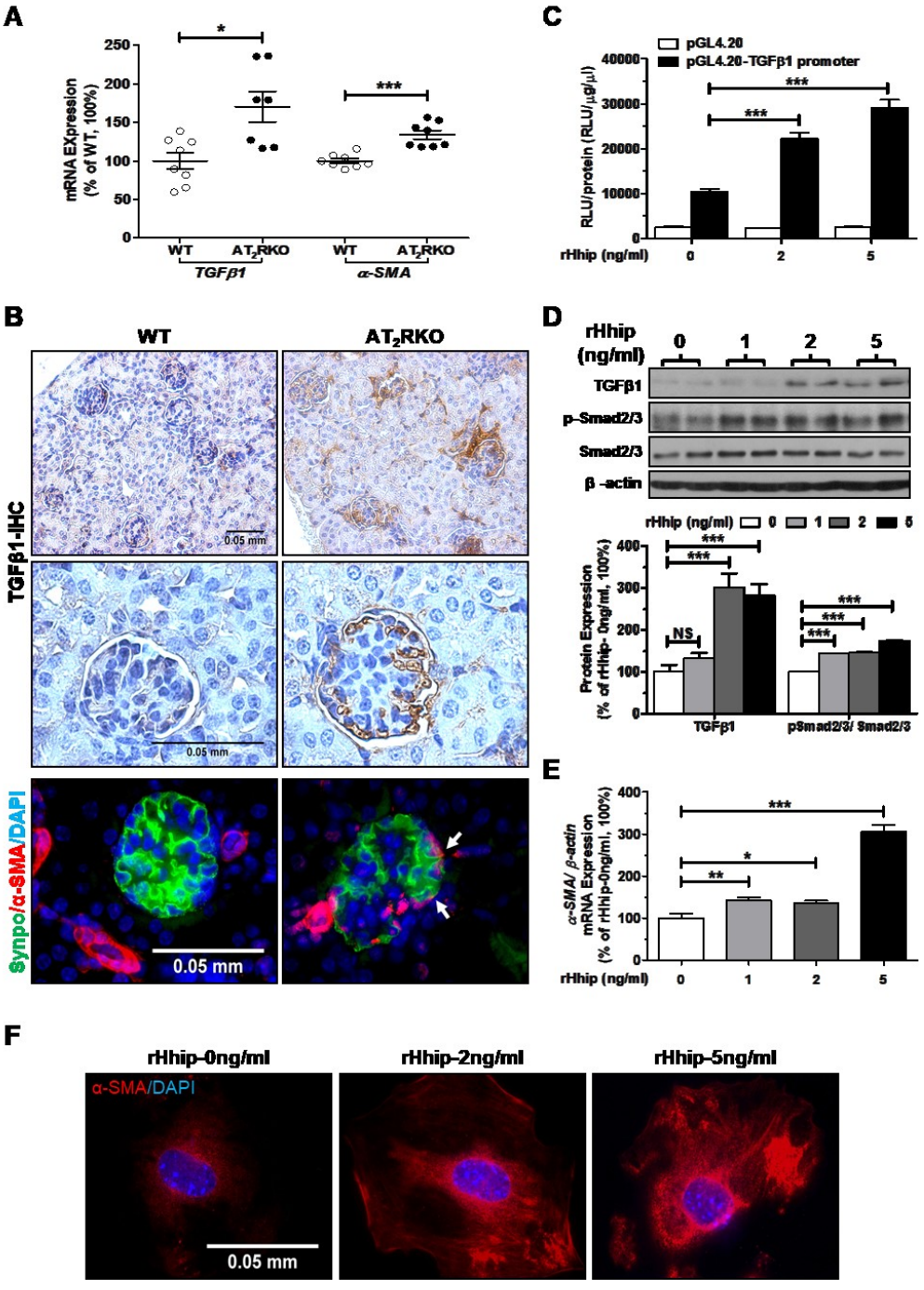
A
mRNA EXpression (% of WT, 100%)
WT
AT2RKO
TGFβ1
α-SMA
B
WT
AT2RKO
TGFβ1-IHC
Sympo/α-SMA/DAPI
0.05 mm
C
pGL4.20
pGL4.20-TGFβ1 promoter
RLU/protein (RLU/μg/μl)
rHhip (ng/ml)
D
rHhip (ng/ml)
TGFβ1
p-Smad2/3
Smad2/3
β -actin
Protein Expression (% of rHhip- 0ng/ml, 100%)
NS
pSmad2/3/ Smad2/3
E
α-SMA/ β-actin mRNA Expression (% of rHhip-0ng/ml, 100%)
F
rHhip-0ng/ml
rHhip-2ng/ml
rHhip-5ng/ml
α-SMA/DAPI

Figure 17. Hhip and TGFβ1-induced EMT. (A, B) *In vivo*. (A) RT-qPCR of *TGFβ1* and *α-SMA* mRNA expression in isolated glomeruli of WT and AT_2RKO at the age of 3 weeks. (B) TGFβ1 IHC and Synpo/α-SMA IF staining in kidneys of WT and AT_2RKO mice at the age of 3 weeks (arrow, Synpo/α-SMA co-localization). (C–F) *In vitro*. (C) pGL4.20-rTGFβ1 promoter activity in mPODs treated with or without rHhip. Promoter activity (RLU) was normalized by the protein concentration (µg/µl). (D) WB analysis in mPODs treated with or without rHhip. (E, F) α-SMA expression in mPODs treated with or without rHhip (E, RT-qPCR; F, IF staining). *$p \leq 0.05$; **$p \leq 0.01$; ***$p \leq 0.001$. NS = non-significant.

Figure 18

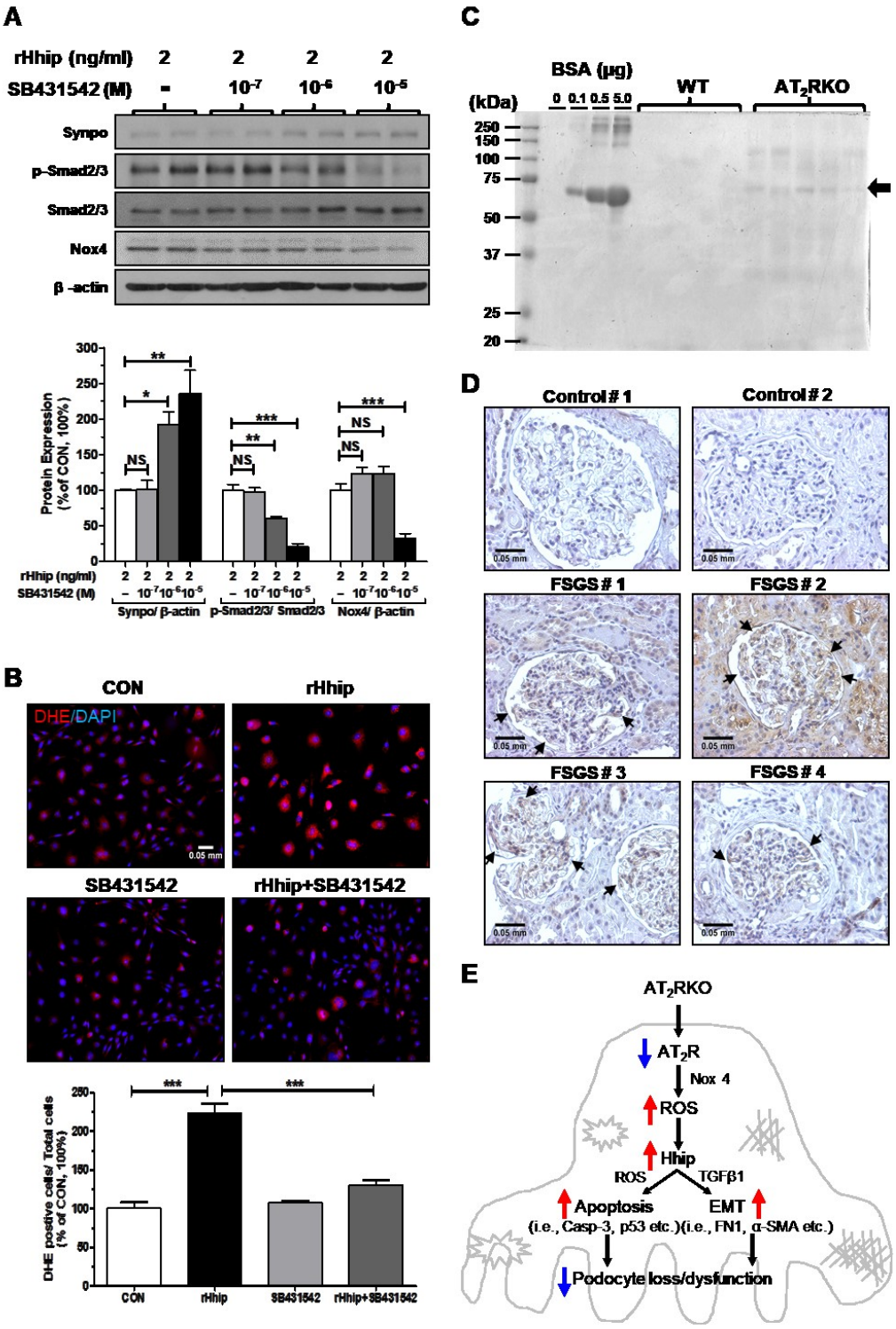
A
rHhip (ng/ml) 2 2 2 2
SB431542 (M) - 10-7 10-6 10-5
Synpo
p-Smad2/3
Smad2/3
Nox4
β -actin
Protein Expression (%of CON, 100%)
Synpo/ β-actin
p-Smad2/3/ Smad2/3
Nox4/ β-actin
B
CON
rHhip
DHE/DAPI
SB431542
rHhip+SB431542
DHE positive cells/ Total cells (% of CON, 100%)
C
BSA (μg)
0 0.1 0.5 5.0
WT
AT2RKO
(kDa)
250
150
100
75
50
37
25
20
D
Control # 1
Control # 2
FSGS # 1
FSGS # 2
FSGS # 3
FSGS # 4
E
AT2RKO
AT2R
Nox 4
ROS
Hhip
ROS
TGFβ1
Apoptosis
EMT
(i.e., Casp-3, p53 etc.)(i.e., FN1, α-SMA etc.)
Podocyte loss/dysfunction

Figure 18. The interaction of Hhip and TGFβRI. (A, B) *In vitro*. (A) WB analysis and (B) DHE staining in mPODs treated with or without TGFβRI inhibitor. (C) Urinary albumin level analyzed by Coomassie Blue gel staining in vivo. (D) HHIP IHC in kidney biopsy samples. (E) A working model of AT_2R deficiency-mediated podocyte loss/dysfunction. In brief, loss of AT_2R via ROS generation (probably mediated by Nox4) stimulates ectopic Hhip expression, which in turn triggers podocyte apoptosis by activation of the caspase-3 and p53 pathways. Concomitantly, the augmented Hhip interacts with TGFβRI/RII to trigger TGFβ1/Smad2/3 signaling and then transform differentiated podocytes into undifferentiated podocyte-derived fibrotic cells.

Supplementary Materials

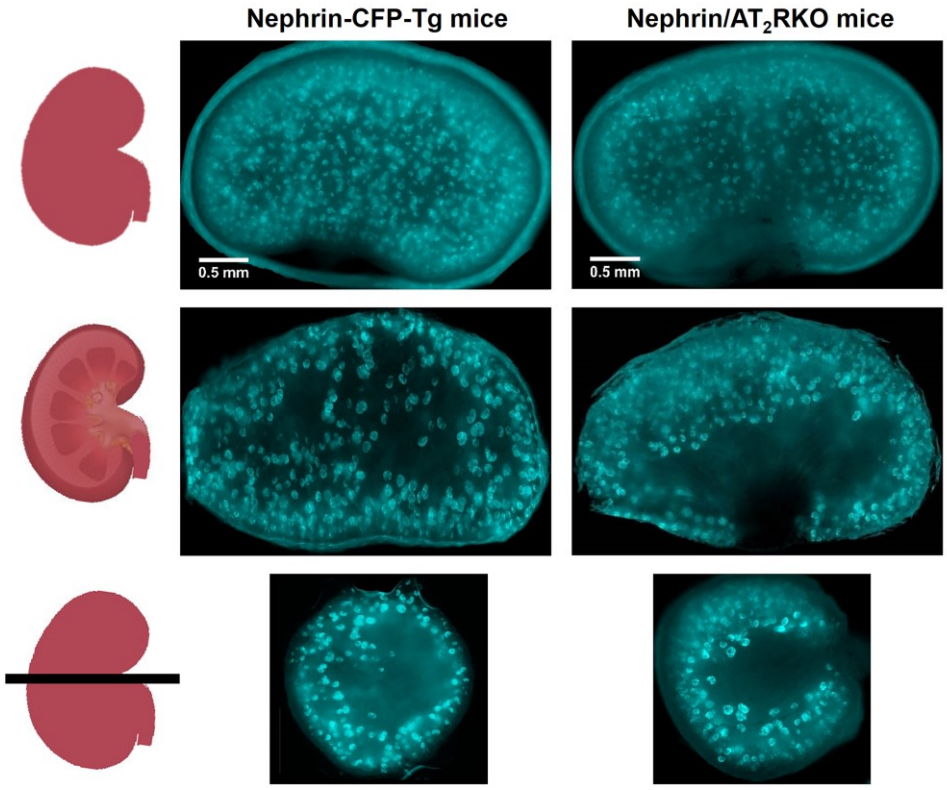

Figure 19. Images of freshly isolated neonatal kidneys (whole-mount and frontal versus transverse sections) from Nephrin-CFP-Tg versus Nephrin/AT_2RKO mice.

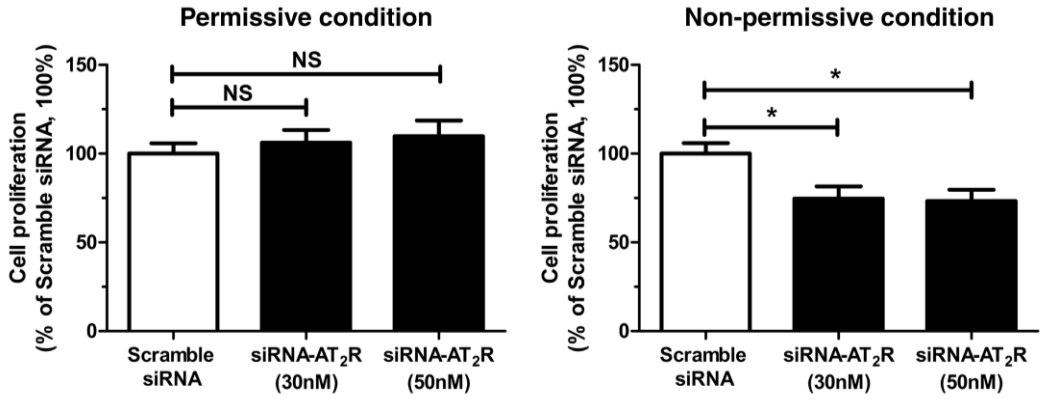

Figure 20. Proliferation study on silencing AT_2R (siRNA) in mPODs under permissive (33°C with 10 U/ml INF-γ) and non-permissive conditions (37°C without INF-γ). *$p \leq$ 0.05. NS = non-significant.

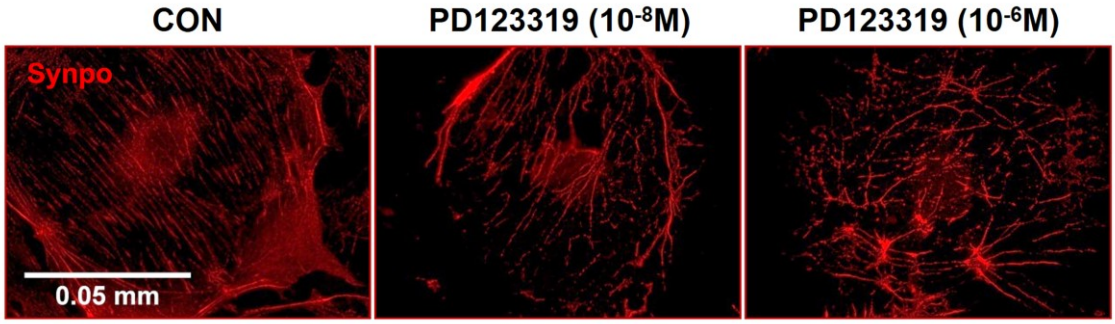

Figure 21. Synpo IF staining in mPODs treated with or without PD123319 in a dose-dependent manner.

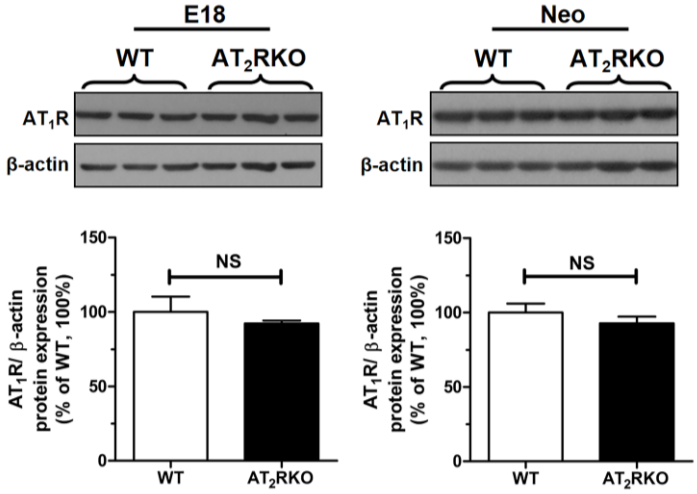

Figure 22. Renal AT_1R protein expression in E18 and neonatal kidneys from wild-type versus AT_2RKO mice analyzed by western blotting.

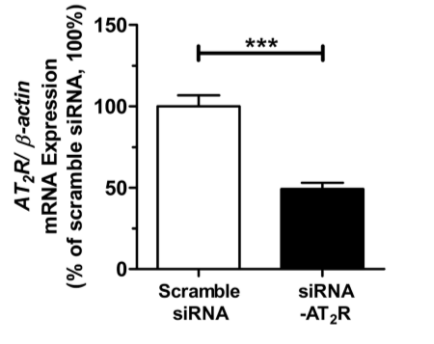

Figure 23. RT-qPCR assessment of *AT_2R* mRNA expression in mPODs treated with AT_2R siRNA (50 nM).

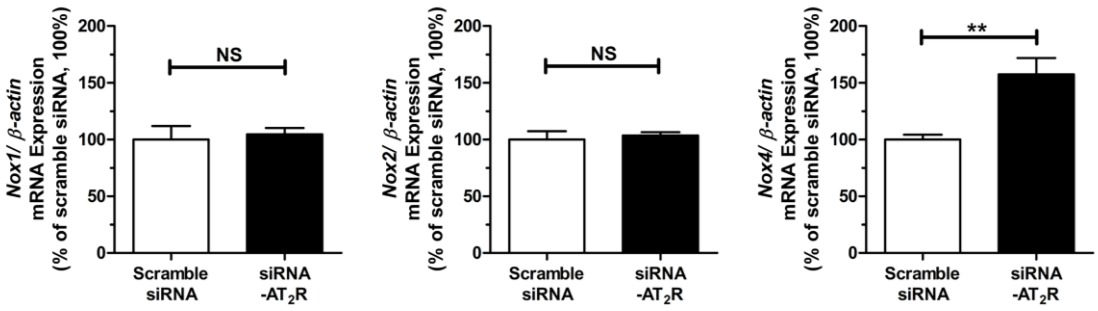

Figure 24. RT-qPCR assessment of *Nox1*, *Nox2*, and *Nox4* mRNA expression in mPODs treated with AT_2R siRNA (50 nM).

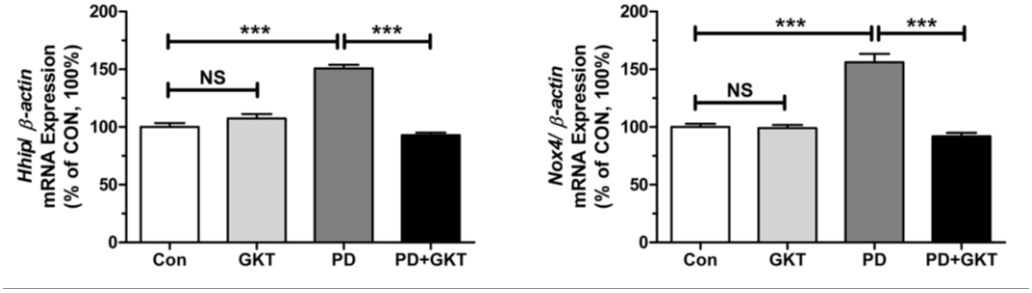

Figure 25. RT-qPCR assessment of *Hhip* and *Nox4* mRNA expression in mPODs treated with GKT (10^{-6} M), PD (10^{-8} M), and PD + GKT. Abbreviation: GKT: GKT137831; PD: PD123319.

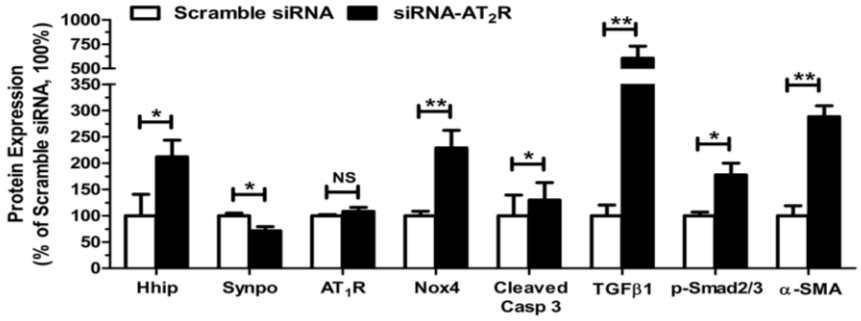

Figure 26. Semi-quantification of Figure 15G *in vitro*. Western blot analysis in mPODs treated with AT_2R siRNA (50 nM). The relative densities of target proteins were compared with that of β-actin. Smad2/3 phosphorylation and cleaved caspse-3 were compared with Smad2/3 and total caspase-3, respectively. Values in scramble siRNA were considered as 100%.

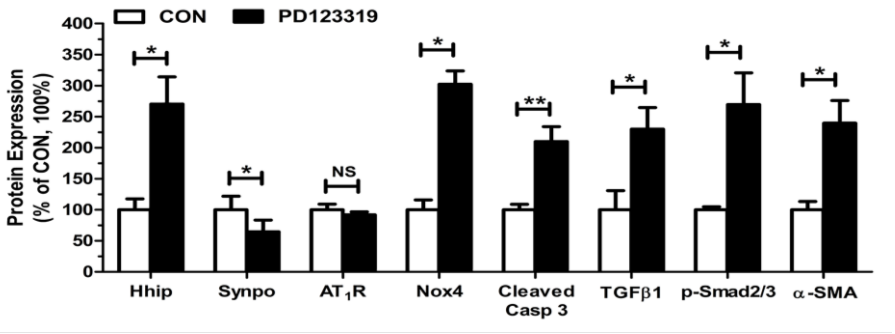

Figure 27. Semi-quantification of Figure 15H *in vitro*. Western blot analysis in mPODs treated with PD123319 (10^{-8} M). The relative densities of target proteins were compared with that of β-actin. Smad2/3 phosphorylation and cleaved caspse-3 were compared with Smad2/3 and total caspase-3, respectively. Values in the control were considered as 100%.

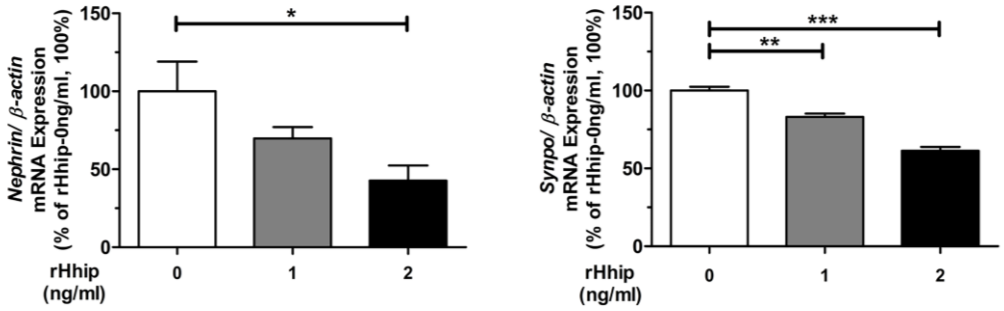

Figure 28. RT-qPCR assessment of *Nephrin* and *Synpo* mRNA expression in mPODs treated with rHhip in a dose-dependent manner.

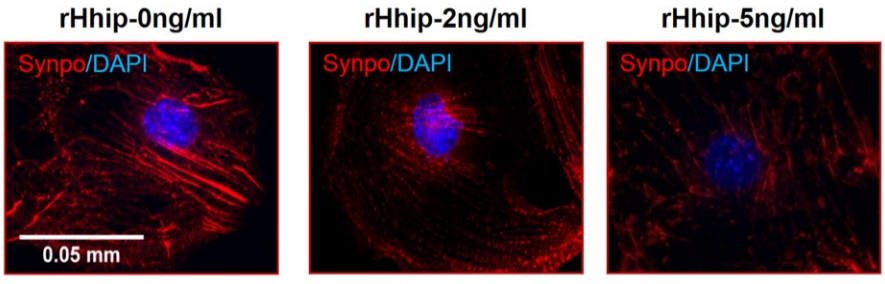

Figure 29. Synpo IF expression in mPODs treated with rHhip in a dose-dependent manner.

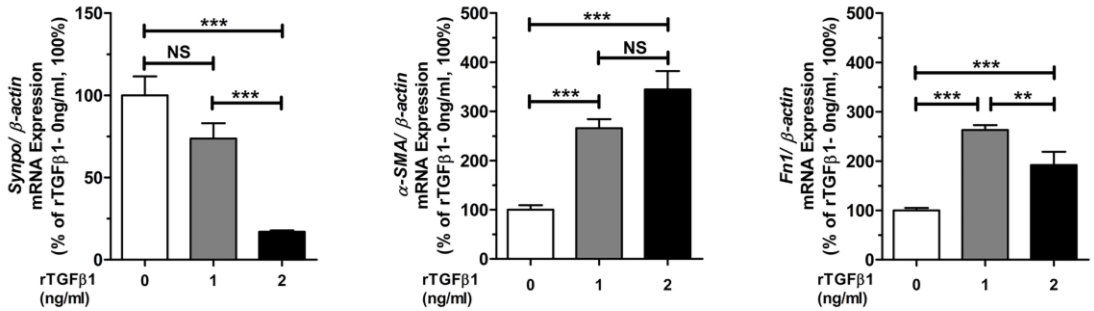

Figure 30. RT-qPCR assessment of *Synpo*, *α-SMA*, and *Fn1* mRNA expression in mPODs treated with rTGFβ1 in a dose-dependent manner.

Figure 31

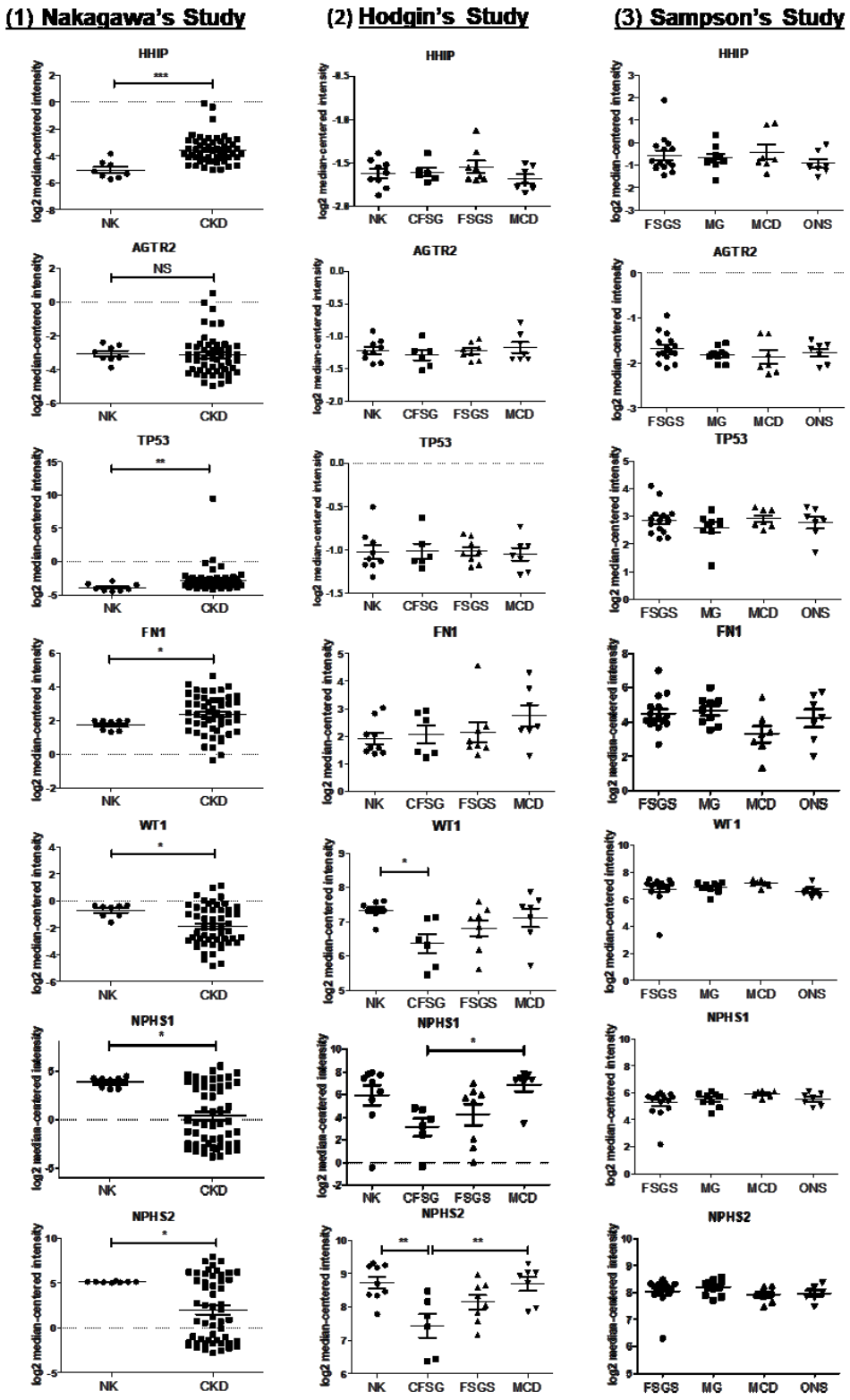
(1) Nakagawa's Study
(2) Hodgin's Study
(3) Sampson's Study
HHIP
AGTR2
TP53
FN1
WT1
NPHS1
NPHS2
log2 median-centered intensity
log2 median-centered intensity
NK
CKD
CFSG
FSGS
MCD
MG
ONS
FSGS
NS
*
**
***

Figure 31. Nephroseq analysis of three publicly available microarray studies performed on human kidney biopsy samples: (1) Nakagawa Chronic Kidney Disease Study; (2) Hodgin Focal Segmental Glomerulosclerosis Glomerular Study; (3) Sampson Nephrotic Syndrome Glomerular Study.

1.3 Discussion

AT_2R deficiency-mediated podocyte loss via activation of ectopic hedgehog interacting protein (Hhip) gene expression

The most significant finding of the present study is that AT_2R deficiency altered podocyte numbers and functions from regular to a depleted and/or a fibrotic-like phenotype. This change in the podocyte resulted in detectable albumin leakage in AT_2RKO mice, at least in part, via increased Hhip expression. Thus, AT_2R plays a critical role in regulating the maturation, integrity, and function of podocyte and exerting renoprotective effects.

The Effects of AT_2R Deficiency in the Embryonic Kidney

AT_2R is highly expressed in fetal tissues and continuously expressed in low abundance in specific adult tissues, but its regulation and function in specific cell types of the kidney during embryonic development has not been established. This receptor is expressed at a high level in fetal UB and metanephric mesenchyme lineage derivatives [21, 92], whereas it is also present to a lesser extent in healthy adult glomerular endothelial cells, podocytes, tubular epithelial cells, renal vasculature, and inner medullary collecting duct [22, 93]. Only 3.1% of AT_2RKO newborn mice exhibit renal dysplasia and other features of CAKUT. Intriguingly, abnormal UB budding accounts for 59.5% of renal malformations in E11 AT_2RKO embryos, suggesting that the majority of these malformations might be underestimated due to undetectable renal specific cells' structural modification or undergo self-correction *in utero* by unclear means [94]. Besides, Song et al. [95] and our previous studies [88] demonstrated that the number of UB tips in E13.5 AT_2RKO embryos was decreased compared to E13.5 WT embryos, suggesting that initial redundant UB budding in these embryos is via reduced UB branching to correct the abnormal UB budding. Thus, AT_2R plays an essential role in regulating reciprocal inductive interactions between the UB and the metanephric mesenchyme. However, it is unclear whether the influence of AT_2R deficiency would subsequently affect glomerulogenesis, nephron number, and kidney function in later life. In the present work, we have a study to investigate the glomerulogenesis with the use of fluorescence microscopy in Nephrin-CFP-Tg vs. Nephrin/AT_2RKO mice. We demonstrated that the embryonic kidneys of E14-E15 Nephrin/AT_2RKO fetus had fewer CFP-positive glomeruli with a grossly smaller

kidney size. However, there is no apparent difference in the glomerular number from E17 to the neonate.

The Impact of AT_2R Deficiency on the Podocyte

Both our present work and previous studies [88] reported that AT_2RKO mice exhibited renal hypoplasia (i.e., abnormally small kidneys with normal morphology and a lower nephron number). Although there is a similar nephron number in AT_2RKO and WT mice, AT_2RKO mice have significantly lower mean glomerular tuft volume from neonate to three weeks of age. Thus, inhibiting AT_2R signaling might regulate the maturation, integrity, and function of glomerular specific cell types (e.g., podocytes). There is accumulating evidence that the AT_2R agonist, CGP42112A, upregulates the functional molecules of the slit diaphragm, and C21, the other AT_2R agonist, administration reduces renal fibrosis and, in combination with ARB, restores glomerular nephrin expression and reduces albuminuria in an experimental animal model of Type 2 diabetes. In three weeks old AT_2RKO mice, we observed significantly decreased podocyte-specific markers, such as nephrin, WT-1, p57, synaptopodin, and podocin, and detectable urinary albumin leakage, indicating that AT_2R regulates the formation and integrity of podocytes.

The Expression Level of AT_1R in Three Week-old AT_2RKO Mice

It has been a challenge to determine the biological function of AT_2R because its role is hidden by the predominant actions of Ang II via AT_1R. In the adult mammalian kidney, AT_1R is expressed primarily in glomeruli and at lower levels in the cortical tubules. Although AT_1R expression increases in glomeruli [96] and renal proximal tubules [97] of adult AT_2RKO mice, we found that AT_1R expression in three week-old AT_2RKO mice did not differ in mRNA and protein levels in isolated glomeruli. This discrepancy might be due to distinct methodology and the age of mice. It has been reported that AT_1R expression is negatively associated with age (i.e., highest level in the fetus and lowest in adult tissue) [98]. This observation could explain why levels of AT_1R are similar between three week-old AT_2RKO and WT mice. Although the level of AT_2R is higher than that of AT_1R in the E14 embryonic kidney, there is no difference between AT_1R and AT_2R at E20 [92]. After birth, the expression levels of both receptors decreases in the kidney, but the level of AT_1R remains much higher than that of

AT_2R in adult kidneys. This dynamic expression of these receptors suggests that both receptors have a distinct biological function to regulate kidney development and maintain healthy kidney function.

The Impact of AT_2R Deficiency on Hhip Expression

Stimulation of AT_2R by Ang II may usually counterbalance AT_1R activation, and that stimulation of AT_2R combined with ARB is therapeutically beneficial. The glomeruli of AT_2RKO mice have been shown to have elevated ROS and Nox4 expression and activated TGFβ1 signaling, suggesting that AT_2R deficiency may increase the effects of Ang II via AT_1R. The mechanisms of ROS-induced apoptosis and TGFβ1-related epithelial–to–mesenchymal transition (EMT) have been well established in the pathogenesis of podocyte loss/dysfunction [99-101]. However, it is not clear if the alterations in podocyte in AT_2RKO mice, such as increased ROS and TGFβ1 activation, are mediated directly through AT_2R deficiency or indirectly through AT_1R.

Our previous study has demonstrated that the offspring of maternal diabetes exhibited impaired kidney development caused by the ROS, Hhip, and TGFβ1 signaling cross-talk. Also, the offspring of maternal diabetes have renal hypoplasia, which is similar to AT_2RKO mice. Hence, we hypothesized that AT_2R deficiency promotes Hhip ectopic expression in podocytes, leading to podocyte loss/dysfunction. To address our hypothesis, we conducted several studies to demonstrate Hhip expression in podocytes *in vivo* and *in vitro*. As expected, Hhip expression was higher in the glomeruli of AT_2RKO mice than in those of WT mice. Indeed, Hhip co-localized with synaptopodin, which is a podocyte-specific protein expressed in the cytosol and increased in immortalized mouse podocytes when AT_2R signalling is inhibited. Also, we observed increased ROS, Nox4 and TGFβ1 in the podocytes of AT_2RKO mice and the AT_2R-knockdown mPODs, suggesting that Hhip might be a mediator causing podocyte loss/dysfunction in those mice. *In vitro*, AT_2R deficiency in mPODs increased Hhip and Nox4 expression, causing the collapse of cytoskeleton actin integrity, likely via the activation of cleaved caspase-3 and the EMT-related TGFβ1–Smad2/3 pathway in podocytes. However, the relationship between ROS, Hhip and TGFβ1 and whether they act separately or in concert to contribute to podocyte dysfunction requires further studies.

The Role of Hhip on ROS Generation

Nox4 is the main NADPH oxidase isoform in the kidney and produces primarily H_2O_2 that regulates renal functions and injuries [86]. Because of an increased Nox4 expression in AT_2RKO mice, we have conducted an *in vitro* study to investigate the impact of H_2O_2 on mPODs. We demonstrated that H_2O_2 stimulated Hhip expression in a dose-dependent manner and increased *de novo* α-SMA synthesis. Then, Nox1/Nox4 inhibitor, GKT137831, attenuated ROS in mPODs in which AT_2R is blocked by using the AT_2R antagonist, PD123319. These data underscore that inhibiting AT_2R signaling via Nox4-derived production of ROS stimulates Hhip expression in mPODs, leading to podocyte injury. Our data further revealed that rHhip was associated with an increased production of ROS, which was attenuated by GKT137831 in mPODs, suggesting a positive autocrine feedback loop of ROS–Hhip, possibly via the activation of Nox4. Additionally, rHhip stimulated an increase in cleaved caspase-3 and acetylated p53 protein expression in mPods, which were similar effects to the inhibition of AT_2R by PD123319. In summary, AT_2R deficiency stimulates Hhip expression, which then may prompt podocyte apoptosis; this process may be mediated, at least in part, via Nox4-derived ROS generation.

The Impact of Hhip on Podocyte Transition

It has been reported that the exogenous TGFβ1 stimulates mitochondrial Nox4 expression in mouse podocyte in a Smad2/3-dependent pathway which is responsible for ROS generation and apoptosis, and that knockdown of either Smad2 or Smad3 prevents Nox4-induced podocyte apoptosis [86, 102]. Our *in vitro* data indicated that rHhip stimulated TGFβ1–Smad2/3 signaling in mPods and also that the effects of increased Nox4 expression and ROS generation were blunted by an inhibitor of TGFβRI, SB431532. These findings suggested that AT_2R deficiency can increase Hhip leading to podocyte apoptosis, while enhanced Hhip further induces TGFβ1–Smad2/3 signaling, Nox4 expression, and ROS generation, forming a vicious cycle, ultimately leading to podocyte loss/dysfunction. On the other hand, TGFβ1 is a profibrotic protein and the most potent inducer capable of initiating and completing the entire EMT processes [73]. We noted that lack of AT_2R stimulated EMT-related inducer and marker, as shown by activation of TGFβ1–Smad2/3 signaling and enhanced α-SMA expression in the podocyte both *in vivo* and *in vitro*. Additionally, the action

of rHhip on TGFβ1–Smad2/3 signaling in mPods was inhibited by SB431532, suggesting that Hhip impairs the podocyte via a TGFβRI-dependent manner. However, it is unclear whether Hhip directly or indirectly interacts with TGFβRI. Although we found that Hhip directly stimulated TGFβ1 expression, the interaction between Hhip and TGFβRI still merits further investigation.

The Application of the Findings on Clinical Studies

FSGS is one of the most common forms of glomerular disease, usually following the disturbances in podocyte structure, number, and function in experimental animals and humans. According to a Nephroseq analysis, patients with FSGS in the Nakagawa CKD Kidney study had upregulated *HHIP*, whereas podocyte markers were downregulated (i.e., *NPHS1*, *NPHS2*, and *WT1*). In human kidney biopsies, we observed an increase of HHIP in the glomeruli of FSGS patients compared with controls, indicating that glomerular cells, including podocytes, displayed an increase of HHIP expression. In human, podocyte depletion may result from upregulation of HHIP in podocytes, which is in line with our findings in mice. However, *AGTR2* levels were not different in patients with CKD and FSGS; the biological functions of AGTR2 might possibly have differences in patients.

1.4 Summary

As a summary of the article 1, we have shown that:

– Loss of AT_2R via Nox4-derived ROS stimulates ectopic Hhip expression, which in turn triggers podocyte apoptosis by activation of the caspase-3 and p53 pathways.

– The augmented Hhip triggers the activation of TGFβ1–Smad2/3 signaling and then drives podocyte transition from normal morphology to a fibrotic-like phenotype.

In conclusion, our data suggest that AT_2R deficiency is linked to podocyte depletion and dysfunction, at least in part, via increased ectopic Hhip expression in podocytes.

1.5 Before Chapter 2

AT_2R is highly implicated in CAKUT in both humans and mice [25, 34, 41]. However, the underlying mechanisms causing the renal malformations in AT_2R variants remain unclear, particularly with respect to the possible molecular, developmental, and *in utero* environmental interactions that lead to the kidney abnormalities. In chapter 1, I study the role of *AT_2R* gene on glomerulogenesis and its relevant mechanisms

CAKUT may occur in offspring of women with gestational diabetes or antecedent diabetes, are the most prevalent of abnormalities observed. In chapter 2, I study whether a diabetic environment *in utero* is postulated to alter the gene expression in developing kidneys and programs progeny for CKD and hypertension in adulthood.

CHAPTER 2

Aliou Y*, **Liao MC***, Zhao XP, Chang SY, Chenier I, Ingelfinger JR, Zhang SL: Post-weaning high-fat diet accelerates kidney injury, but not hypertension programmed by maternal diabetes. Pediatric Research, 2016; 79(3): 416-424. *The first two authors contributed equally to this work.

2.1 Introduction

2.1.1 Maternal Diabetes-induced Perinatal Programming

Diabetes in pregnancy affects health and is related to an increased risk of fetal, neonatal, and long-term complications in the offspring. Maternal diabetes might be pre-gestational diabetes (PGDM) (i.e., Type 1 or Type 2 diabetes diagnosed before pregnancy) or gestational diabetes (GDM) (i.e., diabetes diagnosed during pregnancy). The outcomes of complications, including hypertension, cardiovascular disease, and CKD, are associated with the beginning and length of glucose intolerance during pregnancy and also the severity of maternal diabetes. This phenomenon of maternal environmental factors that can change the phenotype and potential of offspring with enduring consequences later in life is also called perinatal programming. These key influences on lifetime health might reflect the perturbed or adapted biological mechanisms, including epigenetic, cellular, physiological, and metabolic processes. Numerous studies have indicated that CKD and hypertension in adulthood result from perinatal insults and maternal environmental changes in perinatal life [31]. Understanding these influences that occur in the perinatal period has the potential to identify and intervene in those people at higher risk for hypertension and kidney diseases during their lifetimes.

Both PGDM and GDM increase the risk of adverse maternal and children health outcomes. The prevalence of GDM among women who had a live birth is higher than of PDGM in the United States [103]. However, PGDM is associated with higher morbidity when compared to GDM [104]. Maternal diabetes increases infants' risk for macrosomia, congenital malformations, stillbirth, neonatal hypoglycemia, intrauterine growth restriction, and preterm

birth. The reason leading to adverse outcomes in PGDM and GDM is attributed to abnormal glucose levels affecting both the mother and fetus. According to the hyperglycemia and adverse pregnancy outcomes (HAPO) study, there is a linear relationship between maternal glucose levels and adverse pregnancy outcomes [105]. Thus, maternal diabetes is a critical medical condition for both mother and fetus.

There are clinically two distinct phenotypes of abnormal fetal growth which occur in the offspring of maternal diabetes, depending on the degree of diabetes [106]. One is fetal macrosomia and high birth weight (also called Big Baby Syndrome) which is the consequence of fetal overnutrition and occurs in moderately-controlled or well-controlled diabetic pregnancies. The other is fetal microsomia and low birth weight which occurs in severely diabetic pregnancies and is one of the consequences of intrauterine growth restriction (IUGR) when the fetus does not achieve the expected *in utero* growth potential due to genetic and environmental factors. Birth weight is a multiplex interaction between maternal environment and fetal genes. Both nutrients and hormones play an essential role in fetal development. A major nutrient for fetal development is glucose, which is acquired from the maternal circulation. The primary growth hormone for fetal development is insulin secreted by the fetus. In rodent studies, fetuses from mildly diabetic dams with mild hyperglycemia have been shown to have β-cell hyperactivity and hyperinsulinemia, leading to fetal macrosomia [106, 107].

In contrast, fetuses from severely diabetic dams with the extreme hyperglycemia have been shown to possess overstimulated fetal β-cells, resulting in inefficient insulin secretion, further leading to fetal microsomia. In addition to insulin levels from the fetus itself, the extreme glucose level impairs maternal placental growth and reduces placental functions, resulting in fetal growth restriction. Recent genome-wide association study (GWAS) demonstrated that genetically upregulated maternal blood glucose levels are associated with higher offspring birth weight [108], whereas fetal genetics for birth weight has a significant impact on fetal growth and is independent of maternal blood glucose levels [109, 110]. As there is a robust negative relationship between fetal loci associated with birth weight and future cardiometabolic diseases including hypertension, coronary artery disease, and Type 2

diabetes [109], fetal genotype might predominantly affect fetal growth without the same effects for future cardiometabolic diseases.

The Developmental Origins of Health and Disease (DOHaD) concept suggests that poor perinatal influences can increase the risks of hypertension, obesity, and Type 2 diabetes in adulthood [111]. These influences during the perinatal period are strongly linked to the onset and outcome of disorders and diseases in later life. There are several theories to describe the term "perinatal programming." The thrifty phenotype hypothesis suggests the ability of an individual to react to environmental changes (poor nutrition in early life) with an adaptive response (impaired β-cell development and function) [112]. That is to supply the utmost important organs and delay the development of non-urgent systems or organs. However, the ignored organs later become deficient, and diseases (e.g., Type 2 diabetes and the metabolic syndrome) become prevalent. This concept of perinatal programming is thought to compensate for poor developmental conditions actively. Furthermore, Plagemann proposed a further concept suggesting that perinatal programming is a vegetative learning process leading to passive adaptations of an individual [107]. That is, modifications of the intrauterine and neonatal environment may promote the development of a variety of diseases throughout later life. Natural and social environments, epigenomic plasticity, and microstructural plasticity are three key components that interact with each other and establish the phenotype of perinatal programming and DOHaD [113]. The proposal of perinatal hyperinsulinemia as a possible predisposing factor for diabetes and cardiovascular diseases in later life is summarized in Figure 32 [107]. Thus, the possibility to prevent permanently increased disposition for 'diabesity' is via prevention of perinatal hyperglycemia, hyperinsulinemia and overnutrition during critical periods of early development.

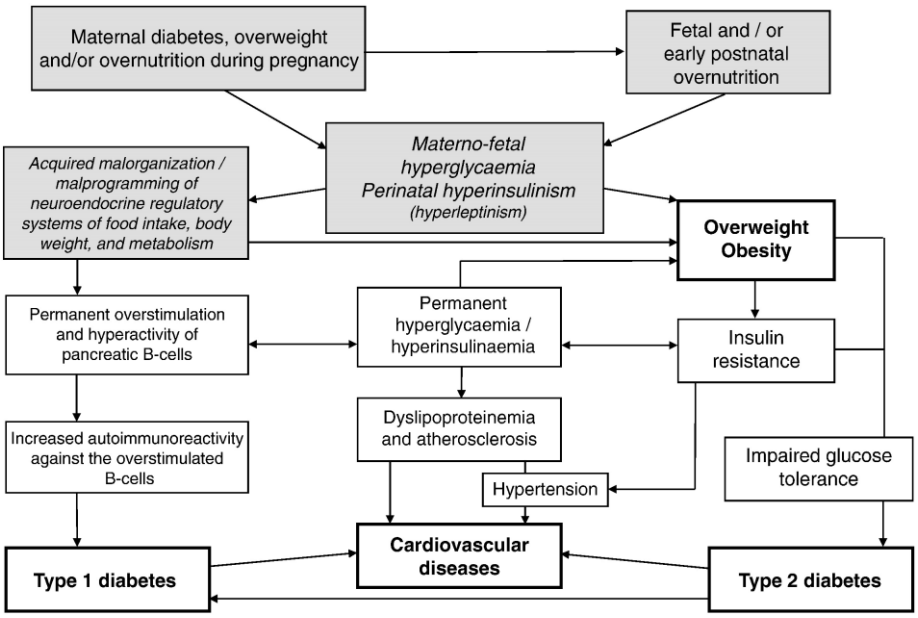

Figure 32. A mechanistic proposal on the early developmental origins of 'diabesity' disposition, acquired by pre- and/or neonatal overfeeding, materno-fetal hyperglycemia, and perinatal hyperinsulinism. Adapted from "Maternal diabetes and perinatal programming," by A. Plagemann, 2011, *Early Human Development, 87(11)*, p. 746, Copyright 2011 with permission from Elsevier. [107]

Numerous epidemiological studies reported a correlation between low birth weight and adverse renal outcome, including glomerular disease, renal failure, and hypertension [114]. Brenner et al. hypothesized that IUGR might cause a reduction of nephron number, which could lead to primary hypertension and progressive renal diseases in later life [115]. The low birth weight, which results from IUGR or prematurity leads to a low nephron number and a decrease of total glomerular filtration surface area. This decrease in glomerular filtration surface area enhances glomerular filtration rate (GFR) of the remaining nephrons and leads to glomerular and systemic hypertension. Hypertension in later life causes glomerular damage and progressive glomerulosclerosis, further reducing the glomerular filtration surface area and forming a vicious cycle, ultimately leading to ESRD. It has been reported that reduced nephron number is related to patients with primary hypertension [116]. Thus, perinatal programming of the renal function reflects renal microstructural changes determined by intrauterine environmental factors.

2.1.2 AT_2R and Perinatal Programming

As mentioned in previous sections, substantial epidemiological evidence demonstrates that traits at birth are associated with diseases in later life. For instance, low birth weight has been linked to increased risk of hypertension, coronary artery disease, and Type 2 diabetes in adulthood. Also, early postnatal weight gain is a strong risk factor for later overweight in offspring of diabetic mothers [117], suggesting that the mode of neonatal nutrition might affect the risk of later overweight. All these findings suggest that the environmental factor during the critical perinatal period determines the risk of disease in later life. Any variation during this critical window induces offspring adaptations including permanent alterations to cell type and number in the organ and the following influence of gene expression pattern. However, there are two different findings from observational studies of the relationship between birth weight and BP in later life. Some studies report that low birth weight is associated with hypertension and cardiovascular diseases in later life [118], whereas others have demonstrated that this relationship could be attributed to a statistical artifact [119]. Recent GWAS demonstrated that the relationship between low birth weight and hypertension in later life is associated with genetic effects, including indirect maternal genotype and direct fetal genotype [120]. Thus, both environmental and genetic factors are key contributing factors for diseases in later life.

The kidney is vulnerable to the perinatal programming effects of maternal undernutrition and also crucial to the regulation of BP. In the rodent, feeding a low-protein diet in pregnancy, which is a model of IUGR, could increase BP in offspring possibly via activation of the RAS and early treatment of the offspring with AT_1R antagonist could blunt this BP-raising effect of maternal undernutrition. AT_2R expression has been shown to be significantly lower in the offspring of maternal undernutrition [121]. Thus, AT_2R might play a role in perinatal programming of hypertension and kidney diseases, suggesting the importance of environmental and genetic factors in the development of disease in later life.

AT_2R is highly expressed in fetal mesenchymal tissues and plays a vital role in regulating cellular differentiation and organ development. Embryonic rodent kidneys express AT_2R in the UB, metanephric mesenchyme, and stroma. AT_2R normally stimulates the timely apoptosis of undifferentiated metanephric mesenchyme cells and plays a crucial role in UB

branching via the balance of cell proliferation and apoptosis [95]. At the same time, emerging UB induces neighboring metanephric mesenchyme cells to conduct a mesenchymal–to–epithelial transition forming epithelial elements of the glomerulus, proximal tubule, and distal tubule. It is striking that the inadequacy of nephron number is caused by abnormal UB branching and that even a minor decline in the efficiency of UB branching produces a profound decrease in nephron endowment [122]. AT_2RKO mice were found to impair UB branching on E13.5, decrease the glomerular size, and display the phenotype of CAKUT and hypertension, suggesting that AT_2R is essential for kidney development and function and might serve as a potential target in the developmental origins of disease in later life [88, 95].

2.1.3 Sex and Gender Effects

Sex and gender differences have become prominent in most diseases because the same disease manifests differently in men and women. The terms ‘sex’ – referring to the biological differences between male and female – and ‘gender’ – the constructed roles, behaviors, expressions and identities of masculinity and femininity in society – have different meanings but are often used vaguely in the literature. The prevalence of non-dialysis-dependent CKD, defined by an estimated GFR (eGFR) of less than 60 mL/min per 1.73 m^2, is higher in women than in men [123]. However, many investigators argue that this difference is possibly due to the longer life expectancy of women and by CKD overdiagnosis based on eGFR equations [124]. Hypertension is a leading cause of death for both men and women [125]. Mean systolic BP in the worldwide population gradually increases with aging in both men and women. Although the prevalence of hypertension is equal in men and women, certain discrepancies emerge between men and women in BP values and risks of cardiovascular diseases. Thus, sex and gender effects should be investigated in the studies of renal and cardiovascular diseases.

Kidney disease and cardiovascular disease are particularly more prevalent in men than in age-matched premenopausal women. However, the value of BP and the consequence of renal and cardiovascular diseases increase in women after menopause. Moreover, kidney function deteriorates faster in men than in women, and men likely tend to adopt unhealthier lifestyles compared to women and sex hormones directly effect on kidney function (i.e., the protective effects of estrogens or the detrimental effects of testosterone). Therefore, sex

hormones are responsible for sexual dimorphism in the pathophysiology of the kidney and cardiovascular system. On the other hand, the RAS regulates the pathophysiology of kidney and cardiovascular systems, suggesting that the RAS appears to be regulated by sex hormones. It has been demonstrated that sex hormones and their receptors play a pivotal role in the progression of kidney disease via different pathophysiological mechanisms such as RAS, oxidative stress, and fibrosis (Table 5) [124].

Numerous studies suggest that several RAS components are regulated by sex hormones and are altered by hormone replacement therapies [126]. The Agt expression is increased by estrogen and testosterone, as well as decreased in liver and kidney following castration in rats [127, 128]. Estrogen down-regulates serum and tissue ACE expression, renal and vascular AT_1R density and expression, whereas testosterone conversely up-regulates ACE activity and tissue AT_1R expression [129, 130]. Accumulating evidences indicate that both women and female rodents exhibit higher Ang (1-7) levels compared with men and male rodents [131]. Renal ACE2 and circulating Ang (1-7) levels are up-regulated by estradiol administration in experimental animals [132]. AT_2R, located on the X chromosome, is mainly expressed in the kidney and vasculature in female rodents compared with male rodents [5]. Besides, the AT_2R/AT_1R ratio is higher in females than in males. In both male and female rodents, renal AT_2R expression is up-regulated by estrogen [133]. However, vascular AT_2R expression is down-regulated by testosterone [134]. Therefore, the decrease of AT_1R density alleviates sodium retention and renal vasoconstriction, whereas the increase of AT_2R density induced by estrogen stimulates natriuresis and vasodilation. Taken together, these studies suggest that estrogen alters the equilibrium of the RAS from the detrimental ACE/Ang II/AT_1R arm to the protective arms (i.e., ACE2/Ang (1-7)/Mas receptor and Ang II/Ang III/AT_2R pathway), suggesting that the influences of sex hormones on the RAS might contribute to sex differences in the progression of renal and cardiovascular diseases.

Several clinical studies indicated that there are inconsistent responses to ARB in both men and women. Miller et al. [135] reported that a higher dosage of ARB is required to control the peripheral vascular and the renal microvascular levels in men compared with women. In contrast, a systematic review indicated that therapy with ARB in hypertensive cohorts is more effective in preventing cardiovascular outcomes in men compared with

women [136]. Therefore, more studies are required to elucidate sex differences in the efficacy of ARB.

Gonadal hormones and sex chromosomes are two possible factors to cause sex differences in the regulation of arterial pressure and kidney function by AT_2R. Previous studies have indicated that chronic low-dose Ang II infusion down-regulates arterial pressure in female rodents, at a concentration that does not affect male rodents [137]. This effect was subsequently found to be regulated via an AT_2R-mediated estrogen-dependent mechanism [138]. Moreover, chronic Ang II infusion increases arterial pressure and the sensitivity of the tubuloglomerular feedback in male mice and female AT_2RKO mice, whereas this response to Ang II is attenuated in wild-type female mice [139]. Also, a study in the four core genotype mouse model has been demonstrated that AT_2R-mediated vasodilation requires both estrogen and the XX chromosome complement [140]. Thus, an enhanced AT_2R-mediated mechanism counterbalances the vasoconstrictive effects of Ang II and attenuates the sensitivity of the tubuloglomerular feedback in females, suggesting that targeting AT_2R can be beneficial in women with renal and cardiovascular disease.

Table 5. Possible mechanisms for sex differences in CKD progression. Adapted from "Sex and gender disparities in the epidemiology and outcomes of chronic kidney disease," by J.J. Carrero, 2018, *Nature Reviews Nephrology, 14(3)*, p. 154, Copyright 2018 with permission from Springer Nature. [124]

Potential mechanism	Supporting evidence	Evidence against
Direct effects of sex steroids on the kidney	• In animals, estrogens have anti-fibrotic and anti-apoptotic effects in the kidney • In animals, testosterone has pro-inflammatory, pro-apoptotic and pro-fibrotic effects in the kidney • In a human case report, testosterone replacement directly modulates renal perfusion in an adolescent with hypogonadism • In animals, female rats of most strains are protected against age-induced renal structural damage	• In humans, oral contraceptive use and estrogen replacement therapy are associated with an increased risk of microalbuminuria and kidney function decline • In humans, testosterone production decreases with lower eGFR. Low testosterone in men with CKD is associated with lower muscle mass and increased mortality. Androgen deprivation therapy is associated with the risk of acute kidney injury • In humans, no sex difference in the rate of development of age-dependent kidney injury is observed
Sex differences in NO metabolism and oxidative stress	• In animals, NO production is better preserved in females than in males, partly as a result of the actions of estrogens. Further, activated ANG II in the aging male kidney favors a pro-oxidant, pro-inflammatory, pro-fibrotic and vasoconstrictive state • In animals, pro-inflammatory mediators of kidney injury are lower, and oxidative stress in the kidney is lower in female rats as compared to male rats, again partly due to the actions of estrogen	NA
Gender-differential impact of comorbidities and lifestyle risk factors	• Men tend to adopt unhealthier lifestyles compared with women. Men with CKD have poorer dietary habits and are less compliant with CKD-specific dietary restrictions • Modifiable risk factors, such as BMI and plasma glucose, accelerate CKD progression in men to a greater extent than in women	• Women may have less renal benefit from dietary protein restriction than men • CKD is not infrequent (3%) in pregnancy. Pregnancy complications, such as gestational hypertension, pre-eclampsia, and diabetes, increase the risk of CKD progression

ANG II, angiotensin II; BMI, body mass index; CKD, chronic kidney disease; eGFR, estimated glomerular filtration rate; NA, not available; NO, nitric oxide.

2.1.4 Research Questions and Hypothesis

For the article 2, we asked the following questions:

Question 1: What are the direct consequences in offspring of the severe maternal diabetes/ IUGR situation on BP and kidney function in later life?

Question 2: What are the long-term outcomes of IUGR offspring who experience overnutrition in early life as a secondary impact on BP and kidney function in adulthood?

Question 3: What are the potential mechanisms of perinatal programming of hypertension and kidney injury?

The adaptations of offspring to the altered intrauterine and postnatal environment have consequences in later life. Previously, our lab has reported that severe maternal diabetes (defined as maternal blood glucose concentration ~30 mM) is associated with IUGR in offspring which have impaired kidney development resulting in relatively small kidneys and nascent nephron deficiency in the neonate, as well as hypertension and kidney injury in adulthood [91, 141, 142]. Moreover, early accelerated weight gain during childhood also increases the risks of hypertension, cardiovascular diseases, and kidney injury in adulthood [114, 143]. Thus, growth during both the prenatal and the immediate postnatal periods is an essential factor for adult hypertension, cardiovascular diseases and kidney injury. Several studies have indicated that increased visceral adiposity is associated with the development of hypertension and CKD [144, 145]. Taken together, we hypothesized that feeding the offspring of severe diabetes dams with a high-fat diet after weaning exacerbates perinatal programming of hypertension and kidney injury.

2.2 Article 2

- **Post-weaning high-fat diet accelerates kidney injury, but not hypertension programmed by maternal diabetes**
- **Pediatric research, 2016; 79(3): 416-424**
- Yessoufou Aliou[1]*, **Min-Chun Liao[1]***, Xin-Ping Zhao[1], Shiao-Ying Chang[1], Isabelle Chenier[1], Julie R. Ingelfinger[2] and Shao-Ling Zhang[1]

  Yessoufou Aliou & Min-Chun Liao. ***The first two authors contributed equally to this work.**

  [1]Centre de recherche du Centre hospitalier de l'Universite de Montreal (CRCHUM), Universite de Montreal, Montréal, Quebec, Canada

  [2]Pediatric Nephrology Unit, Massachusetts General Hospital and Harvard Medical School Boston, Boston, Massachusetts

  Correspondence: Shao-Ling Zhang, Université de Montréal, Centre de Recherche du Centre Hospitalier de l'Université de Montréal (CRCHUM), Tour Viger, 900 Rue Saint-Denis, Montréal, Québec, H2X 0A9, Canada. E-mail: shao.ling.zhang@umontreal.ca
- **Author Contribution**

SLZ is the guarantor of this work, had full access to all study data, and takes responsibility for data integrity and the accuracy of data analysis. SLZ was principal investigators and was responsible for the study conception and design. SLZ also wrote, reviewed, and edited the manuscript. JRI contributed to discussion and reviewed/edited the manuscript. MCL (Figures 33, 34, 35h~k, 36, 38a, 38e), YA (Figures 33, 34, 35a~g, 37, 38b~d), XPZ (Figures 33, 34), SYC (Figures 33, 34), IC (animal management and discussion) and SLZ contributed to the experiments and collection of data. All authors were involved in the analysis and interpretation of data and contributed to the critical revision of the manuscript. MCL contributed to 45% of work.

Abstract

Background: The aim of this study was to establish the underlying mechanisms by which a post-weaning high-fat diet (HFD) accelerates the perinatal programming of kidney injury occurring in the offspring of diabetic mothers.

Methods: Male mice, offspring of nondiabetic and diabetic dams were fed with normal diet (ND) or HFD from 4 to 20 wk of age. Rat renal proximal tubular cells were used *in vitro*.

Results: On ND, the offspring of dams with severe maternal diabetes had an intrauterine growth restriction (IUGR) phenotype and developed mild hypertension and evidence of kidney injury in adulthood. Exposing the IUGR offspring to HFD resulted in rapid weight gain, catch-up growth, and later to profound kidney injury with activation of renal TGFβ1 and collagen type IV expression, increased oxidative stress, and enhanced renal lipid deposition, but not systemic hypertension. Given our data, we speculate that HFD or free fatty acids may accelerate the process of perinatal programming of kidney injury, via increased CD36 and fatty acid-binding protein 4 expression, which may target reactive oxygen species, nuclear factor-kappa B, and TGFβ1 signaling *in vivo* and *in vitro*.

Conclusion: Early postnatal exposure to overnutrition with a HFD increases the risk of development of kidney injury, but not hypertension, in IUGR offspring of dams with maternal diabetes.

Introduction

Diabetes during pregnancy, whether gestational or pregestational diabetes (Type 1 or Type 2 diabetes), results in offspring at high risk of developing hypertension, cardiovascular disease, and chronic kidney disease in adult life. This phenomenon, termed perinatal programming, in which intrauterine events are associated with later adverse changes, has attracted much attention (1–3). Substantial epidemiologic data have also suggested that the offspring whose mothers were diabetic during pregnancy are susceptible to metabolic disturbances induced by postnatal overnutrition, as seen with high-fat diet (HFD) or with increased caloric intake in early life (1–4).

Women who have diabetes during pregnancy and/or are obese and hyperinsulinemic are at risk of delivering macrosomic newborns (high birth weight), and both short- and long-term outcomes of macrosomic neonates are influenced by postnatal overnutrition (1–4). In high-birth-weight neonates, subsequent growth in infancy and risk of becoming obese or diabetic are directly and linearly linked—e.g., the higher the birth weight, the greater the risk of overweight and metabolic disturbances later in life (1–4). In contrast, pregnant women with severe, uncontrolled diabetes or diabetic complications, such as diabetic nephropathy and/or retinopathy, are at high risk of having a microsomic fetus (i.e., a fetus with intrauterine growth restriction (IUGR)) (5,6). Such infants may be markedly small for dates; but many develop excessive weight gain and increased fat deposition in early infancy, a proxy for neonatal overnutrition (7,8). However, the long-term outcome of IUGR offspring who experience overnutrition in early life is incompletely delineated.

Previously, we demonstrated in a mouse model that severe maternal diabetes (defined as maternal blood glucose concentration ~30 mmol/l) is linked to IUGR in offspring (mean decrease 20% of birth weight). Such offspring showed impaired nephrogenesis resulting in nascent nephron deficiency in neonate and manifested hypertension, glucose intolerance, and kidney injury in adulthood. The possible mechanisms involved in those phenomena include reactive oxygen species (ROS) elevation and activation of the nuclear factor-kappa B (NF-κB), TGFβ1, and p53 pathways (9–13).

Compelling evidence from both experimental (14–16) and human studies (17,18) have suggested that perirenal and/or visceral fat depots may mediate the development of chronic kidney disease and hypertension. CD36 (19–22) and fatty acid–binding protein 4 (Fabp4) (23–27) may mediate chronic inflammation, insulin resistance, oxidant stress, and fibrosis involved in proatherogenic hyperlipidemic states such as obesity. In this study, we followed these affected IUGR offspring from 4 to 20 wk of age and compared the metabolic impacts of post-weaning diet (HFD vs. normal diet (ND)) on handling of lipoproteins, hypertension, and renal function. Focusing on the kidney, we hypothesized that feeding the affected IUGR offspring with HFD after weaning would exacerbate the metabolic perturbations and kidney injury in adulthood; we also hypothesized that alteration of renal CD36 and Fabp4 gene expression is associated with these adverse effects.

Materials and Methods

Animal Models

In our established *in vivo* murine model of maternal diabetes induced by a single i.p. streptozotocin (150 mg/kg) injection on gestational day E13 (9–13), male offspring of diabetic dams displayed more pronounced programming phenotypes; hence, we chose to focus on males for this designed HFD study. Male offspring from nondiabetic and diabetic C57/BL6 mice were fed with normal chow (ND) (18% protein with 6.2% fat, calories from protein 24%, fat 18%, and carbohydrate 58%; Harlan Teklad, Montreal, Canada) or HFD (20.5% protein with 36% fat, calories from protein 14%, fat 60%, and carbohydrate 26%; Bio-Serv, Flemington, NJ) from 4 wk until 20 wk of age. All animals were killed at 20 wk of age with high CO_2, and the kidneys removed immediately. BW (g), kidney weight (mg), and TL (mm) were rapidly recorded. The biological samples were processed, collected, and stored accordingly for analysis. Kidneys were either quickly frozen in OCT or fixed overnight in 4% paraformaldehyde at 4 °C before paraffin embedding.

Animal care and the procedures utilized were approved by the Institutional Animal Care Committee of the CRCHUM. Mice were housed under standard humidity and lighting conditions (12-h light–dark cycles) with free access to water and food designed.

Biochemical and Physiological Studies

Plasma NEFA level (mmol/l) was measured using an NEFA kit that detects a variety of free fatty acids (Wako Chemical, Osaka, Japan). Plasma triglycerides (mg/ml) were determined by GPO Trinder kit (Sigma Aldrich, St Louis, MO). Plasma cholesterol (μg/ml) was assessed by the amplex red cholesterol assay kit (Invitrogen, Burlington, Canada). Plasma insulin was measured by mouse ultrasensitive insulin ELISA jumbo kit (Alpco Diagnostics, Salem, NH).

Blood glucose levels were measured with an Accu-Chek Performa glucose meter (Roche Diagnostics, Laval, Canada) in the morning after a 4-h fast, as previously reported (9,10). Mean SBP was monitored by the tail-cuff method with the Visitech BP-2000 Blood Pressure Analysis System for mice (Visitech System, Apex, NC) in longitudinal fashion to minimize stress-related hypertension (9,10). The animals were acclimated to SBP measurement with a 2 wk period of pretraining starting at 4 wk of age (SBP measured 15 times/animal/day, thrice weekly), followed by actual measurement of SBP thrice weekly from 6 wk until 20 wk of age.

Intraperitoneal Glucose Tolerance Test and IST

Intraperitoneal glucose tolerance test and IST were performed according to a standard protocol. Blood glucose was quantified with an Accu-Chek Performa glucose meter. Briefly, intraperitoneal glucose tolerance test was performed after a 6-h fast; 1 mg/g body glucose was injected intraperitoneally, and blood glucose levels were measured at 0, 15, 30, 60, and 120 min. IST was initiated after a 4-h fast. Humulin R (Eli Lilly Canada, Toronto, Canada; 0.75 units/kg) was injected intraperitoneally, and blood glucose levels were measured at 0, 15, 30, 60, and 90 min.

Glomerular Filtration Rate

As reported previously (9), we measured GFR in 20 wk-old male animals by the fluorescein isothiocyanate-inulin method, recommended by the Diabetic Complications Consortium. Urine samples, collected from mice individually housed in metabolic cages, were assayed for albumin/creatinine ratio (ELISA, Albuwell and Creatinine Companion, Exocell, Philadelphia, PA), as reported previously (9,10).

Histology

We assessed hematoxylin and eosin staining of adipocyte collected from both visceral and perirenal fat. The number of adipocytes displayed in microscopic fields (N = 10 fields per animal) were quantitated in a randomized and blinded fashion. Renal morphology was assessed with periodic acid–Schiff and Masson's trichrome staining (9,10). IHC was performed by the standard avidin–biotin–peroxidase complex method (Santa Cruz Biotechnologies, Santa Cruz, CA), as described elsewhere (9,10). The antibodies used included polyclonal p53 and aquaporin 1 (Santa Cruz Biotechnologies); anti-TGFβ1 antibody (R&D Systems, Burlington, Canada); monoclonal anticollagen type IV antibody (Chemicon International, Temecula, CA); polyclonal CD36 antibody (Abcam, Cambridge, MA); Fabp4 antibody (R&D Systems). Oxidative stress in vivo was assessed by dihydroethidium (Sigma-Aldrich, Oakville, Canada) staining in frozen kidney sections as reported previously (13). The classic scoring of glomerulosclerosis (scale from 0 to 4) (39) and tubulo-interstitial injury (scale from 0 to 3) (40) was based on periodic acid–Schiff images. The semi-quantitation of the relative staining values was performed by NIH Image J software (Bethesda, MD) (9,10). The images (N = 6–8 per animal) were analyzed and quantitated in a randomized and blinded fashion.

Real-Time Quantitative PCR

Total RNA extracted from freshly isolated renal cortex was assayed for gene expression by real-time quantitative PCR and calculated using the $\Delta\Delta C_t$ method, as reported previously (9–13). The Fast SYBR green mastermix kit and the 7500 Fast real-time PCR system (Applied Biosystems, Life Technologies, Foster City, CA) were employed for this purpose (9–13). The primer sequences are listed as:

CD36 (S), 5′ -catattggtcaagccagctag-3′; *CD36* (AS), 5′ -agcaacaaacatcaccactcc-3′;

Fabp4 (S), 5′ -aaggtgaagagcatcataaccct-3′; *Fabp4* (AS), 5′ -tcacgcctttcataacacattcc-3′.

***In Vitro* Studies**

The immortalized rat renal proximal tubular cells (IRPTCs) line (passages 15–18) reported previously (9) was employed for our in vitro studies. Caspase-3 activity, ROS generation, and Hoechst staining were measured in IRPTCs treated with or without bovine

serum albumin (BSA, fatty acid free; Sigma-Aldrich) or BSA-bound sodium palmitate (BSA-PA; Sigma-Aldrich) overnight. The preparation of BSA-PA (125 μmol/l and 250 μmol/l) was described in detail by Roduit et al (41). The antibodies used for western blot included NF-κB (p50/p65), p53, and TGFβ1 from Santa Cruz Biotechnology; anti-phospho-p53 (Ser 15) from Abcam.

Statistical Analysis

Statistical significance between the experimental groups was analyzed by one-way ANOVA, by using Graphpad Software, Prism 5.0 (La Jolla, CA). A probability level of $p \leq 0.05$ was considered to be statistically significant and followed by a Bonferroni analysis with adjustment for multiple comparisons (9–13).

Results

Growth Curves of Offspring

We compared the growth pattern of four subgroups of male offspring of nondiabetic (control) and diabetic dams—e.g., control offspring on ND (Con-ND, $N = 17$); control offspring on HFD (Con-HF, $N = 15$); diabetic offspring on ND (Dia-ND, $N = 12$), and diabetic offspring on HFD (Dia-HF, $N = 12$). Similar to previous reports (9–11), Dia-ND mice born with IUGR continued to have lower body weight (BW, g) throughout life (mean BW in cross-section time-point measurement decreased 20%; $P \leq 0.01$; Figure 33a). HFD increased BW of both Con-HF and Dia-HF animals over time. Offspring of diabetic dams were more sensitive to HFD as compared to those of control dams, as they showed the steepest climb in BW—i.e., a catch-up pattern from 4 to 5 wk ($P < 0.05$; Figure 33c). In contrast, significant BW gain in Con-HF mice (vs. Con-ND mice) began only at 8 wk of age ($P < 0.05$; Figure 33b).

Metabolic Parameters

At 20 wk, as compared with Con-ND mice, Dia-ND animals had increased plasma levels of nonesterified fatty acids (NEFA) (Figure 33d; $P < 0.01$), triglycerides (Figure 33e; $P < 0.01$), and cholesterol (Figure 33f; $P < 0.05$), but not insulin (Figure 33g). HFD was associated with elevated plasma levels of NEFA ($P < 0.05$), triglycerides ($P < 0.05$), cholesterol ($P < 0.01$), and insulin ($P < 0.01$) in Con-HF animals, but this was not seen in Dia-HF groups (Figure 33d–g). Intraperitoneal glucose tolerance test (Figure 33h,i) and insulin

sensitivity test (IST) (Figure 33j) were performed at 19 wk before animals were killed. The fasting blood glucose concentration (mmol/l) at baseline of the four subgroups did not differ from each other (Con-ND (8.31 ± 0.34) vs. Dia-ND (8.0 ± 0.36); Con-HF (10.45 ± 0.47) vs. Dia-HF (9.71 ± 0.53); Figure 33h). HFD impaired glucose tolerance in both Con-HF and Dia-HF offspring at similar levels (Figure 33h,i; $P < 0.01$), despite the fact that Dia-ND already displayed a mild degree of impaired glucose tolerance ($P < 0.05$) when compared with Con-ND, as we also showed previously (10). Con-HF animals showed less insulin sensitivity through the entire IST procedure ($P < 0.01$), while a similar IST pattern was observed for the other three groups (Figure 33j).

Mean Systolic Blood Pressure

Longitudinal measurement of systolic blood pressure (SBP) (Figure 34a), recorded from 6 to 20 wk of age, revealed that Dia-ND have significantly higher SBP over the follow-up period when compared with Con-ND, as previously reported (10). HFD animals displayed normal SBP (mm Hg) at 10 to 20 wk of age, irrespective of whether they were offspring of dams with maternal diabetes or not (Figure 34a).

Kidney Function and Adipocyte Morphology

As compared with Con-ND mice, Dia-ND animals exhibited significantly increased ($P \leq 0.05$) urinary albumin/creatinine ratio (Figure 34b) and glomerular filtration rate (GFR; $P \leq 0.01$; Figure 34c).

HFD was associated with a significantly increased albumin/creatinine ratio ($P \leq 0.05$) in both groups of offspring compared with respective ND groups (Figure 34b). However, HFD was not associated with changes of GFR/ tibia length (TL) ratio in either control or diabetic animals (Figure 34c). The kidney weight/TL (mm) ratio among the four groups of animals remains unchanged either in ND or HFD condition.

As compared with Con-ND, Dia-ND mice had a decreased number of adipocytes ($P < 0.01$) collected from both perirenal and visceral fat. These changes were more pronounced in HFD offspring (Con-HF, $P < 0.01$; Dia-HF, $P < 0.05$; Figure 34d,e).

Renal Expression of Extracellular Matrix Protein

Consistent with previous reports (9,10), Dia-ND offspring at 20 wk showed enhanced extracellular matrix protein accumulation seen by periodic acid–Schiff (Figure 35a) and Masson's trichrome (Figure 35b) staining, resulting in glomerulosclerosis ($P < 0.01$; Figure 35h) and tubulointerstitial injury ($P < 0.05$; Figure 35i).

Our immunohistochemistry (IHC) data indicate that the kidneys of Dia-ND offspring also had increased expression of TGFβ1 (Figure 35c) and collagen type IV (Figure 35d) localized to both glomeruli ($P < 0.01$; Figure 35j) and tubulointerstitium ($P < 0.05$; Figure 35k). And most importantly, HFD enhanced these changes in both groups of offspring ($P < 0.01$), particularly in the kidneys of Dia-HF mice.

Oil Red Staining, Oxidative Stress, and Apoptosis in Kidney

Within the kidneys of HFD animals (Con-HF vs. Dia-HF) at 20 wk of age, there was increased oil red staining (Figure 35e), elevated oxidative stress on dihydroethidium staining (e.g., the nonfluorescent dihydroethidium is oxidized to fluorescent ethidium by superoxide anion ($O_2^{\bullet -}$)) (Figure 35f) and augmented apoptotic events on p53-IHC staining (Figure 35g) in both glomeruli ($P < 0.05$; Figure 35j) and tubulointerstitium ($P < 0.05$; Figure 35k).

Renal CD36 and Fabp4 Expression

As compared with Con-ND mice, renal CD36 (Figure 36a, mRNA; Figure 36c, protein) and Fabp4 (Figure 36b, mRNA; Figure 36d, protein) expression were increased in renal cortex in Dia-ND ($P < 0.05$) and both HFD-fed groups (Con-HF vs. Dia-HF). Moreover, IHC staining (Figure 37) revealed that increased CD36 and Fabp4 were predominantly localized in the proximal tubular cells, particularly in the kidneys of Dia-HF mice (Figure 37a) colocalizing with aquaporin 1 immunostaining (Figure 37b,c).

***In Vitro* Studies**

We performed *in vitro* experiments using bovine serum albumin (BSA)-bound sodium palmitate (BSA-PA) to treat IRPTCs (9) to confirm our *in vivo* observations. Palmitic acid is the most common saturated fatty acid in the human body. Because of the low solubility in aqueous solutions, palmitic acid needs binding proteins to increase its concentration and

solubility in vascular and interstitial compartments. Albumin serves as the major vehicle for fatty acid transport through the plasma. BSA-PA stimulated both CD36 and Fapb4 protein expression in a dose-dependent manner (Figure 38a) in IRPTCs. Moreover, BSA-PA (125 μmol/l) was associated with significantly induced ROS generation (Figure 38b; $P < 0.01$), increased apoptosis (Caspase-3 activity, Figure 38c, $P < 0.01$; Hoechst staining, Figure 38d, $P < 0.01$; and phosphorylation of p53, Figure 38e) and augmented NF-κB (i.e., p50/p65) as well as TGFβ1 protein expression (Figure 38e, $P < 0.01$) in IRPTCs.

Discussion

This study indicates that IUGR offspring of diabetic dams post-weaning fed with HFD showed "rapid" weight gain, catch-up growth, and subsequently displayed features of profound kidney injury associated with increased CD36 and Fabp4 expression. However, they did not have hypertension in adulthood.

In agreement with most human and experimental observations (1–3,7,8), we observed "rapid" catch-up growth in young Dia-HF offspring from 5 to 8 wk of age. Con-HF offspring became obese over time, with elevated plasma lipids at 20 wk of age (i.e., NEFA, triglycerides, and cholesterol), whereas Dia-HF offspring had similar BW and lipid levels as Con-ND at 20 wk of age, underscoring the finding that postnatal HFD feeding has a differential impact on the growth pattern in the offspring of both nondiabetic and diabetic dams.

Similar observations were also reported in the small litter rat model in which smaller young offspring were exposed to HFD feeding (4,28,29). The implications of those findings were that HFD enhanced insulin sensitivity and fatty-acid oxidation in the skeletal muscle and increased plasma levels of leptin, insulin, and adiponectin to maintain BW and metabolic homeostasis in the normal range (4,28,29). Since increasing lipid oxidation might improve insulin sensitivity (30,31), in this study, when compared with Con-HF mice, Dia-HF animals with normal lipid metabolism and plasma insulin levels had a rapid insulin response and higher insulin sensitivity by IST measurement, hinting that enhanced lipid oxidation might have occurred in these animals. Taken together, our data suggest that Dia-HF animals might use HF as the fuel or energy to balance their BW and metabolism.

In humans, increased intrarenal and perirenal fat is associated with an increased risk of hypertension and chronic kidney disease (17,18). However, the observations of obesity-induced hypertension in animals are varied (32). For instance, Kennedy et al. (32) recently reviewed blood pressure responses in obese mouse models such as Lep $^{ob/ob}$, LepR $^{db/db}$, and HFD-induced obesity; responses of blood pressure include an increase, decrease, or no change, largely depending on strain, sex, age, environment, and the method of measuring BP. In this study, we did not observe an impact from HFD on the development of hypertension in either Con-HF or Dia-HF mice; our results are similar to reported observations in 5 out of 6 nephrectomized rats fed with HFD (33) and obese ZSF1 rats (34). Previously, the mild hypertension we noted in Dia-ND animals (9,10) was mainly because of renal hypertrophy related to renal hyperfiltration with increased GFR. However, we noted that Dia-HF mice at 20 wk of age showed kidney weight/TL and GFR/TL ratios comparable to Con-ND animals, which might be a partial explanation for their normotensive status.

Renal injury has been reported previously in our Dia-ND mice (9–13). In this work, we found that HFD augmented TGFβ1 and collagen IV gene expression, increased renal lipid accumulation, as well as heightened oxidative stress in both glomerular and tubular compartments in the kidneys of Dia-HF mice, resulting in significant glomerulosclerosis, tubular fibrosis, and apoptosis. Although our findings are consonant with other reports (14–16), results reported in remnant kidney rats receiving HFD (33) seem to ameliorate these parameters/pathways to prevent kidney injury. Currently, we do not have further explanation for this discrepancy beside species differences.

Emerging evidence suggested that CD36 (19–22) and Fabp4 (23–27) are highly implicated in the pathogenesis of HFD-induced cell damage. For example, intrarenal CD36 has been identified as a novel mediator in renal diseases associated with proteinuria and renal dysfunction (35). The elevated level of serum/plasma/urinary Fabp4 is considered a predictor or biomarker for renal dysfunction in diabetes and cardiovascular diseases (23–27). Hence, we further hypothesized that these affected IUGR offspring fed with HFD would develop metabolic perturbations and kidney injury in adulthood that might be associated with alterations of both renal CD36 and Fabp4 gene expression.

Our data showed that HFD enhanced renal CD36 and Fabp4 expression, which predominantly localized to PTCs (confirmed by colocalization in PTCs with the PTC biomarker, aquaporin 1), but not in glomeruli, suggesting that it is plausible that apparent CD36- and Fabp4-mediated PTC changes might be secondary to proteinuria and/or lipiduria.

We validated our *in vivo* findings with *in vitro* studies in IRPTCs and investigated the functional impact of free fatty acids (i.e., BSA-PA) on renal CD36 and Fabp4 expression and its related molecular mechanism(s). We observed that BSA-PA stimulated both CD36 and Fabp4 protein expression in a dose-dependent manner in IRPTCs. CD36 has been shown to mediate PTC apoptosis (36) and to influence the binding and uptake of albumin in PTCs to promote proteinuria (35). The activated CD36 in PTCs targets JNK, ROS, and inflammatory cytokines to facilitate renal dysfunction (22). CD36 deficiency attenuates TGFβ1 signaling, NF-κB activity, and renal fibrosis in hypercholesterolemic mice (37), whereas CD36 overexpression leads to lipid accumulation in PTCs (20). On the other hand, Fabp4 was reported to be actively expressed in the peritubular and glomerular region to mediate renal dysfunction in diseased kidney (26,27). Fabp4, via the ER stress-JNK pathway, mediated vascular inflammation in the pathogenesis of cardiovascular disorders associated with obesity and diabetes (38). Thus, we tested those potential mechanisms in IRPTCs in culture, and our data suggested that BSA-PA induced ROS generation, enhanced apoptosis (via phosphorylation of p53), and activated NF-κB (i.e., p50/p65) and TGFβ1 protein expression in IRPTCs. These data would support the concept that CD36 and Fabp4, induced by free fatty acids, may contribute to the substantial PTC damages resulting in tubulointerstitial fibrosis and apoptosis.

Taken together, our observations suggest a synergistic contribution by CD36 and Fabp4 to renal dysfunction and injury. Our data indicate that, in addition to HFD-induced glomerular injury, HFD via increased CD36 and Fabp4 expression in PTCs may target ROS, NF-κB, and TGFβ1 signaling to accelerate the process of maternal diabetes–induced perinatal programming of kidney injury. In conclusion, early postnatal exposure to HFD in IUGR offspring of diabetic dams increases the risk of development of subsequent kidney injury, but not hypertension.

Acknowledgements

The authors owe special thanks to John S.D. Chan (CRCHUM, Montreal, QC, Canada) for his unconditional support and valuable comments on this manuscript. Editorial assistance was provided by the CRCHUM's Research Support Office.

Statement of Financial Support

This project was supported by grants to S.-L.Z. from the Canadian Institutes of Health Research (MOP115025) and Canadian Diabetes Association (OG-3-13-4073-SZ).

Disclosure

None.

References of Article 2

1. Plagemann A. Maternal diabetes and perinatal programming. Early Hum Dev 2011;87:743–7.
2. Plagemann A, Harder T, Rodekamp E, Kohlhoff R. Rapid neonatal weight gain increases risk of childhood overweight in offspring of diabetic mothers. J Perinat Med 2012;40:557–63.
3. Plagemann A, Harder T, Schellong K, Schulz S, Stupin JH. Early postnatal life as a critical time window for determination of long-term metabolic health. Best Pract Res Clin Endocrinol Metab 2012;26:641–53.
4. Spencer SJ. Early life programming of obesity: the impact of the perinatal environment on the development of obesity and metabolic dysfunction in the offspring. Curr Diabetes Rev. 2012;8:55–68.
5. Holemans K, Aerts L, Van Assche FA. Fetal growth restriction and consequences for the offspring in animal models. J Soc Gynecol Investig 2003;10:392–9.
6. Van Assche FA, Holemans K, Aerts L. Long-term consequences for offspring of diabetes during pregnancy. Br Med Bull 2001;60:173–82.
7. Perälä MM, Männistö S, Kaartinen NE, et al. Body size at birth is associated with food and nutrient intake in adulthood. PLoS One 2012;7:e46139.
8. Crowther NJ, Cameron N, Trusler J, Toman M, Norris SA, Gray IP. Influence of catch-up growth on glucose tolerance and beta-cell function in 7-year-old children: results from the birth to twenty study. Pediatrics 2008;121:e1715–22.
9. Chang SY, Chen YW, Zhao XP, et al. Catalase prevents maternal diabetes-induced perinatal programming via the Nrf2-HO-1 defense system. Diabetes 2012;61:2565–74.
10. Chen YW, Chenier I, Tran S, Scotcher M, Chang SY, Zhang SL. Maternal diabetes programs hypertension and kidney injury in offspring. Pediatr Nephrol 2010;25:1319–29.
11. Tran S, Chen YW, Chenier I, et al. Maternal diabetes modulates renal morphogenesis in offspring. J Am Soc Nephrol 2008;19:943–52.

12. Zhang SL, Chen YW, Tran S, Chenier I, Hébert MJ, Ingelfinger JR. Reactive oxygen species in the presence of high glucose alter ureteric bud morphogenesis. J Am Soc Nephrol 2007;18:2105–15.

13. Chen YW, Chenier I, Chang SY, Tran S, Ingelfinger JR, Zhang SL. High glucose promotes nascent nephron apoptosis via NF-kappaB and p53 pathways. Am J Physiol Renal Physiol 2011;300:F147–56.

14. Declèves AE, Mathew AV, Cunard R, Sharma K. AMPK mediates the initiation of kidney disease induced by a high-fat diet. J Am Soc Nephrol 2011;22:1846–55.

15. Odermatt A. The Western-style diet: a major risk factor for impaired kidney function and chronic kidney disease. Am J Physiol Renal Physiol 2011;301:F919–31.

16. Soumura M, Kume S, Isshiki K, et al. Oleate and eicosapentaenoic acid attenuate palmitate-induced inflammation and apoptosis in renal proximal tubular cell. Biochem Biophys Res Commun 2010;402:265–71.

17. Foster MC, Hwang SJ, Porter SA, Massaro JM, Hoffmann U, Fox CS. Fatty kidney, hypertension, and chronic kidney disease: the Framingham Heart Study. Hypertension 2011;58:784–90.

18. Chandra A, Neeland IJ, Berry JD, et al. The relationship of body mass and fat distribution with incident hypertension: observations from the Dallas Heart Study. J Am Coll Cardiol 2014;64:997–1002.

19. Hajri T, Han XX, Bonen A, Abumrad NA. Defective fatty acid uptake modulates insulin responsiveness and metabolic responses to diet in CD36-null mice. J Clin Invest 2002;109:1381–9.

20. Kang HM, Ahn SH, Choi P, et al. Defective fatty acid oxidation in renal tubular epithelial cells has a key role in kidney fibrosis development. Nat Med 2015;21:37–46.

21. Kennedy DJ, Kuchibhotla S, Westfall KM, Silverstein RL, Morton RE, Febbraio M. A CD36-dependent pathway enhances macrophage and adipose tissue inflammation and impairs insulin signalling. Cardiovasc Res 2011;89:604–13.

22. Kennedy DJ, Chen Y, Huang W, et al. CD36 and Na/K-ATPase-α1 form a proinflammatory signaling loop in kidney. Hypertension 2013;61:216–24.

23. Ishimura S, Furuhashi M, Watanabe Y, et al. Circulating levels of fatty acid-binding protein family and metabolic phenotype in the general population. PLoS One 2013;8:e81318.

24. Furuhashi M, Ishimura S, Ota H, et al. Serum fatty acid-binding protein 4 is a predictor of cardiovascular events in end-stage renal disease. PLoS One 2011;6:e27356.

25. Yeung DC, Xu A, Tso AW, et al. Circulating levels of adipocyte and epidermal fatty acid-binding proteins in relation to nephropathy staging and macrovascular complications in type 2 diabetic patients. Diabetes Care 2009;32:132–4.

26. Tanaka M, Furuhashi M, Okazaki Y, et al. Ectopic expression of fatty acid-binding protein 4 in the glomerulus is associated with proteinuria and renal dysfunction. Nephron Clin Pract 2014;128:345–51.

27. Okazaki Y, Furuhashi M, Tanaka M, et al. Urinary excretion of fatty acid-binding protein 4 is associated with albuminuria and renal dysfunction. PLoS One 2014;9:e115429.

28. Prior LJ, Velkoska E, Watts R, Cameron-Smith D, Morris MJ. Undernutrition during suckling in rats elevates plasma adiponectin and its receptor in skeletal muscle regardless of diet composition: a protective effect? Int J Obes (Lond) 2008;32:1585–94.

29. Velkoska E, Cole TJ, Dean RG, Burrell LM, Morris MJ. Early undernutrition leads to long-lasting reductions in body weight and adiposity whereas increased intake increases cardiac fibrosis in male rats. J Nutr 2008;138:1622–7.

30. Bruce CR, Hoy AJ, Turner N, et al. Overexpression of carnitine palmitoyltransferase-1 in skeletal muscle is sufficient to enhance fatty acid oxidation and improve high-fat diet-induced insulin resistance. Diabetes 2009;58:550–8.

31. Murrow BA, Hoehn KL. Mitochondrial regulation of insulin action. Int J Biochem Cell Biol 2010;42:1936–9.

32. Kennedy AJ, Ellacott KL, King VL, Hasty AH. Mouse models of the metabolic syndrome. Dis Model Mech 2010;3:156–66.

33. Kim HJ, Vaziri ND, Norris K, An WS, Quiroz Y, Rodriguez-Iturbe B. High-calorie diet with moderate protein restriction prevents cachexia and ameliorates oxidative stress, inflammation and proteinuria in experimental chronic kidney disease. Clin Exp Nephrol 2010;14:536–47.

34. Hamdani N, Franssen C, Lourenço A, et al. Myocardial titin hypophosphorylation importantly contributes to heart failure with preserved ejection fraction in a rat metabolic risk model. Circ Heart Fail 2013;6:1239–49.

35. Baines RJ, Chana RS, Hall M, Febbraio M, Kennedy D, Brunskill NJ. CD36 mediates proximal tubular binding and uptake of albumin and is upregulated in proteinuric nephropathies. Am J Physiol Renal Physiol 2012;303:F1006–14.

36. Susztak K, Ciccone E, McCue P, Sharma K, Böttinger EP. Multiple metabolic hits converge on CD36 as novel mediator of tubular epithelial apoptosis in diabetic nephropathy. PLoS Med 2005;2:e45.

37. Okamura DM, López-Guisa JM, Koelsch K, Collins S, Eddy AA. Atherogenic scavenger receptor modulation in the tubulointerstitium in response to chronic renal injury. Am J Physiol Renal Physiol 2007;293:F575–85.

38. Xu A, Vanhoutte PM. Adiponectin and adipocyte fatty acid binding protein in the pathogenesis of cardiovascular disease. Am J Physiol Heart Circ Physiol 2012;302:H1231–40.

39. El Nahas AM, Bassett AH, Cope GH, Le Carpentier JE. Role of growth hormone in the development of experimental renal scarring. Kidney Int 1991;40:29–34.

40. Véniant M, Heudes D, Clozel JP, Bruneval P, Ménard J. Calcium blockade versus ACE inhibition in clipped and unclipped kidneys of 2K-1C rats. Kidney Int 1994;46:421–9.

41. Roduit R, Masiello P, Wang SP, Li H, Mitchell GA, Prentki M. A role for hormone-sensitive lipase in glucose-stimulated insulin secretion: a study in hormone-sensitive lipase-deficient mice. Diabetes 2001;50:1970–5.

Figures

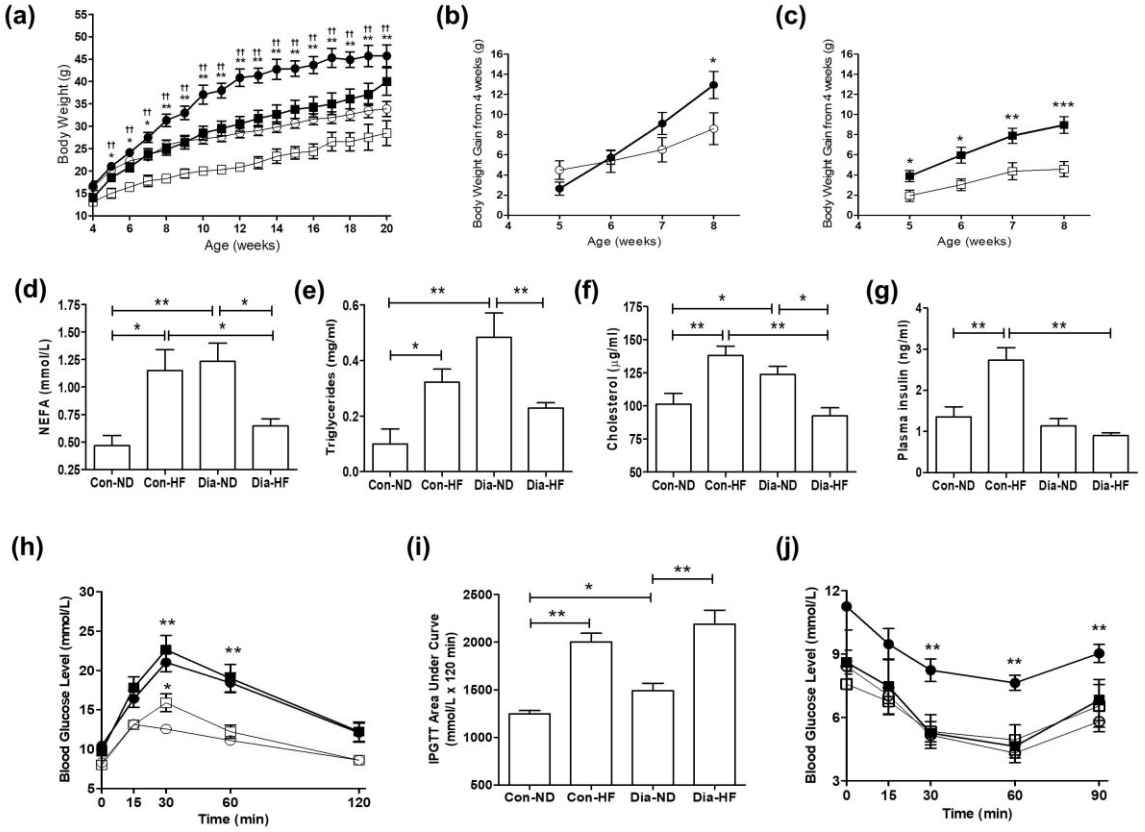

Figure 33. Metabolic parameters in offspring. (a) Growth follow-up in four subgroups of male offspring from the age of 4 to 20 wk. (○) Con-ND; (●) Con-HF; (□) Dia-ND; (■) Dia-HF; *, $P \leq 0.05$; **$P \leq 0.01$ vs. Con-ND; ††$P \leq 0.01$ vs. Dia-ND. (b,c) Body weight gain in male offspring from the age of 4 to 8 wk (b: offspring from control dams and c: offspring from diabetic dams). (○) Con-ND; (●) Con-HF; (□) Dia-ND; (■) Dia-HF; *$P \leq$ 0.05; **$P \leq 0.01$. (d–g) Plasma metabolic profile measurements (d: NEFA (mmol/l); e: triglycerides (mg/ml); f: cholesterol (µg/ml); and g: insulin (ng/ml)) in four subgroups of 20-wk-old male offspring. *$P \leq 0.05$; **$P \leq 0.01$. (h) IPGTT measurement. IPGTT was performed after a 6-h fast; 1 mg/g body glucose was injected intraperitoneally, and blood glucose levels were measured at 0, 15, 30, 60, and 120 min. (○) Con-ND; (●) Con-HF; (□) Dia-ND; (■) Dia-HF; *$P \leq 0.05$; **$P \leq 0.01$ vs. Con-ND. (i) IPGTT area under curve; *$P \leq 0.05$; **$P \leq 0.01$. (j) IST measurement. IST was initiated after a 4-h fast. Humulin R (0.75 units/kg) was injected intraperitoneally, and blood glucose levels were measured

at 0, 15, 30, 60, and 90 min after Humulin R injection. (○) Con-ND; (●) Con-HF; (□) Dia-ND; (■) Dia-HF; $^{**}P \leq 0.01$; $^{**}P \leq 0.01$ vs. Con-ND. Values represent the mean ± SEM. IPGTT, intraperitoneal glucose tolerance test.

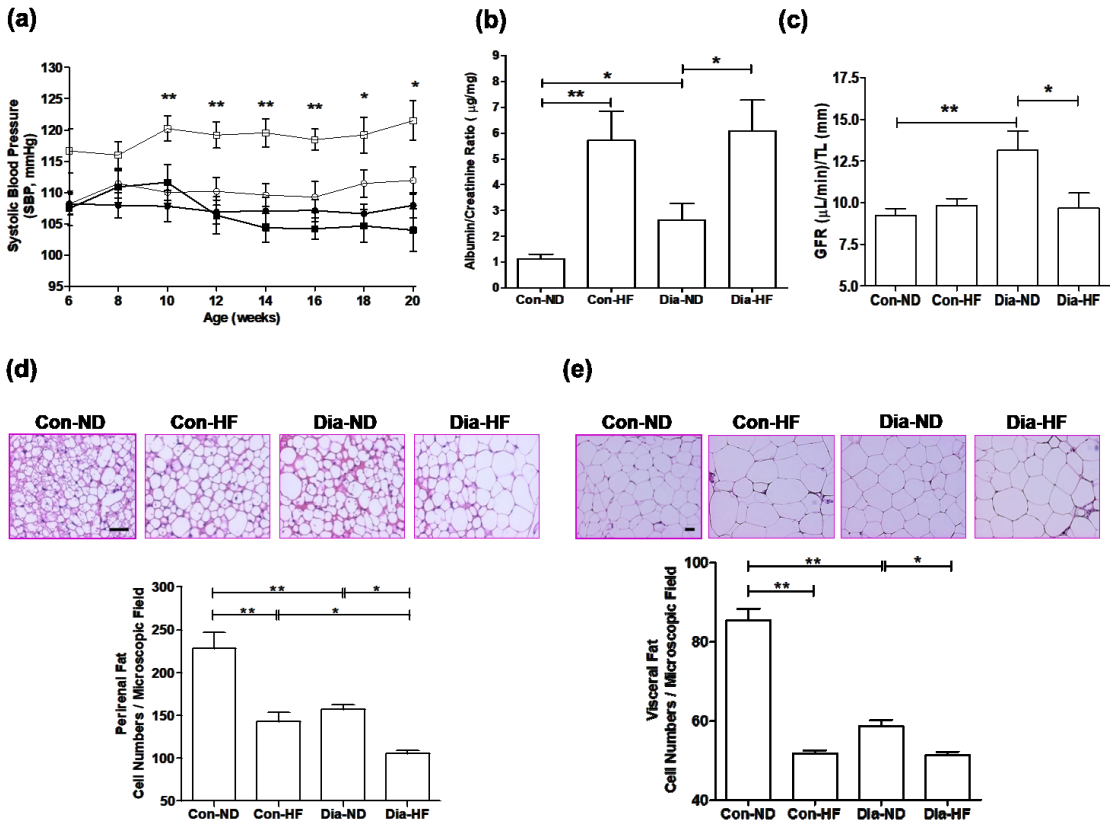

Figure 34. Blood pressure, renal function, and adipocyte morphology. (a) Longitudinal SBP measurement. (○) Con-ND; (●) Con-HF; (□) Dia-ND; (■) Dia-HF; $^{*}P \leq 0.05$; $^{**}P \leq 0.01$ vs. Con-ND. (b) Urinary ACR measurement; $^{*}P \leq 0.05$; $^{**}P \leq 0.01$. (c) GFR/TL ratio; $^{*}P \leq 0.05$; $^{**}P \leq 0.01$. (d) H&E staining- perirenal fat (magnification: ×200) with semi-quantitation of adipocyte number per microscopic field (N = 10 fields per animal). $^{*}P \leq 0.05$; $^{**}P \leq 0.01$. (e) H&E staining- visceral fat (magnification: ×100) with semi-quantitation of adipocyte number per microscopic field (N = 10 fields per animal). $^{*}P \leq 0.05$; $^{**}P \leq 0.01$. Values represent the mean ± SEM. ACR, albumin/creatinine ratio; GFR, glomerular filtration rate; H&E, hematoxylin and eosin; SBP, systolic blood pressure; TL, tibia length. Scale bars = 50 μm.

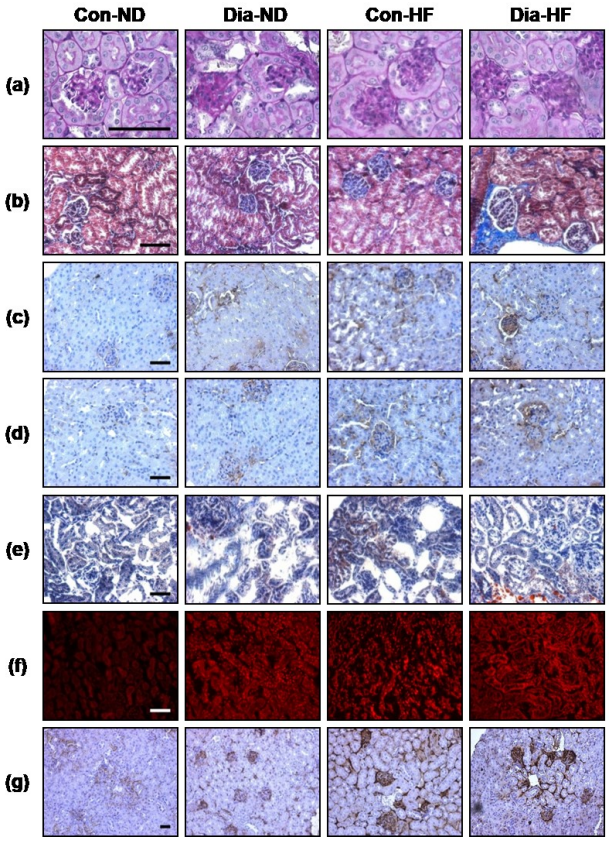

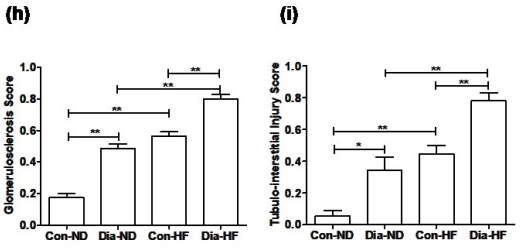

(j)

Glomerular	Con-ND	Dia-ND	Con-HF	Dia-HF
Masson	100.0 ± 15.1	223.5 ± 22.8 **	223.5 ± 17.9 **	256.5± 19.3 **
TGF-β1	100.0 ± 6.2	202.4 ± 16.9 **	210.1 ± 21.5 **	346.3 ± 24.9 **;††; ‡‡
Coll IV	100.0 ± 5.4	173.2 ± 15.8 *	178.2 ± 14.1 *	247.3 ± 22.0 **;†; ‡
Oil-Red	100.0 ± 11.9	350.6 ± 98.9 **	282.5 ± 33.2 **	345.8 ± 35.7 **
DHE	100.0 ± 2.8	119.1 ± 4.5 *	172.3 ± 5.4 **; ††	194.3 ± 6.6 **;††; ‡
p53	100.0 ± 19.5	413.1 ± 61.8 *	839.7 ± 207.2 **; †	1335.0 ± 86.7 **; ††; ‡‡

(k)

Tubular	Con-ND	Dia-ND	Con-HF	Dia-HF
Masson	100.0 ± 11.0	231.6 ± 22.5 *	244.8 ± 33.6 *	367.4 ± 33.2 **; ††; ‡
TGF-β1	100.0 ± 9.2	188.7 ± 20.7 *	243.3 ± 11.8 **	337.8 ± 32.1 **; ††; ‡
Coll IV	100.0 ± 5.9	197.0 ± 15.3 *	223.5 ± 28.1 **	359.6 ± 33.7 **; ††; ‡‡
Oil-Red	100.0 ± 9.7	221.8 ± 61.8 *	268.5 ± 21.2 **	408.5 ± 19.9 **; ††; ‡‡
DHE	100.0 ± 3.7	126.2 ± 6.4 *	149.4 ± 4.8 **	185.9 ± 8.2 **; ††; ‡‡
p53	100.0 ± 7.4	399.7 ± 26.8 **	535.0 ± 35.1 **; †	777.7 ± 67.8 **; ††; ‡‡

Figure 35. Renal morphology. (a) PAS staining (magnification: ×600). (b) Masson's trichrome staining (magnification: ×200). (c) IHC-TGFβ1 staining (magnification: ×200). (d) IHC-collagen type IV (magnification: ×200). (e) Oil red deposition (magnification: ×200). (f) DHE staining (magnification: ×200). (g) IHC-p53 staining (magnification: ×100). (h) Classic scoring of glomerulosclerosis based on PAS images. Grade 0, normal glomeruli; grade 1, presence of mesangial expansion/thickening of the basement membrane. (i) Classic scoring of tubulointerstitial injury based on PAS images. Grade 0, normal tubules; grade 1, the tubulointerstitial lesions involving less than 25% of the field. (j–k) Semi-quantitation of the relative staining values in both (j) glomerular and (k) tubular compartment. The value in Con-ND animals was 100% ± SEM. *$P \leq 0.05$; **$P \leq 0.01$ vs. Con-ND; †$P \leq 0.05$ vs. Dia-ND; ‡$P \leq 0.05$ vs. Con-HF. Values represent the mean ± SEM. DHE, dihydroethidium; PAS, periodic acid–Schiff. Scale bars = 50 μm.

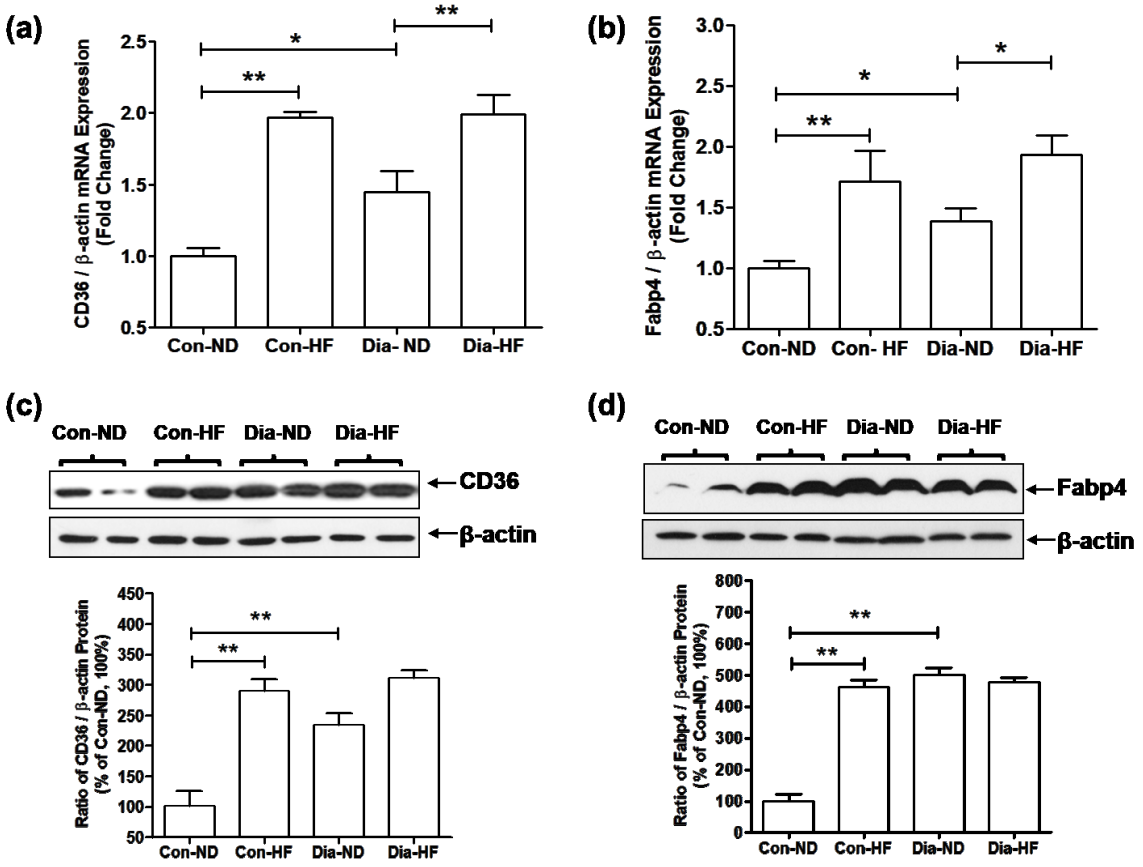

Figure 36. Renal CD36 & Fabp 4 gene expression. (a, c) Renal CD36 and (b, d) Fabp4 gene expression in the renal cortex of four subgroups of 20-wk-old male offspring. (a and b) qRT-PCR analysis. (c and d) Western blot analysis. The relative densities of CD36 and Fabp4 were compared with their own β-actin mRNA or protein. The values of Con-ND animals were considered as 100%. Each point represents the mean ± SEM of three independent experiments. *$P \leq 0.05$; **$P \leq 0.01$.

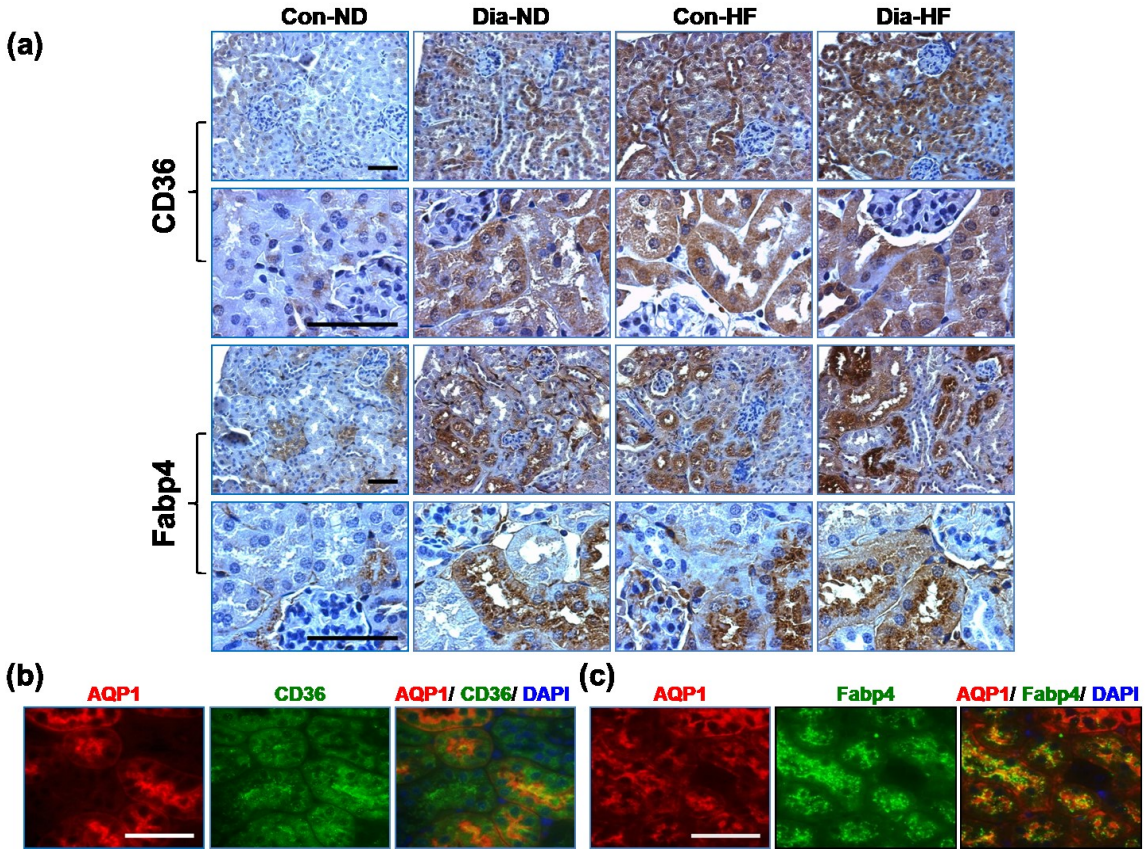

Figure 37. Renal CD36 & Fabp 4 localization. (a) IHC staining images of CD36 and Fabp4 in the kidneys of four subgroups of 20 wk-old male offspring (magnification: ×200; ×600). (b) The colocalization of AQP1 (red) with CD36 (green) in the kidneys of Dia-HF animals (magnification: ×600). (c) The colocalization of AQP1 (red) with Fabp4 (green) in the kidneys of Dia-HF animals (magnification: ×600). AQP1, aquaporin 1; Fabp4, fatty acid–binding protein 4. Scale bars = 50 μm.

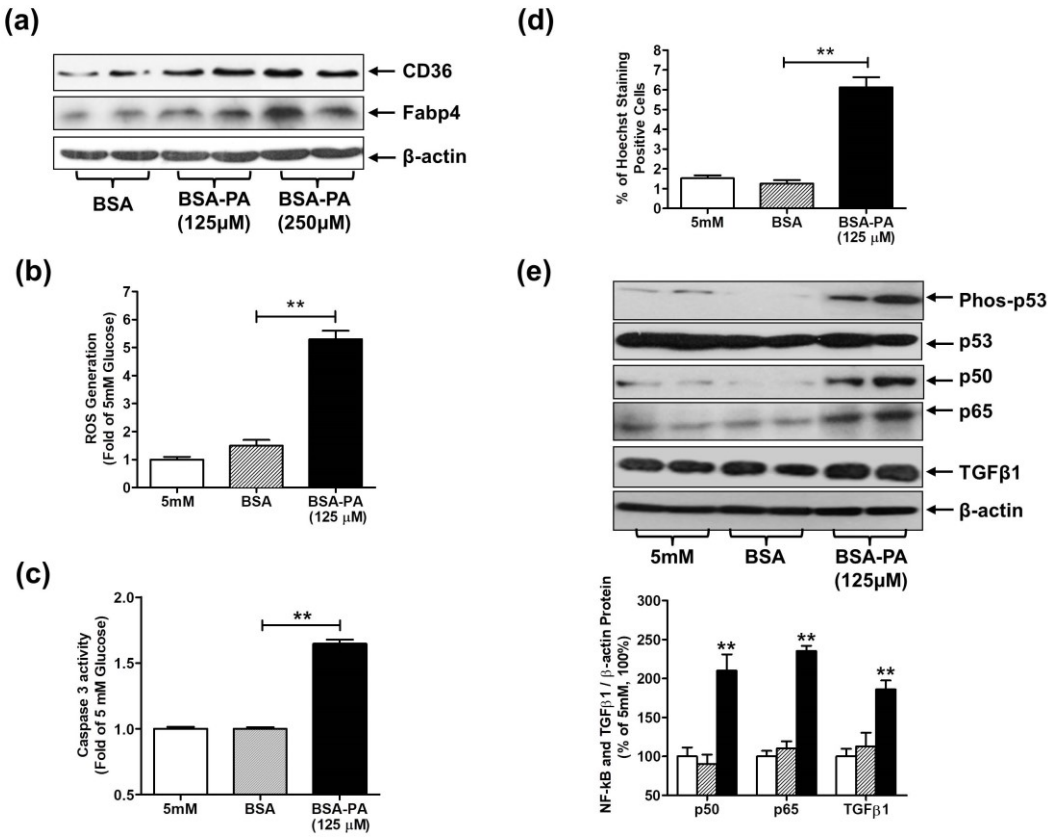

Figure 38. BSA-PA effects in IRPTCs. IRPTCs were incubated with 0.5% BSA, 125 μM BSA-PA or 250 μM BSA-PA for 24 hours. (a) CD36 and Fabp4 protein expression analyzed by western blot. (b) ROS generation. (c) Caspase-3 activity assay. (d) Quantification of Hoechst staining–positive cells. (e) Western blot of phosphorylation of p53, NF-κB (i.e., p50/p65), and TGFβ1 protein expression. The relative densities of gene expression were compared with their own β-actin, and the gene expression protein ratio in 5 mmol/l glucose medium was considered as 100%. IRPTC in 5 mmol/l glucose (white bar); BSA (shadowed bar), and BSA-PA (black bar). Each point represents the mean ± SEM of three independent experiments. *$P \leq 0.05$; **$P \leq 0.01$. BSA-PA, bovine serum albumin–bound sodium palmitate; IRPTC, immortalized rat renal proximal tubular cell; NF-κB, nuclear factor-kappa B.

2.3 Discussion

Post-weaning high-fat diet accelerates kidney injury, but not hypertension programmed by maternal diabetes

Several research questions were addressed in the present study, and the primary findings suggested that (1) IUGR offspring of diabetic dams fed with standard chow diet developed mild hypertension and evidence of kidney injury in adulthood; (2) IUGR offspring of diabetic dams post-weaning fed with high-fat diet resulted in rapid weight gain, catch-up growth, and subsequently developed profound kidney injury in adulthood, but not systemic hypertension; and (3) those features of severe kidney injury were associated with increased CD36 and Fabp4 expression in proximal tubular cells.

The Impact of Postnatal Overnutrition on the Growth Pattern

In the present study, offspring of diabetic dams fed with normal chow (Dia-ND) had a mean birth weight decrease of 20% and continued to have a lower body weight throughout the study, which is similar to previous observations [91, 141, 146]. We also found significantly rapid catch-up growth in offspring of diabetic dams fed with HFD (Dia-HF) from 5 to 8 weeks of age, which is in line with most human and experimental animal studies [107, 147-150]. Although a high-fat diet increased the body weight of Con-HF and Dia-HF offspring over time, there were different plasma lipid profiles in both groups. Con-HF offspring increased plasma NEFA, triglycerides and cholesterol at 20 weeks of age, suggesting that these offspring became obese with lipid abnormalities. In contrast to Con-HF offspring, Dia-HF offspring had similar body weights and plasma lipid profiles as offspring of non-diabetic dams fed with normal chow (Con-ND) at 20 weeks of age. These findings demonstrate that postnatal overnutrition has a differential impact on the growth pattern in the offspring of both non-diabetic and diabetic dams.

Our observation was consistent with previous studies using rats, which showed that rats exposed to a high-fat diet after weaning developed an increased fat mass with elevated plasma insulin, leptin and adiponectin levels [151, 152]. In addition, the IUGR offspring of diabetic rats displayed normal or elevated plasma insulin levels, glucose intolerance, and increased fat mass [153, 154]. In our study, Con-HF offspring had increased plasma insulin

with decreased insulin sensitivity, whereas Dia-HF offspring had regular plasma insulin with increased insulin sensitivity, underscoring that a maternal diabetes milieu might have an impact on offspring insulin production and functions. Thus, we speculated that Dia-HF offspring might enhance the utilization of high fat as the fuel or energy source and store the excess lipids in adipose tissues to balance their body weight and metabolism.

The Impact of Postnatal Overnutrition on Adipose Morphology and BP

Hypertrophic adipose morphology (i.e., adipose tissue with fewer but larger adipocytes) is positively associated with insulin resistance, diabetes, and cardiovascular disease [155]. Because both perirenal and visceral fat among Con-HF, Dia-HF, and Dia-ND offspring have fewer but larger adipocytes compared to Con-ND, it is expected that those offspring are associated with a range of metabolic disturbances, including alternation of plasma glucose, lipid and insulin levels, insulin resistance and susceptibility to cardiometabolic disease.

Besides, the accumulation of fat in the perirenal and renal sinus is associated with an increased prevalence of hypertension and chronic kidney disease [156, 157]. However, there were inconsistent observations in demonstrating hypertension in different experimental obese mouse models. It is likely due to differences in background strain, age, gender, modes of inducing obesity (e.g., diet versus monogenic), and the method of measuring hypertension. For example, there are different BP responses in mouse models of the absence of the leptin signaling pathways [158]. Leptin positively relates to adiposity and increases BP when infused chronically into lean rodents. Thus, mouse models with a deficiency of intact leptin signaling pathways would be expected to have low BP. Indeed, $Lep^{ob/ob}$ mice are hypotensive. However, studies in $LepR^{db/db}$ mice are conflicting, reporting that the mice are hypotensive or hypertensive [159, 160]. In this study, we did not observe the impact of HFD-induced obesity on systolic blood pressure in either Con-HF or Dia-HF offspring. Dia-ND displayed mild hypertension; the possible explanation was attributed to renal hypertrophy related to renal hyperfiltration accompanied by increased GFR. However, the kidney weight/TL and GFR/TL ratios in Dia-HF mice at 20 weeks of age were similar to Con-ND, which might be a partial interpretation of normotension in those mice.

The Impact of Postnatal Overnutrition on Kidney Function

We previously reported that kidney injury in adulthood resulted from a severe maternal diabetic environment [91, 141, 146], which was observed in Dia-ND offspring in this study. Obesity is a significant risk factor for the progression of kidney injury. Obesity-induced kidney diseases have been characterized by proteinuria, glomerulosclerosis, and tubular fibrosis. Thus, increased high fat intake is related to the onset and progression of kidney diseases. We found that Dia-HF offspring increased renal TGFβ1 and collagen IV gene expression, renal lipid accumulation, and ROS generation in both glomerular and tubular compartments of the kidney. These findings suggest that HFD might be another insult resulting in profound kidney injury in Dia-HF offspring.

Accumulation of lipid and dysfunction of fatty acid oxidation in the tubular epithelial cells have been proposed to have a pathogenic role in the development of renal fibrosis. Several studies suggested that CD36 and Fabp4 are highly associated with the pathogenesis of HFD-induced cell damage [161-165]. CD36, a long-chain fatty acid transporter, can facilitate the uptake of long-chain fatty acids. It has been reported that increased CD36 expression in the kidney is associated with proteinuria and renal dysfunction [162]. Fabp4, an intracellular lipid chaperone, is expressed in the adipocytes, macrophages, and renal peritubular capillaries. Also, the altered level and localization of Fabp4 in the kidney is associated with proteinuria and renal dysfunction [165]. Therefore, we speculated that alteration of CD36 and Fabp4 expression might have an impact of IUGR offspring fed with HFD on the development of metabolic disorders and kidney injury in adulthood. In this study, we observed that HFD increased CD36 and Fabp4 expression, which localized to the proximal tubular cells. It is likely that those changes might be secondary to proteinuria and renal dysfunction.

The Mechanisms of HFD-induced Kidney Injury

We used immortalized rat renal proximal tubular cell line (IRPTCs) as an *in vitro* model to examine the functional impact of free fatty acids (i.e., BSA-PA) on renal CD36 and Fabp4 expression and its related molecular mechanism. We found that BSA-PA induced dose-dependent augmentations in CD36 and Fabp4 in IRPTCs. CD36 has multiple roles in lipid accumulation, inflammatory signaling, apoptosis, and kidney fibrosis through activation of

NF-κB, PKC-NADPH oxidase, mitogen-activated protein kinases (MAPKs), and TGF-β signaling pathways [166]. For example, the activation of CD36 in proximal tubular cells by diet-induced obesity targets inflammatory cytokines and ROS, leading to renal dysfunction [163]. CD36 has been demonstrated to mediate proximal tubular apoptosis induced by free fatty acid palmitate via activation of pro-apoptotic p38 MAPK and caspase-3 [167]. On the other hand, Fabp4 was detected in both the glomerular cells (e.g., endothelial cells, macrophages, and mesangial cells) and proximal tubular cells in both mouse and human kidneys, and those ectopic expressions have been involved in the pathogenesis of kidney diseases [168]. In macrophages, Fabp4 increases the accumulation of cholesterol ester and stimulates inflammatory responses through the activation of the NF-κB signaling pathway [168]. Therefore, we examined those potential mechanisms in IRPTCs, and our data suggested that BSA-PA stimulated ROS generation, enhanced apoptosis, and activated NF-κB and TGF-β signaling pathways in IRPTCs. Those findings possibly suggest that free fatty acids may induce the augmentation of CD36 and Fabp4 expression in proximal tubular cells causing these substantial damages, further leading to tubulointerstitial fibrosis and apoptosis.

2.4 Summary

As a summary of the article 2, we have shown that:

– Offspring of dams with severe maternal diabetes had an IUGR phenotype and developed mild hypertension and kidney injury in adulthood.

– IUGR offspring of diabetic dams post-weaning fed with high-fat diet resulted in rapid weight gain, catch-up growth, and subsequently developed profound kidney injury in adulthood, but not systemic hypertension.

– The features of severe kidney injury were associated with increased CD36 and Fabp4 expression in proximal tubular cells.

In conclusion, our studies suggest that post-weaning exposure to HFD in IUGR offspring of diabetic dams increases the risk of development of kidney injury in adulthood, but not hypertension.

CHAPTER 3

3.1 Introduction

Infants born to mothers with gestational diabetes have an increased risk of congenital malformations. CAKUT are the most prevalent of all fetal congenital malformations and frequent causes of CKD and ESRD in children. Moreover, the offspring of a diabetic mother may have long-term sequelae that can lead to hypertension and CKD later in life. Many data indicate that adult hypertension and kidney diseases are initiated in childhood. The possible causes of such adult hypertension and kidney diseases are multifactorial and involve genetics and *in utero* environmental factors. Intriguingly, AT_2RKO mice exhibit a spectrum of CAKUT and also develop hypertension in adulthood. Therefore, we aim to understand the impacts of AT_2R deficiency and *in utero* environment of the diabetic mother on offspring that develop hypertension and kidney diseases later in life and attempt to elucidate the underlying mechanisms.

In this study, we first examined the impact of AT_2R deficiency on the glomerular endowment in embryonic and three week-old mouse kidneys and the underlying molecular mechanisms. The results suggest that AT_2R deficiency impaired glomerulogenesis in embryonic kidneys that exhibited renal hypoplasia. Also, we observed podocyte loss and dysfunction in AT_2RKO mice and this phenotype was mediated, at least in part, via increased Hhip expression in podocytes.

We also examined the impact of the *in utero* environment of the severe diabetic mother on the adult-onset of hypertension and kidney injury. Although many studies have supported this concept, the underlying molecular mechanisms are still far from being fully understood. We therefore investigated the long-term outcomes of IUGR offspring with overnutrition in early life and the underlying mechanisms. Our data suggested that IUGR offspring of diabetic dams developed mild hypertension and kidney injury in adulthood. Fed with a high-fat diet after weaning, those offspring displayed profound kidney injury in adulthood, but not systemic hypertension. It also appeared that increased CD36 and Fabp4 expression in proximal tubular cells accelerated maternal diabetes-induced perinatal programming of kidney injury.

The impacts of AT_2R and hyperglycemia milieu *in utero* on offspring were studied in chapter 1 and chapter 2, respectively. We next interested in the interaction between these influences and aimed to understand the underlying mechanisms.

3.1.1 Interactions of AT_2R with estrogen and its receptors

Sex has an impact on the incidence and prevalence of several kidney diseases as well as the rate of progression of these disorders. Kidney disease is particularly more prevalent in men than in age-matched premenopausal women [123, 124]. In the experimental animal models of aging and Type 2 diabetes, female animals are low risk in the progression of kidney diseases [169]. Studies through gonadectomy or administration of sex hormones to manipulation of the hormonal environment replicate these effects on kidney disease progression, indicating that sex hormone environment rather than genetic differences is responsible for sex differences [123, 124, 126]. In the experimental animal model, estrogen increases AT_2R expression in the kidney in both male and female rats, indicating a positive regulatory interaction [170]. On the other hand, the action of Ang II via AT_2R upregulates ovarian estrogen production and induces ovulation in rabbits [171]. These findings highlight the possibility that there is a reciprocally positive regulation between AT_2R and estrogen.

Several studies reported that the AT_2R/AT_1R ratio is greater in the vasculature and kidney in female than in male animals [5, 124, 172]. Since the *AT_2R* is located on the X chromosome, genetic inequalities are arising from the differences in the sex chromosome complement. However, in the four core genotype mouse model it has been found that the X-chromosome, independently of estrogen, increases renal and brain AT_2R/AT_1R mRNA ratio [173]. The finding indicates that the dosage of *AT_2R* gene underpins, in part, the greater functional role of the AT_2R in females as compared to males.

Estrogens play an essential role in multiple physiology and pathophysiology, ranging from the development of the reproductive system and maintenance of cardiovascular homeostasis to tumorigenesis [174]. Steroid hormone receptors are universal and can be located in both the cytoplasm and the plasma membrane of the cell. Estrogen receptor (ER) has two main forms: ERα and ERβ, which are encoded by the genes *Esr1* and *Esr2*, respectively [175]. Both ERα and ERβ have different tissue distribution and transcriptional

activation domains. Also, these receptors may play different and even opposite roles in controlling the cellular response to estrogens in cells expressing both estrogen receptors [176]. In the rodent, ERα and ERβ are regulated by estrogen and expressed in the renal cortex [177]. Of note, ERs are also found to be localized on podocytes by histochemical studies [178] and expressed in isolated podocytes [179]. Interestingly, there are several estrogen response elements (EREs) for the binding of ERα and ERβ on rat and human AT_2R promoters, indicating that the expression of AT_2R may be regulated by estrogen via ERα and ERβ [180].

3.1.2 Objectives/ Hypothesis

In current studies, we observed that AT_2R deficiency impaired glomerulogenesis, resulting in podocyte loss and dysfunction via ectopic Hhip expression in the podocyte. Also, the hyperglycemic milieu *in utero* accelerated the process of perinatal programming of kidney injury and hypertension in the offspring of diabetic mothers. However, the impact of AT_2R deficiency on the long-term outcomes of those offspring was not addressed.

We previously established a functional relationship between AT_2R and ACE2 in adult mice, indicating that AT_2R deficiency enhanced the development of diabetic nephropathy via upregulation of ROS generation and downregulation of ACE2 expression [97]. In addition, one study reported that podocyte-specific overexpression of human ACE2 delayed the development of diabetic nephropathy with the partial protection of podocyte loss in the STZ-induced type I diabetic mouse model [181]. According to those findings and the results of this thesis, we hypothesized that AT_2R deficiency accelerates maternal diabetes-induced perinatal programming via activation of intrarenal RAS and perturbation of ACE2-mediated counterbalance mechanisms.

3.2 Materials and Methods

Animals and Experimental Design

To understand the causes and potential mechanisms of the developmental origins of health and disease, scientists recommend studies with larger human cohorts, starting early in pregnancy or even around the time of conception, to obtain more information on the exact background and potential mechanisms. Although the epidemiological analysis can minimize confounding factors, such studies still cannot demonstrate the causal relationship between initial programming and the later onset of diseases. Thus, animal studies are an ideal method to demonstrate causal relationships and to study the underlying mechanisms. In the studies, we chose STZ-induced diabetic mouse model in AT_2RKO mice to investigate the interaction between AT_2R deficiency and the hyperglycemic intrauterine milieu.

AT_2RKO mice (C57BL/6) were obtained from Dr. Tadashi Inagami (Vanderbilt University School of Medicine, Nashville, TN, USA). As mentioned in article 2, we used a maternal diabetic murine model (Figure 40) induced by a single intraperitoneal injection of streptozotocin (Sigma-Aldrich Canada, Oakville, ON, Canada) at a dose of 150 mg/kg of body weight on gestational day E13. The offspring (male/female) of non-diabetic and diabetic dams of wild-type (WT, C57BL/6) and AT_2RKO mice were followed until 20 weeks of age. All animals were euthanized at 20 weeks of age with CO_2, and the kidneys were removed immediately. BW (g), kidney weight (mg), and tibia length (mm) were rapidly recorded. The biological samples were processed, collected, and stored accordingly for analysis. Kidneys were fixed overnight in 4% paraformaldehyde at 4°C before paraffin embedding. Mature glomerular isolation from both WT and AT_2RKO mice was performed by using the iron-magnet method, as mentioned in article 1.

Animal care in these experiments met the standards set forth by the Canadian Council on Animal Care, and the procedures utilized were approved by the Institutional Animal Care Committee of the Centre de Recherche du Centre Hospitalier de l'Université de Montréal (CRCHUM). All WT and AT_2RKO mice were housed under standard humidity and lighting conditions (12 hours light–dark cycles). Animals were allowed free access to standard mouse chow and water *ad libitum*.

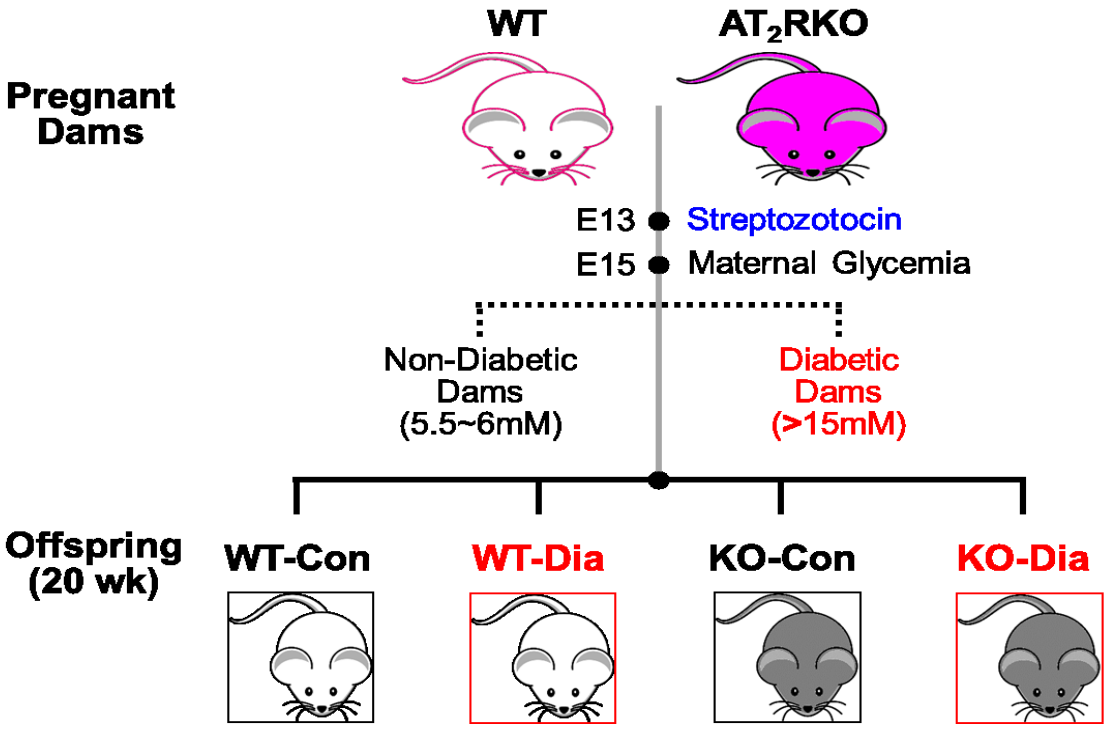

Figure 39. Maternal diabetic murine model. *In vivo* murine model of maternal diabetes induced by a single intraperitoneal injection of streptozotocin (150 mg/kg) injection on gestational day E13 in both wild-type (WT, C57BL/6 mice) and AT_2RKO (C57BL/6 background mice) pregnant dams. On E15, we measured the glycemia to determine the diabetic dams (defined as maternal blood glucose concentration > 15mM). Non-Diabetic dams were injected with saline by a single intraperitoneal injection on gestational day E13. Both male (M) and female (F) offspring of non-diabetic (control) and diabetic dams of wild-type (WT) and AT_2RKO (KO) mice were followed until 20 weeks of age—e.g., offspring of WT control dams (WT-Con), offspring of WT diabetic dams (WT-Dia), offspring of AT_2RKO control dams (KO-Con), and offspring of AT_2RKO diabetic dams (KO-Dia).

Blood Pressure Measurements

Mean systolic blood pressure (SBP) was monitored by the tail-cuff method with the Visitech BP-2000 Blood Pressure Analysis System for mice (Visitech System Inc., Apex, NC, USA) as mentioned in article 2. The animals were acclimated to SBP measurement with a 2 weeks period of pre-training starting at 12 weeks of age (SBP measured 15 times/animal/day,

thrice weekly), followed by actual measurement of SBP thrice weekly from 14 weeks until 20 weeks of age.

Glomerular Filtration Rate (GFR) Measurement

We estimated GFR in 20 week-old male and female animals by the fluorescein isothiocyanate-inulin (FITC-inulin) method as recommended by the Diabetic Complications Consortium and mentioned in article 2. In brief, each mouse received a single intravenous bolus of 5% FITC-inulin, after which seven blood samples were collected from the saphenous vein at 3, 7, 10, 15, 35, 55, and 75 minutes post-FITC-inulin injection. Plasma fluorescence concentration at each time point was measured by Fluoroscan Ascent FL (Labsystems, Helsinki, Finland) with 485 nm excitation and read at 538 nm emission. The GFR was calculated according to the equation: $GFR = I/(A/\alpha + B/\beta)$, where I was the amount of FITC-inulin bolus delivered, A and α were the y intercept and decay constant of the rapid (initial) decay phase, respectively, and B and β were the y intercept and decay constant of the slow decay phase, respectively [182].

Renal Histology

Kidney sections were stained with Periodic-Acid Schiff (PAS) to reveal renal morphologic changes. The changes of morphology features—glomerulosclerosis (based on PAS images, scale from 0 to 4) were scored with the scorer blinded to the group, as mentioned in article 2. Relative staining was quantified with NIH Image J software (Bethesda, MD, USA).

Podocytes were identified by immunofluorescence (IF) staining of podocyte markers including p57 (H-91) and synaptopodin (Synpo) (P-19) antibodies (1:100, both from Santa Cruz Biotechnology, Santa Cruz, CA, USA). Podocyte number in WT and AT_2RKO mice kidneys at 20 weeks of age was determined on 3.5-mm formalin fixed sections stained with p57 antibody (marker of podocyte). Cells stained positive for p57 were counted in glomerular cross-sections (30–35 glomeruli per mouse, N = 6/group), as mentioned in article 1.

Podocyte Cell Line

Immortalized mouse podocyte cell line (mPODs) were a generous gift of Dr. Stuart J Shankland (University of Washington, WA, USA) and cultured as described in article 1. Before the treatment periods, mPODs for analyzing estrogen influences were maintained in

charcoal-stripped fetal bovine serum for at least 2 days before starting the experiments to exclude residual estrogenic action of culture medium.

Real-time quantitative polymerase chain reaction (RT-qPCR)

RT-qPCR [The Fast SYBR® green master mix kit and the 7500 Fast Real-Time PCR system (Applied Biosystems, Life Technologies, Foster City, CA, USA)] was performed to quantify the relative expression of *Agtr2, Esr1, Esr2 and ribosomal protein L13A (RPL13A)* in isolated glomeruli and mPODs as described in article 1 with specific primers.

Statistical analysis

The data are expressed as means ± SEM. Statistical significance between the experimental groups was analyzed by one-way or two-way ANOVA (analysis of variance) and the Bonferroni post-tests as appropriate. $p \leq 0.05$ values were considered to be statistically significant.

3.3 Unpublished Results

Mean Systolic Blood Pressure

Longitudinal measurement of systolic blood pressure (SBP) (Figure 40), recorded from 14 to 20 weeks of age, revealed that KO-Dia-Female have significantly higher SBP over the follow-up period when compared with WT-Con-Female. SBP was not significantly different in male mice among all the groups. This finding suggested that AT_2R deficiency enhances maternal diabetes-induced perinatal programmed hypertension in the female progeny.

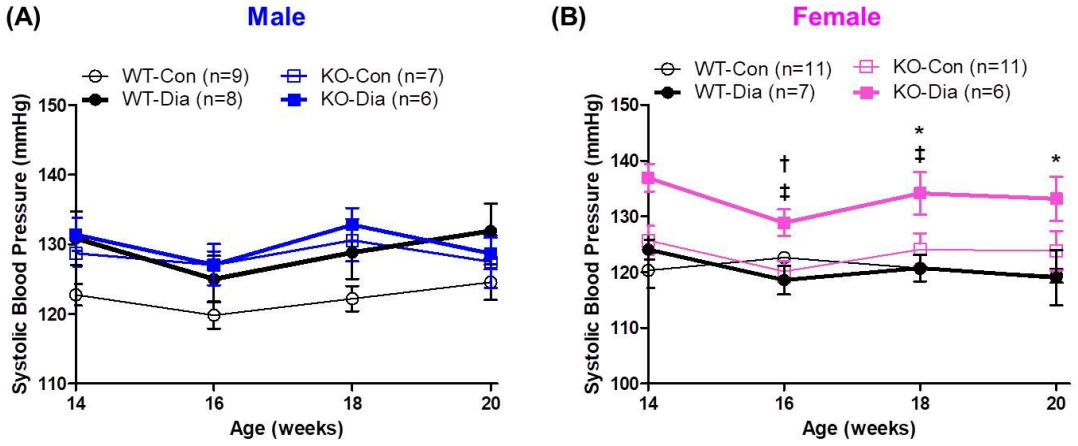

Figure 40. Systolic blood pressure in the offspring of non-diabetic (Con) and diabetic (Dia) dams of wild-type (WT) and AT2RKO (KO) mice. Longitudinal systolic blood pressure measurement in male (M, left graph) and female (F, right graph) mice. (○) WT-Con-M; (●) WT-Dia-M; (□) KO-Con-M; (■) KO-Dia-M; (○) WT-Con-F; (●) WT-Dia-F; (□) KO-Con-F; (■) KO-Dia-F. * $p \leq 0.05$, KO-Dia versus WT-Con; † $p \leq 0.05$, KO-Dia versus KO-Con; ‡ $p \leq 0.05$ KO-Dia versus WT- Dia.

Renal Morphology and Function

Compared to the offspring of non-diabetic dams, both WT and KO mice showed enhanced extracellular matrix protein accumulation seen by periodic acid–Schiff (PAS) staining (Figure 41A,B), irrespective of their sex, suggesting that those mice have glomerular diseases. AT_2RKO mice exhibited increased kidney injury compared to WT animals. These damages were more pronounced in the female KO-Dia offspring. Similar patterns were found in the glomerular filtration rate (Figure 41C). Those findings suggested that the offspring of diabetic mothers have an increased risk of kidney injury, and loss of AT_2R might enhance maternal diabetes-induced perinatal programmed kidney injury in the female progeny.

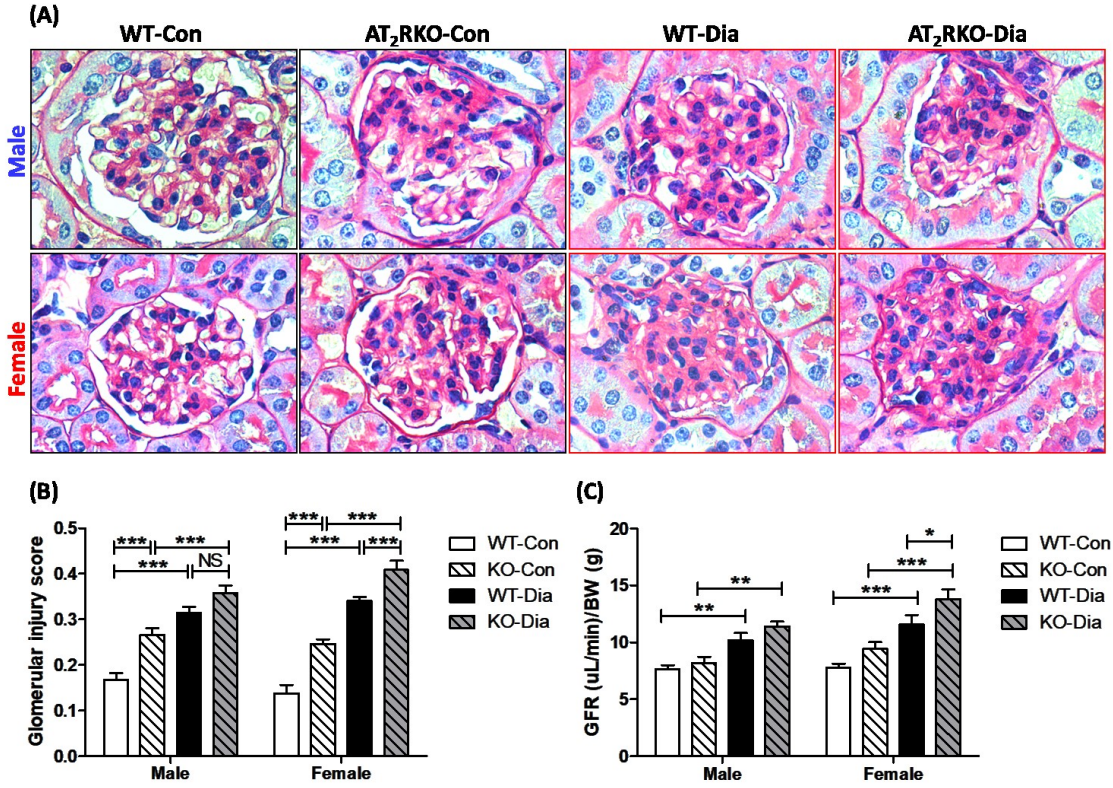

Figure 41. Renal morphology and function. (A) PAS staining (magnification: ×600). (B) Classic scoring of glomerulosclerosis based on PAS images. Grade 0, normal glomeruli; grade 1, presence of mesangial expansion/thickening of the basement membrane. ***$p \leq$ 0.001. NS = non-significant. (C) Glomerular filtration rate (GFR) measurement. *$p \leq$ 0.05; **$p \leq 0.01$; ***$p \leq 0.001$.

Podocyte Number and Morphology

Similar to previous findings, both WT and KO mice exhibited podocyte loss compared to the offspring of non-diabetic dams (Figure 4A,B), irrespective of their sex, and this result was indeed in line with synaptopodin expression levels as observed by IF (Figure 41C). An enhanced podocyte loss was observed in both male and female KO-Dia offspring, suggesting that AT_2R deficiency increases maternal diabetes-induced perinatal programmed podocyte loss.

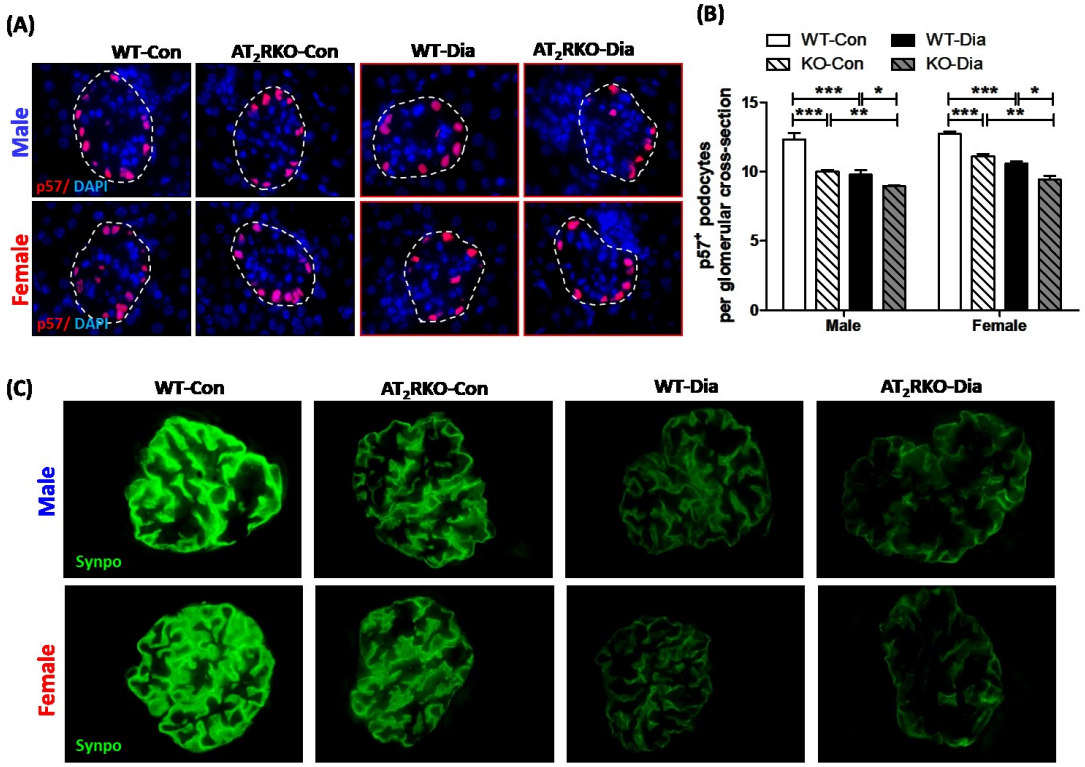

Figure 42. Podocyte number and marker analysis. (A) Podocyte marker p57 IF staining (B) Semi-quantification of p57 positively stained cells per glomerulus cross-section. *$p \leq 0.05$; **$p \leq 0.01$; ***$p \leq 0.001$. (C) Podocyte marker synaptopodin (Synpo) IF staining.

Estrogen Receptors Expression in Isolated Glomeruli and mPODs

Compared to the offspring of non-diabetic dams, both WT and KO mice of diabetic dams expressed significantly lower level of *Esr1* in isolated glomeruli, except female KO mice (Figure 43A). This might be due to female KO mice have lower basal level of *Esr1*. Compared

with WT mice, KO mice showed enhanced *Esr2* mRNA basal level in the glomeruli (Figure 43A,B). In addition, compared to the offspring of non-diabetic dams, the offspring of diabetic dams expressed higher *Esr2* in female WT mice than that in male WT. However, this change did not display in the male and female AT_2RKO mice. To further confirm the impact of estradiol on ERs expression in the podocytes, we applied estradiol to mPODs (Figure 43C-D). Our RT-qPCR data indicated that estradiol stimulates *Esr2* expression in mPODs, while *Esr1* remains unchanged. Interestingly, AT_2R mRNA was also upregulated by estradiol in mPODs, suggesting that estradiol might stimulate ERβ and AT_2R expression in mPODs.

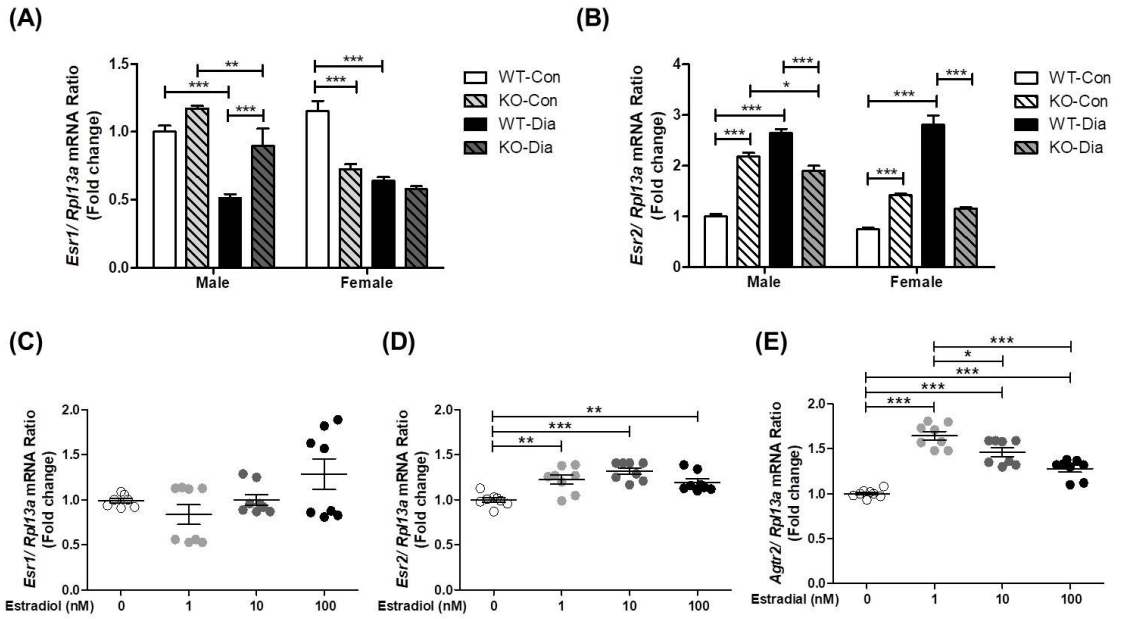

Figure 43. Estrogen receptors expression in isolated glomeruli and effect of estradiol on estrogen receptors and AT_2R expression in cultured podocytes. (A,B) RT-qPCR assessment of (A) *Esr1* and (B) *Esr2* expression in isolated glomeruli from the offspring (male/female) of non-diabetic and diabetic dams of wild-type (WT) and AT_2RKO (KO) mice at the age of 20 weeks. (C-D) RT-qPCR assessment of (C) *Esr1*, (D) *Esr2* and (E) *Agtr2* expression in mPODs. *$p \leq 0.05$; **$p \leq 0.01$; ***$p \leq 0.001$.

3.4 Discussion

The present study indicates a synergistic effect of the hyperglycemic milieu *in utero* and AT_2R deficiency on the long-term outcome of kidney injuries, especially on female

progeny. We observed that this synergistic effect appeared in female offspring from AT_2RKO diabetic dams with the increased SBP, accompanying an increase GFR. The features of kidney injuries and depletion of podocyte number were found in offspring from AT_2RKO diabetic dams, more severe in female progeny.

The genetic effect of AT_2R deficiency has been reported to be either increased [25] or unchanged [26] on baseline blood pressure in male mice via invasive blood pressure measurement. This discrepancy could be due to differences in the genetic background of the mouse strains or other factors, such as methods of blood pressure measurement, sex, age or environmental stress that might affect baseline blood pressure. In the present study, male offspring from AT_2RKO non-diabetic dams have a trend of increased SBP compared to male offspring from wild-type non-diabetic dams, which is similar to previous findings [97]. The environmental effect of hyperglycemic milieu *in utero* on blood pressure was hypertensive in female AT_2RKO mice or normotensive in female wild-type mice and male mice, as previous reported that ~50% of offspring from diabetic dams manifested hypertension [141]. The present studies demonstrate a synergistic effect of the genetic and environmental factors on the elevation of blood pressure in female offspring from diabetic dams.

Podocyte dysfunction has been proposed as a key contributor to many forms of progressive glomerular diseases which account for 90% of chronic kidney disease [183]. Similar to article 1, we showed that AT_2R deficiency mice displayed podocyte loss and dysfunction at 20 weeks of age. In addition, this phenotype was observed in offspring from wild-type diabetic dams and further deterioration in offspring from AT_2RKO diabetic dams. Interestingly, this deterioration in AT_2RKO diabetic progeny was more prominent in females than males. Thus, female mice might be sensitive to the impact of AT_2R deficiency and the hyperglycemic milieu *in utero* on kidney diseases.

Literature indicates that ERα regulates the estrogen-mediated protection effect against apoptosis in podocytes [184]. In the present study, ERα was downregulated in the isolated glomeruli of male offspring from diabetic dams, while the basal level of ERα was dramatically decreased in the female AT_2RKO mice, suggesting that maternal diabetes induces perinatal programming of kidney injury in the podocyte of offspring and also AT_2R deficiency in female progeny aggravates this phenomenon. On the other hand, the previous report

demonstrates that estradiol protects against diabetic glomerulosclerosis by regulating the phenotype of podocyte via increasing the ERβ protein expression and modulating apoptotic and anti-inflammatory signaling pathways [179]. The present study was shown that ERβ was upregulated in isolated glomeruli of offspring from wild-type diabetic dams and of offspring from AT_2RKO non-diabetic dams, while this change did not display in offspring from AT_2RKO diabetic dams. This can be partially explained the podocyte loss in offspring from AT_2RKO diabetic dams, suggesting AT_2R deficiency is associated with the lack of protective roles mediated by estrogen via ERβ in the podocyte. Although the changing ERα-ERβ ratio was observed in our *in vivo* study, the actual level of plasma estrogen has not been measured. Our *in vitro* study was shown that estradiol stimulated ERβ and AT_2R expression, suggesting the enhanced protective role and anti-apoptotic effect of female gender on the podocyte. However, the protective role mediated by estrogen via estrogen receptors on podocyte remains unclear.

In summary, the recent studies suggest that AT_2R deficiency accelerated features of nephropathy in the female progeny of diabetic dams, which might be due to loss of the estrogen-mediated protective effects by modulating the ERα-ERβ ratio in the podocyte.

3.5 Future Works

Based on these recent findings, we speculate that in the female progeny, AT_2R deficiency enhances the process of the hyperglycemic intrauterine milieu induced perinatal programming of kidney injury and hypertension. We need further studies to understand the underlying mechanisms and the sex difference. In brief, we would like to investigate the expression and function of the RAS components as well as the level and activity status of sex hormones.

To detect the urinary albumin leakage caused by podocyte loss, the urinary albumin/creatinine ratio (ACR) will be measured to identify the kidney injury. To understand the impact of AT_2R deficiency on the RAS, the expression of RAS components will be examined in both mRNA and protein levels. Moreover, we will measure testosterone and estrogen levels by mass spectrometry to understand whether sex differences play roles in maternal diabetes-programmed kidney injury.

In conclusion, AT_2R deficiency accelerated features of nephropathy in the female progeny of diabetic dams. Hopefully, these experiments will help us to understand the underlying mechanisms of how the interaction between AT_2R deficiency and the hyperglycemic intrauterine milieu. Our proposed working model is summarized in Figure 43. The genetic effect of AT_2R on the sequence of the final nephron formation and the function of podocytes has been addressed in article 1. In addition, the environmental effect of the hyperglycemic milieu *in utero* on the long-term outcomes of kidney diseases and hypertension in the offspring has been discussed in article 2. The interaction of those effects on the long-term outcomes of kidney diseases and hypertension was synergistic, especially in female progeny. However, the possible mechanisms of changing the ERα-ERβ ratio in the podocyte of AT_2RKO mice and how AT_2R deficiency accelerates renal dysfunction need to be evaluated in future studies. In summary, both AT_2R deficiency and maternal environmental changes predispose offspring to a deteriorative long-term outcome of kidney function, especially on the podocyte dysfunction.

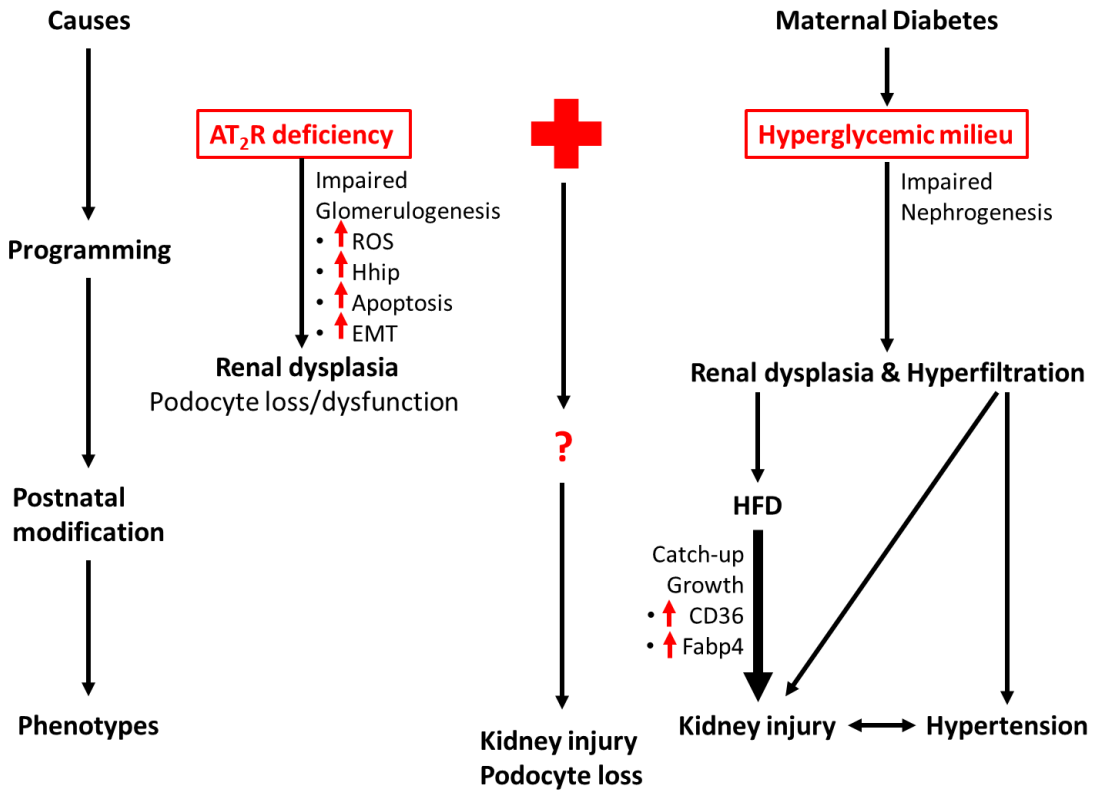

Figure 44. Proposed working model.

CHAPTER 4 – REFERENCES

1. Forrester, S.J., et al., *Angiotensin II Signal Transduction: An Update on Mechanisms of Physiology and Pathophysiology.* Physiol Rev, 2018. **98**(3): p. 1627-1738.
2. Paul, M., A. Poyan Mehr, and R. Kreutz, *Physiology of local renin-angiotensin systems.* Physiol Rev, 2006. **86**(3): p. 747-803.
3. Nehme, A., et al., *An Update on the Tissue Renin Angiotensin System and Its Role in Physiology and Pathology.* J Cardiovasc Dev Dis, 2019. **6**(2).
4. Dandona, P., et al., *Angiotensin II and inflammation: the effect of angiotensin-converting enzyme inhibition and angiotensin II receptor blockade.* J Hum Hypertens, 2007. **21**(1): p. 20-7.
5. Chow, B.S. and T.J. Allen, *Angiotensin II type 2 receptor (AT2R) in renal and cardiovascular disease.* Clin Sci (Lond), 2016. **130**(15): p. 1307-26.
6. Kawai, T., et al., *AT1 receptor signaling pathways in the cardiovascular system.* Pharmacol Res, 2017. **125**(Pt A): p. 4-13.
7. Carey, R.M., *AT2 Receptors: Potential Therapeutic Targets for Hypertension.* Am J Hypertens, 2017. **30**(4): p. 339-347.
8. Carey, R.M., *Newly discovered components and actions of the renin-angiotensin system.* Hypertension, 2013. **62**(5): p. 818-22.
9. Chai, S.Y., et al., *The angiotensin IV/AT4 receptor.* Cell Mol Life Sci, 2004. **61**(21): p. 2728-37.
10. Seikaly, M.G., B.S. Arant, Jr., and F.D. Seney, Jr., *Endogenous angiotensin concentrations in specific intrarenal fluid compartments of the rat.* J Clin Invest, 1990. **86**(4): p. 1352-7.
11. Navar, L.G., et al., *Tubular fluid concentrations and kidney contents of angiotensins I and II in anesthetized rats.* J Am Soc Nephrol, 1994. **5**(4): p. 1153-8.
12. Navar, L.G., et al., *Renal responses to AT1 receptor blockade.* Am J Hypertens, 2000. **13**(1 Pt 2): p. 45S-54S.
13. Navar, L.G., H. Kobori, and M. Prieto-Carrasquero, *Intrarenal angiotensin II and hypertension.* Curr Hypertens Rep, 2003. **5**(2): p. 135-43.

14. Casarini, D.E., et al., *Angiotensin I-converting enzyme activity in tubular fluid along the rat nephron.* Am J Physiol, 1997. **272**(3 Pt 2): p. F405-9.
15. Hackenthal, E., et al., *Morphology, physiology, and molecular biology of renin secretion.* Physiol Rev, 1990. **70**(4): p. 1067-116.
16. de Gasparo, M., et al., *International union of pharmacology. XXIII. The angiotensin II receptors.* Pharmacol Rev, 2000. **52**(3): p. 415-72.
17. Dasgupta, C. and L. Zhang, *Angiotensin II receptors and drug discovery in cardiovascular disease.* Drug Discov Today, 2011. **16**(1-2): p. 22-34.
18. Karnik, S.S., et al., *International Union of Basic and Clinical Pharmacology. XCIX. Angiotensin Receptors: Interpreters of Pathophysiological Angiotensinergic Stimuli [corrected].* Pharmacol Rev, 2015. **67**(4): p. 754-819.
19. Turu, G., et al., *Differential beta-arrestin binding of AT1 and AT2 angiotensin receptors.* FEBS Lett, 2006. **580**(1): p. 41-5.
20. Yosypiv, I.V., *Renin-angiotensin system in ureteric bud branching morphogenesis: implications for kidney disease.* Pediatr Nephrol, 2014. **29**(4): p. 609-20.
21. Kakuchi, J., et al., *Developmental expression of renal angiotensin II receptor genes in the mouse.* Kidney Int, 1995. **47**(1): p. 140-7.
22. Ozono, R., et al., *Expression of the subtype 2 angiotensin (AT2) receptor protein in rat kidney.* Hypertension, 1997. **30**(5): p. 1238-46.
23. Zhang, J. and R.E. Pratt, *The AT2 receptor selectively associates with Gialpha2 and Gialpha3 in the rat fetus.* J Biol Chem, 1996. **271**(25): p. 15026-33.
24. Feng, Y.H., Y. Sun, and J.G. Douglas, *Gbeta gamma -independent constitutive association of Galpha s with SHP-1 and angiotensin II receptor AT2 is essential in AT2-mediated ITIM-independent activation of SHP-1.* Proc Natl Acad Sci U S A, 2002. **99**(19): p. 12049-54.
25. Ichiki, T., et al., *Effects on blood pressure and exploratory behaviour of mice lacking angiotensin II type-2 receptor.* Nature, 1995. **377**(6551): p. 748-50.
26. Hein, L., et al., *Behavioural and cardiovascular effects of disrupting the angiotensin II type-2 receptor in mice.* Nature, 1995. **377**(6551): p. 744-7.

27. Tanaka, M., et al., *Vascular response to angiotensin II is exaggerated through an upregulation of AT1 receptor in AT2 knockout mice.* Biochem Biophys Res Commun, 1999. **258**(1): p. 194-8.
28. Siragy, H.M., et al., *Sustained hypersensitivity to angiotensin II and its mechanism in mice lacking the subtype-2 (AT2) angiotensin receptor.* Proc Natl Acad Sci U S A, 1999. **96**(11): p. 6506-10.
29. Masaki, H., et al., *Cardiac-specific overexpression of angiotensin II AT2 receptor causes attenuated response to AT1 receptor-mediated pressor and chronotropic effects.* J Clin Invest, 1998. **101**(3): p. 527-35.
30. Tsutsumi, Y., et al., *Angiotensin II type 2 receptor overexpression activates the vascular kinin system and causes vasodilation.* J Clin Invest, 1999. **104**(7): p. 925-35.
31. Ingelfinger, J.R., et al., *World Kidney Day 2016: Averting the legacy of kidney disease-focus on childhood.* Pediatr Nephrol, 2016. **31**(3): p. 343-8.
32. Queisser-Luft, A., et al., *Malformations in newborn: results based on 30,940 infants and fetuses from the Mainz congenital birth defect monitoring system (1990-1998).* Arch Gynecol Obstet, 2002. **266**(3): p. 163-7.
33. Sanna-Cherchi, S., et al., *Genetic approaches to human renal agenesis/hypoplasia and dysplasia.* Pediatr Nephrol, 2007. **22**(10): p. 1675-84.
34. Yosypiv, I.V., *Congenital anomalies of the kidney and urinary tract: a genetic disorder?* Int J Nephrol, 2012. **2012**: p. 909083.
35. Nicolaou, N., et al., *Genetic, environmental, and epigenetic factors involved in CAKUT.* Nat Rev Nephrol, 2015. **11**(12): p. 720-31.
36. Chesnaye, N., et al., *Demographics of paediatric renal replacement therapy in Europe: a report of the ESPN/ERA-EDTA registry.* Pediatr Nephrol, 2014. **29**(12): p. 2403-10.
37. Wuhl, E., et al., *Timing and outcome of renal replacement therapy in patients with congenital malformations of the kidney and urinary tract.* Clin J Am Soc Nephrol, 2013. **8**(1): p. 67-74.
38. Dressler, G.R., *The cellular basis of kidney development.* Annu Rev Cell Dev Biol, 2006. **22**: p. 509-29.
39. Davidson, A.J., *Mouse kidney development*, in *StemBook*. 2008: Cambridge (MA).

40. Schell, C., N. Wanner, and T.B. Huber, *Glomerular development--shaping the multi-cellular filtration unit.* Semin Cell Dev Biol, 2014. **36**: p. 39-49.
41. Nishimura, H., et al., *Role of the angiotensin type 2 receptor gene in congenital anomalies of the kidney and urinary tract, CAKUT, of mice and men.* Mol Cell, 1999. **3**(1): p. 1-10.
42. Levin, A., et al., *Global kidney health 2017 and beyond: a roadmap for closing gaps in care, research, and policy.* Lancet, 2017. **390**(10105): p. 1888-1917.
43. Ku, E., et al., *Hypertension in CKD: Core Curriculum 2019.* Am J Kidney Dis, 2019.
44. Kemp, B.A., et al., *AT(2) receptor activation induces natriuresis and lowers blood pressure.* Circ Res, 2014. **115**(3): p. 388-99.
45. Padia, S.H., et al., *Conversion of renal angiotensin II to angiotensin III is critical for AT2 receptor-mediated natriuresis in rats.* Hypertension, 2008. **51**(2): p. 460-5.
46. Bosnyak, S., et al., *Stimulation of angiotensin AT2 receptors by the non-peptide agonist, Compound 21, evokes vasodepressor effects in conscious spontaneously hypertensive rats.* Br J Pharmacol, 2010. **159**(3): p. 709-16.
47. Benndorf, R.A., et al., *Angiotensin II type 2 receptor deficiency aggravates renal injury and reduces survival in chronic kidney disease in mice.* Kidney Int, 2009. **75**(10): p. 1039-49.
48. Hashimoto, N., et al., *Overexpression of angiotensin type 2 receptor ameliorates glomerular injury in a mouse remnant kidney model.* Am J Physiol Renal Physiol, 2004. **286**(3): p. F516-25.
49. Wang, Y., et al., *Anti-fibrotic Potential of AT2 Receptor Agonists.* Front Pharmacol, 2017. **8**: p. 564.
50. Chow, B.S., et al., *Relaxin requires the angiotensin II type 2 receptor to abrogate renal interstitial fibrosis.* Kidney Int, 2014. **86**(1): p. 75-85.
51. Pollak, M.R., et al., *The glomerulus: the sphere of influence.* Clin J Am Soc Nephrol, 2014. **9**(8): p. 1461-9.
52. Vaughan, M.R. and S.E. Quaggin, *How do mesangial and endothelial cells form the glomerular tuft?* J Am Soc Nephrol, 2008. **19**(1): p. 24-33.
53. Costantini, F. and R. Kopan, *Patterning a complex organ: branching morphogenesis and nephron segmentation in kidney development.* Dev Cell, 2010. **18**(5): p. 698-712.

54. Lindstrom, N.O., et al., *Conserved and Divergent Molecular and Anatomic Features of Human and Mouse Nephron Patterning.* J Am Soc Nephrol, 2018. **29**(3): p. 825-840.
55. Lindstrom, N.O., et al., *Integrated beta-catenin, BMP, PTEN, and Notch signalling patterns the nephron.* Elife, 2015. **3**: p. e04000.
56. Nagata, M., *Glomerulogenesis and the role of endothelium.* Curr Opin Nephrol Hypertens, 2018. **27**(3): p. 159-164.
57. Kobayashi, A., et al., *Six2 defines and regulates a multipotent self-renewing nephron progenitor population throughout mammalian kidney development.* Cell Stem Cell, 2008. **3**(2): p. 169-81.
58. Oxburgh, L., *Kidney Nephron Determination.* Annu Rev Cell Dev Biol, 2018. **34**: p. 427-450.
59. Halt, K.J., et al., *CD146(+) cells are essential for kidney vasculature development.* Kidney Int, 2016. **90**(2): p. 311-324.
60. Hu, Y., et al., *Hemovascular Progenitors in the Kidney Require Sphingosine-1-Phosphate Receptor 1 for Vascular Development.* J Am Soc Nephrol, 2016. **27**(7): p. 1984-95.
61. Ichimura, K., et al., *Three-dimensional architecture of podocytes revealed by block-face scanning electron microscopy.* Sci Rep, 2015. **5**: p. 8993.
62. Kriz, W., *TRPC6 - a new podocyte gene involved in focal segmental glomerulosclerosis.* Trends Mol Med, 2005. **11**(12): p. 527-30.
63. Perico, L., et al., *Podocyte-actin dynamics in health and disease.* Nat Rev Nephrol, 2016. **12**(11): p. 692-710.
64. Mundel, P., et al., *Synaptopodin: an actin-associated protein in telencephalic dendrites and renal podocytes.* J Cell Biol, 1997. **139**(1): p. 193-204.
65. Imasawa, T. and R. Rossignol, *Podocyte energy metabolism and glomerular diseases.* Int J Biochem Cell Biol, 2013. **45**(9): p. 2109-18.
66. Jiang, J. and C.C. Hui, *Hedgehog signaling in development and cancer.* Dev Cell, 2008. **15**(6): p. 801-12.
67. Chuang, P.T. and A.P. McMahon, *Vertebrate Hedgehog signalling modulated by induction of a Hedgehog-binding protein.* Nature, 1999. **397**(6720): p. 617-21.

68. D'Cruz, R., et al., *Lineage-specific roles of hedgehog-GLI signaling during mammalian kidney development.* Pediatr Nephrol, 2019.
69. Zhou, D., R.J. Tan, and Y. Liu, *Sonic hedgehog signaling in kidney fibrosis: a master communicator.* Sci China Life Sci, 2016. **59**(9): p. 920-9.
70. Briscoe, J. and P.P. Therond, *The mechanisms of Hedgehog signalling and its roles in development and disease.* Nat Rev Mol Cell Biol, 2013. **14**(7): p. 416-29.
71. Hu, M.C., et al., *GLI3-dependent transcriptional repression of Gli1, Gli2 and kidney patterning genes disrupts renal morphogenesis.* Development, 2006. **133**(3): p. 569-78.
72. Bouchard, M., *Transcriptional control of kidney development.* Differentiation, 2004. **72**(7): p. 295-306.
73. Bates, C.M., et al., *Role of N-myc in the developing mouse kidney.* Dev Biol, 2000. **222**(2): p. 317-25.
74. Shirakawa, T., et al., *A novel heterozygous GLI2 mutation in a patient with congenital urethral stricture and renal hypoplasia/dysplasia leading to end-stage renal failure.* CEN Case Rep, 2018. **7**(1): p. 94-97.
75. Chuang, P.T., T. Kawcak, and A.P. McMahon, *Feedback control of mammalian Hedgehog signaling by the Hedgehog-binding protein, Hip1, modulates Fgf signaling during branching morphogenesis of the lung.* Genes Dev, 2003. **17**(3): p. 342-7.
76. Zhou, X., et al., *Identification of a chronic obstructive pulmonary disease genetic determinant that regulates HHIP.* Hum Mol Genet, 2012. **21**(6): p. 1325-35.
77. Kayed, H., et al., *Localization of the human hedgehog-interacting protein (Hip) in the normal and diseased pancreas.* Mol Carcinog, 2005. **42**(4): p. 183-92.
78. Olsen, C.L., et al., *Hedgehog-interacting protein is highly expressed in endothelial cells but down-regulated during angiogenesis and in several human tumors.* BMC Cancer, 2004. **4**: p. 43.
79. Cain, J.E. and N.D. Rosenblum, *Control of mammalian kidney development by the Hedgehog signaling pathway.* Pediatr Nephrol, 2011. **26**(9): p. 1365-71.
80. Zhao, X.P., et al., *Maternal diabetes modulates kidney formation in murine progeny: the role of hedgehog interacting protein (HHIP).* Diabetologia, 2014. **57**(9): p. 1986-96.

81. Zhao, X.P., et al., *Hedgehog Interacting Protein Promotes Fibrosis and Apoptosis in Glomerular Endothelial Cells in Murine Diabetes.* Sci Rep, 2018. **8**(1): p. 5958.

82. Miyata, K.N., et al., *Increased urinary excretion of hedgehog interacting protein (uHhip) in early diabetic kidney disease.* Transl Res, 2019.

83. Sauer, H., M. Wartenberg, and J. Hescheler, *Reactive oxygen species as intracellular messengers during cell growth and differentiation.* Cell Physiol Biochem, 2001. **11**(4): p. 173-86.

84. Ye, Z.W., et al., *Oxidative stress, redox regulation and diseases of cellular differentiation.* Biochim Biophys Acta, 2015. **1850**(8): p. 1607-21.

85. Garrido, A.M. and K.K. Griendling, *NADPH oxidases and angiotensin II receptor signaling.* Mol Cell Endocrinol, 2009. **302**(2): p. 148-58.

86. Yang, Q., et al., *Nox4 in renal diseases: An update.* Free Radic Biol Med, 2018. **124**: p. 466-472.

87. Kondo, S., et al., *Expression of NADPH oxidase and production of reactive oxygen species contribute to ureteric bud branching and nephrogenesis.* J Med Invest, 2019. **66**(1.2): p. 93-98.

88. Chen, Y.W., et al., *Deficiency of intrarenal angiotensin II type 2 receptor impairs paired homeo box-2 and N-myc expression during nephrogenesis.* Pediatr Nephrol, 2008. **23**(10): p. 1769-77.

89. Chen, Y.W., et al., *Reactive oxygen species and nuclear factor-kappa B pathway mediate high glucose-induced Pax-2 gene expression in mouse embryonic mesenchymal epithelial cells and kidney explants.* Kidney Int, 2006. **70**(9): p. 1607-15.

90. Zhang, S.L., et al., *Reactive oxygen species in the presence of high glucose alter ureteric bud morphogenesis.* J Am Soc Nephrol, 2007. **18**(7): p. 2105-15.

91. Tran, S., et al., *Maternal diabetes modulates renal morphogenesis in offspring.* J Am Soc Nephrol, 2008. **19**(5): p. 943-52.

92. Norwood, V.F., et al., *Differential expression of angiotensin II receptors during early renal morphogenesis.* Am J Physiol, 1997. **272**(2 Pt 2): p. R662-8.

93. Suzuki, K., et al., *Angiotensin II type 1 and type 2 receptors play opposite roles in regulating the barrier function of kidney glomerular capillary wall.* Am J Pathol, 2007. **170**(6): p. 1841-53.

94. Oshima, K., et al., *Angiotensin type II receptor expression and ureteral budding.* J Urol, 2001. **166**(5): p. 1848-52.
95. Song, R., et al., *Angiotensin II AT2 receptor regulates ureteric bud morphogenesis.* Am J Physiol Renal Physiol, 2010. **298**(3): p. F807-17.
96. Saavedra, J.M., et al., *Increased AT(1) receptor expression and mRNA in kidney glomeruli of AT(2) receptor gene-disrupted mice.* Am J Physiol Renal Physiol, 2001. **280**(1): p. F71-8.
97. Chang, S.Y., et al., *Angiotensin II type II receptor deficiency accelerates the development of nephropathy in type I diabetes via oxidative stress and ACE2.* Exp Diabetes Res, 2011. **2011**: p. 521076.
98. Gao, J., et al., *Ontogeny of angiotensin type 2 and type 1 receptor expression in mice.* J Renin Angiotensin Aldosterone Syst, 2012. **13**(3): p. 341-52.
99. Daehn, I., et al., *Endothelial mitochondrial oxidative stress determines podocyte depletion in segmental glomerulosclerosis.* J Clin Invest, 2014. **124**(4): p. 1608-21.
100. Das, R., et al., *Transforming Growth Factor beta1-induced Apoptosis in Podocytes via the Extracellular Signal-regulated Kinase-Mammalian Target of Rapamycin Complex 1-NADPH Oxidase 4 Axis.* J Biol Chem, 2015. **290**(52): p. 30830-42.
101. Loeffler, I. and G. Wolf, *Epithelial-to-Mesenchymal Transition in Diabetic Nephropathy: Fact or Fiction?* Cells, 2015. **4**(4): p. 631-52.
102. Das, R., et al., *Upregulation of mitochondrial Nox4 mediates TGF-beta-induced apoptosis in cultured mouse podocytes.* Am J Physiol Renal Physiol, 2014. **306**(2): p. F155-67.
103. Deputy, N.P., et al., *Prevalence and Changes in Preexisting Diabetes and Gestational Diabetes Among Women Who Had a Live Birth - United States, 2012-2016.* MMWR Morb Mortal Wkly Rep, 2018. **67**(43): p. 1201-1207.
104. Fong, A., et al., *Pre-gestational versus gestational diabetes: a population based study on clinical and demographic differences.* J Diabetes Complications, 2014. **28**(1): p. 29-34.
105. Landon, M.B., et al., *The relationship between maternal glycemia and perinatal outcome.* Obstet Gynecol, 2011. **117**(2 Pt 1): p. 218-24.

106. Aerts, L. and F.A. Van Assche, *Intra-uterine transmission of disease.* Placenta, 2003. **24**(10): p. 905-11.
107. Plagemann, A., *Maternal diabetes and perinatal programming.* Early Hum Dev, 2011. **87**(11): p. 743-7.
108. Tyrrell, J., et al., *Genetic Evidence for Causal Relationships Between Maternal Obesity-Related Traits and Birth Weight.* JAMA, 2016. **315**(11): p. 1129-40.
109. Horikoshi, M., et al., *Genome-wide associations for birth weight and correlations with adult disease.* Nature, 2016. **538**(7624): p. 248-252.
110. Hughes, A.E., et al., *Fetal Genotype and Maternal Glucose Have Independent and Additive Effects on Birth Weight.* Diabetes, 2018. **67**(5): p. 1024-1029.
111. Fleming, T.P., et al., *Origins of lifetime health around the time of conception: causes and consequences.* Lancet, 2018. **391**(10132): p. 1842-1852.
112. Hales, C.N. and D.J. Barker, *The thrifty phenotype hypothesis.* Br Med Bull, 2001. **60**: p. 5-20.
113. Dotsch, J., *Perinatal programming - myths, fact, and future of research.* Mol Cell Pediatr, 2014. **1**(1): p. 2.
114. Dotsch, J., et al., *Perinatal programming of renal function.* Curr Opin Pediatr, 2016. **28**(2): p. 188-94.
115. Brenner, B.M. and G.M. Chertow, *Congenital oligonephropathy and the etiology of adult hypertension and progressive renal injury.* Am J Kidney Dis, 1994. **23**(2): p. 171-5.
116. Keller, G., et al., *Nephron number in patients with primary hypertension.* N Engl J Med, 2003. **348**(2): p. 101-8.
117. Spencer, S.J., *Early life programming of obesity: the impact of the perinatal environment on the development of obesity and metabolic dysfunction in the offspring.* Curr Diabetes Rev, 2012. **8**(1): p. 55-68.
118. Jarvelin, M.R., et al., *Early life factors and blood pressure at age 31 years in the 1966 northern Finland birth cohort.* Hypertension, 2004. **44**(6): p. 838-46.
119. Tu, Y.K., et al., *Why evidence for the fetal origins of adult disease might be a statistical artifact: the "reversal paradox" for the relation between birth weight and blood pressure in later life.* Am J Epidemiol, 2005. **161**(1): p. 27-32.

120. Warrington, N.M., et al., *Maternal and fetal genetic effects on birth weight and their relevance to cardio-metabolic risk factors.* Nat Genet, 2019. **51**(5): p. 804-814.
121. McMullen, S., D.S. Gardner, and S.C. Langley-Evans, *Prenatal programming of angiotensin II type 2 receptor expression in the rat.* Br J Nutr, 2004. **91**(1): p. 133-40.
122. Sakurai, H. and S.K. Nigam, *In vitro branching tubulogenesis: implications for developmental and cystic disorders, nephron number, renal repair, and nephron engineering.* Kidney Int, 1998. **54**(1): p. 14-26.
123. Neugarten, J. and L. Golestaneh, *Influence of Sex on the Progression of Chronic Kidney Disease.* Mayo Clin Proc, 2019. **94**(7): p. 1339-1356.
124. Carrero, J.J., et al., *Sex and gender disparities in the epidemiology and outcomes of chronic kidney disease.* Nat Rev Nephrol, 2018. **14**(3): p. 151-164.
125. Dai, S., et al., *Executive summary--report from the Canadian Chronic Disease Surveillance System: hypertension in Canada, 2010.* Chronic Dis Can, 2010. **31**(1): p. 46-7.
126. White, M.C., R. Fleeman, and A.C. Arnold, *Sex differences in the metabolic effects of the renin-angiotensin system.* Biol Sex Differ, 2019. **10**(1): p. 31.
127. Klett, C., et al., *Regulation of hepatic angiotensinogen synthesis and secretion by steroid hormones.* Endocrinology, 1992. **130**(6): p. 3660-8.
128. Chen, Y.F., A.J. Naftilan, and S. Oparil, *Androgen-dependent angiotensinogen and renin messenger RNA expression in hypertensive rats.* Hypertension, 1992. **19**(5): p. 456-63.
129. Seltzer, A., et al., *Estrogens regulate angiotensin-converting enzyme and angiotensin receptors in female rat anterior pituitary.* Neuroendocrinology, 1992. **55**(4): p. 460-7.
130. Chinnathambi, V., et al., *Gestational exposure to elevated testosterone levels induces hypertension via heightened vascular angiotensin II type 1 receptor signaling in rats.* Biol Reprod, 2014. **91**(1): p. 6.
131. Sullivan, J.C., et al., *Differences in angiotensin (1-7) between men and women.* Am J Physiol Heart Circ Physiol, 2015. **308**(9): p. H1171-6.
132. Ji, H., et al., *Role of angiotensin-converting enzyme 2 and angiotensin(1-7) in 17beta-oestradiol regulation of renal pathology in renal wrap hypertension in rats.* Exp Physiol, 2008. **93**(5): p. 648-57.

133. Baiardi, G., et al., *Estrogen upregulates renal angiotensin II AT1 and AT2 receptors in the rat.* Regul Pept, 2005. **124**(1-3): p. 7-17.
134. Mishra, J.S., G.D. Hankins, and S. Kumar, *Testosterone downregulates angiotensin II type-2 receptor via androgen receptor-mediated ERK1/2 MAP kinase pathway in rat aorta.* J Renin Angiotensin Aldosterone Syst, 2016. **17**(4).
135. Miller, J.A., et al., *Gender differences in the renal response to renin-angiotensin system blockade.* J Am Soc Nephrol, 2006. **17**(9): p. 2554-60.
136. Rabi, D.M., et al., *Reporting on sex-based analysis in clinical trials of angiotensin-converting enzyme inhibitor and angiotensin receptor blocker efficacy.* Can J Cardiol, 2008. **24**(6): p. 491-6.
137. Sampson, A.K., et al., *Enhanced angiotensin II type 2 receptor mechanisms mediate decreases in arterial pressure attributable to chronic low-dose angiotensin II in female rats.* Hypertension, 2008. **52**(4): p. 666-71.
138. Sampson, A.K., et al., *The arterial depressor response to chronic low-dose angiotensin II infusion in female rats is estrogen dependent.* Am J Physiol Regul Integr Comp Physiol, 2012. **302**(1): p. R159-65.
139. Brown, R.D., et al., *Sex differences in the pressor and tubuloglomerular feedback response to angiotensin II.* Hypertension, 2012. **59**(1): p. 129-35.
140. Pessoa, B.S., et al., *Angiotensin II type 2 receptor- and acetylcholine-mediated relaxation: essential contribution of female sex hormones and chromosomes.* Hypertension, 2015. **66**(2): p. 396-402.
141. Chen, Y.W., et al., *Maternal diabetes programs hypertension and kidney injury in offspring.* Pediatr Nephrol, 2010. **25**(7): p. 1319-29.
142. Chen, Y.W., et al., *High glucose promotes nascent nephron apoptosis via NF-kappaB and p53 pathways.* Am J Physiol Renal Physiol, 2011. **300**(1): p. F147-56.
143. Ben-Shlomo, Y., et al., *Immediate postnatal growth is associated with blood pressure in young adulthood: the Barry Caerphilly Growth Study.* Hypertension, 2008. **52**(4): p. 638-44.
144. Chandra, A., et al., *The relationship of body mass and fat distribution with incident hypertension: observations from the Dallas Heart Study.* J Am Coll Cardiol, 2014. **64**(10): p. 997-1002.

145. Odermatt, A., *The Western-style diet: a major risk factor for impaired kidney function and chronic kidney disease.* Am J Physiol Renal Physiol, 2011. **301**(5): p. F919-31.
146. Chang, S.Y., et al., *Catalase prevents maternal diabetes-induced perinatal programming via the Nrf2-HO-1 defense system.* Diabetes, 2012. **61**(10): p. 2565-74.
147. Plagemann, A., et al., *Rapid neonatal weight gain increases risk of childhood overweight in offspring of diabetic mothers.* J Perinat Med, 2012. **40**(5): p. 557-63.
148. Plagemann, A., et al., *Early postnatal life as a critical time window for determination of long-term metabolic health.* Best Pract Res Clin Endocrinol Metab, 2012. **26**(5): p. 641-53.
149. Perala, M.M., et al., *Body size at birth is associated with food and nutrient intake in adulthood.* PLoS One, 2012. **7**(9): p. e46139.
150. Crowther, N.J., et al., *Influence of catch-up growth on glucose tolerance and beta-cell function in 7-year-old children: results from the birth to twenty study.* Pediatrics, 2008. **121**(6): p. e1715-22.
151. Prior, L.J., et al., *Undernutrition during suckling in rats elevates plasma adiponectin and its receptor in skeletal muscle regardless of diet composition: a protective effect?* Int J Obes (Lond), 2008. **32**(10): p. 1585-94.
152. Velkoska, E., et al., *Early undernutrition leads to long-lasting reductions in body weight and adiposity whereas increased intake increases cardiac fibrosis in male rats.* J Nutr, 2008. **138**(9): p. 1622-7.
153. Holemans, K., L. Aerts, and F.A. Van Assche, *Fetal growth restriction and consequences for the offspring in animal models.* J Soc Gynecol Investig, 2003. **10**(7): p. 392-9.
154. Dabelea, D., *The predisposition to obesity and diabetes in offspring of diabetic mothers.* Diabetes Care, 2007. **30 Suppl 2**: p. S169-74.
155. Tandon, P., R. Wafer, and J.E.N. Minchin, *Adipose morphology and metabolic disease.* J Exp Biol, 2018. **221**(Pt Suppl 1).
156. Ricci, M.A., et al., *Morbid obesity and hypertension: The role of perirenal fat.* J Clin Hypertens (Greenwich), 2018. **20**(10): p. 1430-1437.
157. Foster, M.C., et al., *Fatty kidney, hypertension, and chronic kidney disease: the Framingham Heart Study.* Hypertension, 2011. **58**(5): p. 784-90.

158. Kennedy, A.J., et al., *Mouse models of the metabolic syndrome.* Dis Model Mech, 2010. **3**(3-4): p. 156-66.
159. Bodary, P.F., et al., *Leptin regulates neointima formation after arterial injury through mechanisms independent of blood pressure and the leptin receptor/STAT3 signaling pathways involved in energy balance.* Arterioscler Thromb Vasc Biol, 2007. **27**(1): p. 70-6.
160. Su, W., et al., *Hypertension and disrupted blood pressure circadian rhythm in type 2 diabetic db/db mice.* Am J Physiol Heart Circ Physiol, 2008. **295**(4): p. H1634-41.
161. Kang, H.M., et al., *Defective fatty acid oxidation in renal tubular epithelial cells has a key role in kidney fibrosis development.* Nat Med, 2015. **21**(1): p. 37-46.
162. Baines, R.J., et al., *CD36 mediates proximal tubular binding and uptake of albumin and is upregulated in proteinuric nephropathies.* Am J Physiol Renal Physiol, 2012. **303**(7): p. F1006-14.
163. Kennedy, D.J., et al., *CD36 and Na/K-ATPase-alpha1 form a proinflammatory signaling loop in kidney.* Hypertension, 2013. **61**(1): p. 216-24.
164. Furuhashi, M., et al., *Serum fatty acid-binding protein 4 is a predictor of cardiovascular events in end-stage renal disease.* PLoS One, 2011. **6**(11): p. e27356.
165. Tanaka, M., et al., *Ectopic expression of fatty acid-binding protein 4 in the glomerulus is associated with proteinuria and renal dysfunction.* Nephron Clin Pract, 2014. **128**(3-4): p. 345-51.
166. Yang, X., et al., *CD36 in chronic kidney disease: novel insights and therapeutic opportunities.* Nat Rev Nephrol, 2017. **13**(12): p. 769-781.
167. Susztak, K., et al., *Multiple metabolic hits converge on CD36 as novel mediator of tubular epithelial apoptosis in diabetic nephropathy.* PLoS Med, 2005. **2**(2): p. e45.
168. Furuhashi, M., *Fatty Acid-Binding Protein 4 in Cardiovascular and Metabolic Diseases.* J Atheroscler Thromb, 2019. **26**(3): p. 216-232.
169. Silbiger, S.R. and J. Neugarten, *The impact of gender on the progression of chronic renal disease.* Am J Kidney Dis, 1995. **25**(4): p. 515-33.
170. Macova, M., et al., *Estrogen reduces aldosterone, upregulates adrenal angiotensin II AT2 receptors and normalizes adrenomedullary Fra-2 in ovariectomized rats.* Neuroendocrinology, 2008. **88**(4): p. 276-86.

171. Yoshimura, Y., et al., *Angiotensin II induces ovulation and oocyte maturation in rabbit ovaries via the AT2 receptor subtype.* Endocrinology, 1996. **137**(4): p. 1204-11.
172. Armando, I., et al., *Estrogen upregulates renal angiotensin II AT(2) receptors.* Am J Physiol Renal Physiol, 2002. **283**(5): p. F934-43.
173. Dadam, F.M., et al., *Sex chromosome complement involvement in angiotensin receptor sexual dimorphism.* Mol Cell Endocrinol, 2017. **447**: p. 98-105.
174. Valdivielso, J.M., C. Jacobs-Cacha, and M.J. Soler, *Sex hormones and their influence on chronic kidney disease.* Curr Opin Nephrol Hypertens, 2019. **28**(1): p. 1-9.
175. Greene, G.L., et al., *Sequence and expression of human estrogen receptor complementary DNA.* Science, 1986. **231**(4742): p. 1150-4.
176. Hurst, A.G., et al., *Independent downstream gene expression profiles in the presence of estrogen receptor alpha or beta.* Biol Reprod, 2004. **71**(4): p. 1252-61.
177. Esqueda, M.E., T. Craig, and C. Hinojosa-Laborde, *Effect of ovariectomy on renal estrogen receptor-alpha and estrogen receptor-beta in young salt-sensitive and -resistant rats.* Hypertension, 2007. **50**(4): p. 768-72.
178. Bhat, H.K., et al., *Localization of estrogen receptors in interstitial cells of hamster kidney and in estradiol-induced renal tumors as evidence of the mesenchymal origin of this neoplasm.* Cancer Res, 1993. **53**(22): p. 5447-51.
179. Catanuto, P., et al., *17 beta-estradiol and tamoxifen upregulate estrogen receptor beta expression and control podocyte signaling pathways in a model of type 2 diabetes.* Kidney Int, 2009. **75**(11): p. 1194-1201.
180. Mishra, J.S., et al., *Estrogen Receptor-beta Mediates Estradiol-Induced Pregnancy-Specific Uterine Artery Endothelial Cell Angiotensin Type-2 Receptor Expression.* Hypertension, 2019. **74**(4): p. 967-974.
181. Nadarajah, R., et al., *Podocyte-specific overexpression of human angiotensin-converting enzyme 2 attenuates diabetic nephropathy in mice.* Kidney Int, 2012. **82**(3): p. 292-303.
182. Qi, Z., et al., *Characterization of susceptibility of inbred mouse strains to diabetic nephropathy.* Diabetes, 2005. **54**(9): p. 2628-37.
183. Assady, S., et al., *Glomerular podocytes in kidney health and disease.* Lancet, 2019. **393**(10174): p. 856-858.

184. Kummer, S., et al., *Estrogen receptor alpha expression in podocytes mediates protection against apoptosis in-vitro and in-vivo.* PLoS One, 2011. **6**(11): p. e27457